

Test of a solar crop dryer



Test of a solar crop dryer

**Søren Østergaard Jensen
Danish Technological Institute**

**Erik Fløjgaard Kristensen
Danish Institute of Agricultural Sciences**

**Torkil Forman
Aidt Miljø A/S**

January 2001

Preface

The report describes the tests carried out on a solar crop dryer. The work is part of the project “Test and Research Project into the Drying of Food and Wood Products with Solar Heat” financed by Danida (Danish International Development Assistance) via the Danish Embassy in Ghana. The project was established based on an initiative by the Energy Commission of Ghana.

The present report describes the experience gained on tests carried out in Denmark on a solar crop dryer. The tests were an important part of the development of the solar crop dryer, which later was shipped to Ghana for further tests and use. The present report describes in chronological order the tests carried out and the experience gained.

Participants in the tests:

Aidt Miljø A/S

Torkil Forman

Department of Agricultural Engineering, Danish Institute of Agricultural Sciences

Erik Fløjgaard Kristensen

Jens Kristian Kristensen

Solar Energi Centre Denmark, Danish Technological Institute

Søren Østergaard Jensen

William Otto

Test of a solar crop dryer

1st printing, 1st edition

© Danish Technological Institute

Energy division

ISBN: 87-7756-583-5

ISSN: 1600-3780

List of contents

1.	Introduction	3
2.	Initial design	4
2.1.	Solar crop dryer	4
2.1.1.	Collector	5
2.1.2.	Fan	7
2.1.3.	PV	8
2.1.4.	Ductworks	9
2.1.5.	Drying bed	10
2.2.	Measuring equipment	10
2.2.1.	Sensors	12
2.2.2.	Data logging	15
2.2.3.	Processing of the measured data	15
2.3.	Measuring results	15
2.3.1.	Drying capacity	22
2.3.2.	Collector efficiency	24
2.3.3.	Flow rate	27
2.3.4.	Pressure drop	27
3.	Modified design	31
3.1.	Collector	31
3.2.	Ductworks	32
3.3.	Drying bed	32
3.4.	Pressure drop	33
3.5.	Measuring results	34
3.5.1.	Drying capacity	40
3.5.2.	Temperature of the air to the drying bed	42
3.5.3.	Collector efficiency	42
3.6.	Measurements with at new air speed sensor	46
3.6.1.	Efficiency	47
4.	Test including measuring of the power to the fan	52
4.1.	Measuring results	52
4.1.1.	Drying capacity	52
4.1.2.	Air flow rate	54
4.1.4.	Voltage and current from the PV-panels	56
4.1.3.	Efficiency	57
5.	Test with a filter in the inlets to the collector and with/without a maximum power point tracker	59
5.1.	Filter	59
5.2.	Maximum power point tracker	59
5.3.	Measuring results	60
5.3.1.	Temperature of the air to the drying bed	66
6.	Test with thermal mass in the pressure chamber under the drying bed	67
6.1.	Thermal mass	67
6.2.	Measuring results	68

6.2.1.	Heat losses from the ductworks	71
6.2.2.	Efficiency	72
7.	Economical consideration	74
7.1.	Conclusion	80
8.	Conclusion	81
9.	References	84
Appendix A	Data sheet for the fan	85
Appendix B	Data sheet for the PV-panels	87
Appendix C	Weather conditions in Accra	89

1. Introduction

One of the major goals of the project “Test and Research Project into the Drying of Food and Wood Products with Solar Heat” was to develop and test a solar crop dryer for use in Ghana.

Based on a survey in Ghana (Jensen, Frank and Kristensen, 1999) it was decided to develop a dryer for drying of maize for seed as the increase in value of the crop due to the drying here would be high – the dryer may, however, also be used to dry other crops or other items – one unit will e.g. be erected in Ghana to test drying of fish. The capacity of the dryer was defined to be 500 kg having a collector area of approx. 25 m². It was decided to let the dryer consist of 5 separate units each with a transparent collector area of 4.77 m² and a capacity of approx. 100 kg. The modulized concept has several benefits: If one drying bed is operated improperly this will not affect the total quantity of crops being dried at that time. It is possible to dry different crops (creating different pressure drop) side by side without risking that the crop with the highest pressure drop will be dried improperly. Small dc fans are often cheaper than larger dc fans. The system will be less complex, and an even air distribution over the drying bed is easier obtainable. Finally it is possible to start with only one unit and then gradually increase the capacity of the solar dryer - this will make it easier to invest in a solar dryer.

It was further decided that the fans of the dryer should be powered directly by PV-panels in order to make the dryer independent of an often unreliable, missing or expensive grid.

The dryer is going to be erected and tested at Silwood Farms situated close to Accra. Silwood Farms has total land acreage of 210 acres where 176 acres are used for cultivating maize - the rest is used for growing pineapples. A majority of the maize is processed into seed. The main harvest season for maize at Silwood Farms is August/September with a smaller harvest period in January. During the rest of the year other crops may be dried in the solar crop dryer.

The solar crop dryer was developed and produced in Denmark by Aidt Miljø A/S in corporation with the Department of Agricultural Engineering and Solar Energi Centre Denmark. As an important part of the development of the solar crop dryer, a unit was tested in Denmark. The report describes briefly the dryer and the modifications made to the original design based on the tests. Main focus of the report is the results from the tests on the prototype.

The second chapter of the report contains the description, measuring equipment and test on the initial design of the solar crop dryer. The third to sixth chapter contain only descriptions of the modifications made to the dryer and the measuring equipment and the most important measuring results. Several other smaller tests have been carried out than the tests described in chapter 3-6, however, the tests described in chapter 3-6 include the major findings of the tests carried out. Chapter seven contains some preliminary economical considerations.

2. Initial design

2.1. Solar crop dryer

The prototype test unit had a capacity of approx. 100 kg and a collector area of 4.77 m². Figure 2.1 shows the principle of the dryer while figure 2.2 shows a picture of the first design.

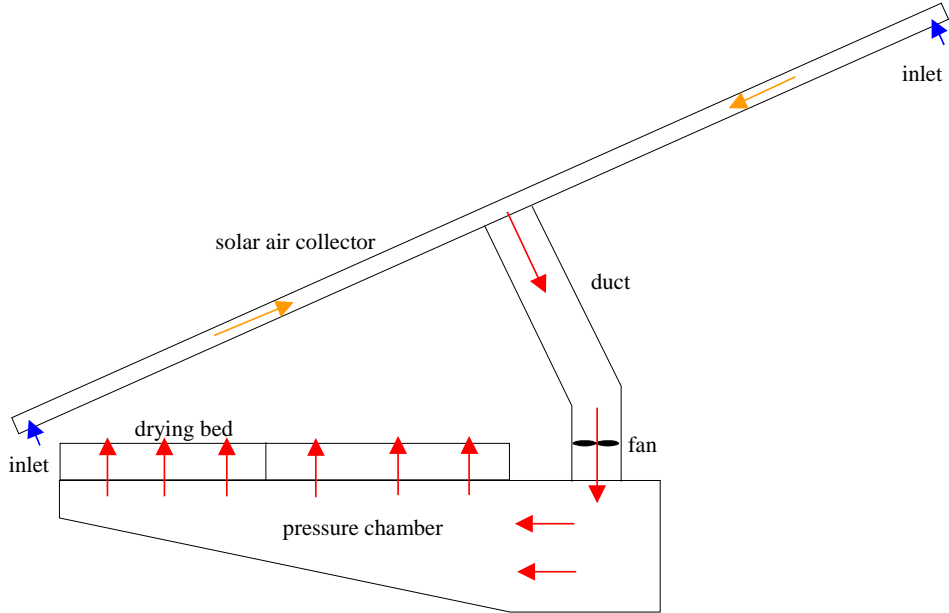


Figure 2.1. The principle of the concept in the solar crop dryer. The coloured arrows show the air stream through the system.



Figure 2.2. Photo of the first design of the solar crop dryer.

The components of the solar crop dryer was:

- **Collector:** Outer dimensions: 4900 x 1070 mm². Transparent area: 4.77 m². Cover: 10 mm double walled ribbed UV-stabilized polycarbonate. Absorber: Black felt mat. Air intake at the back in both ends and air outlet in the middle at the back.
- **Fan:** 300 m³/h at 40 Pa. 12 V dc motor.
- **PV:** 2 panels of 12 V, 14 W_p.
- **Duct between collector and drying bed:** Internal cross section: 16.9 x 17.3 mm² = 0.0299 m².
- **Drying bed:** 6 trays of 890 x 297 mm² (outer dimensions), inner dimensions 826 x 273 mm² = in total 1.35 m². The height was 125 mm giving a total drying volume of 0.168 m³. The trays were made of plywood with a plastic net in the bottom.

2.1.1. Collector

The solar air collector of the dryer was based on the matrix principle – i.e. the air flow was through the absorber. The absorber was a 2 mm temperature-resistant black porous felt mat where through the air was sucked as shown in figure 2.3.

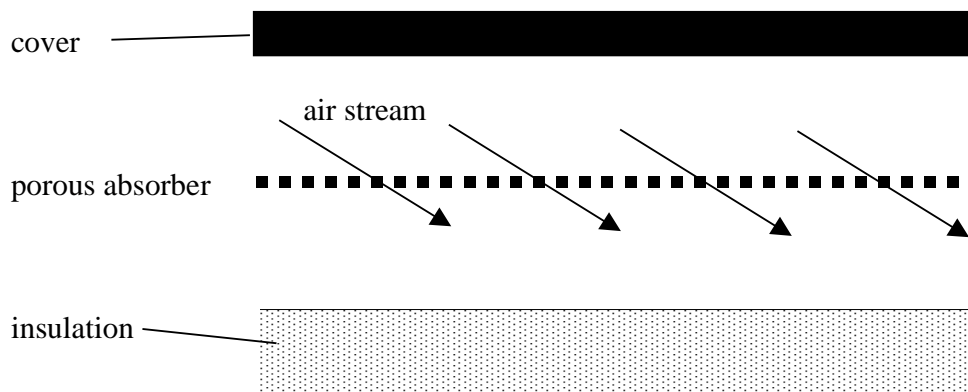


Figure 2.3. The principle of the collector in the solar dryer.

Figure 2.1 shows that there was an air inlet at both ends at the back of the collector and an outlet at the middle also at the back of the collector. The aim of two inlets is to reduce the pressure loss across the collector. Figure 2.4 shows the internal dimensions of the collector and the location and dimensions of the inlets and outlet. The air was sucked in between the cover and the absorber, then through the absorber end let to the outlet, which was situated below the absorber.

Figure 2.5 shows the materials of the collector while figures 2.6 and 2.7 show a section of the inlet and the outlet respectively.

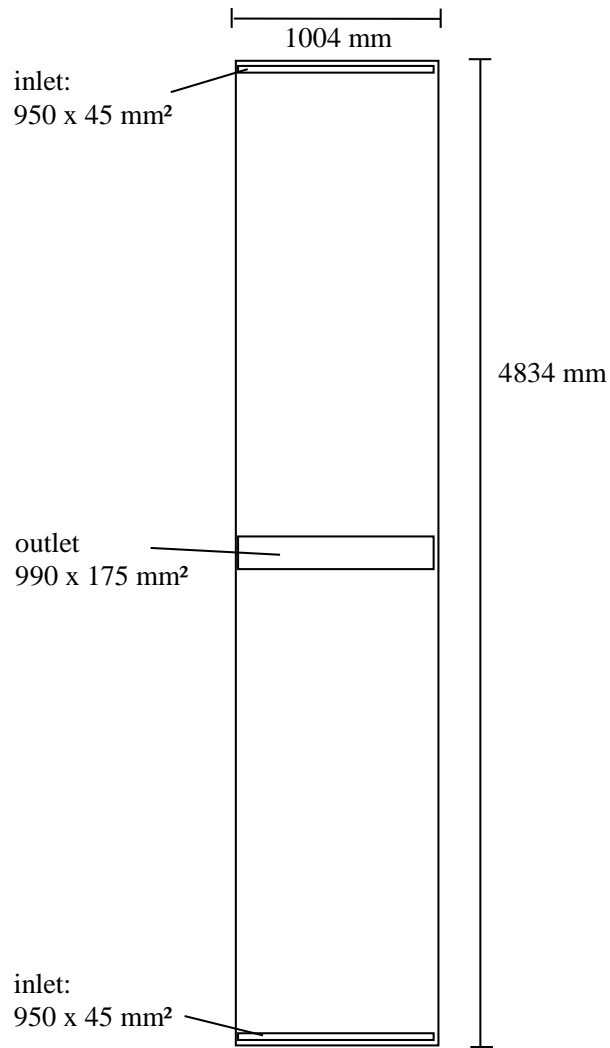


Figure 2.4. The internal dimensions of the collector and the location and dimensions of the inlets and outlet.

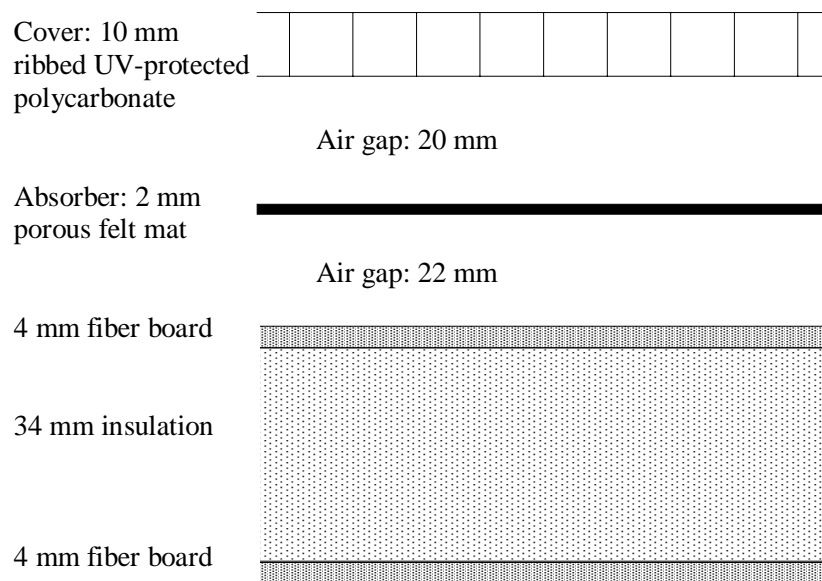


Figure 2.5. The materials of the collector.

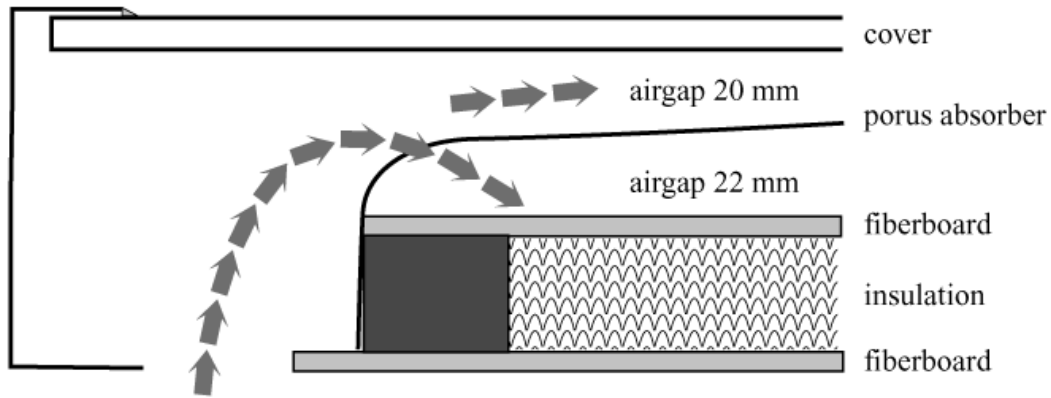


Figure 2.6. Section showing the inlet to the collector.

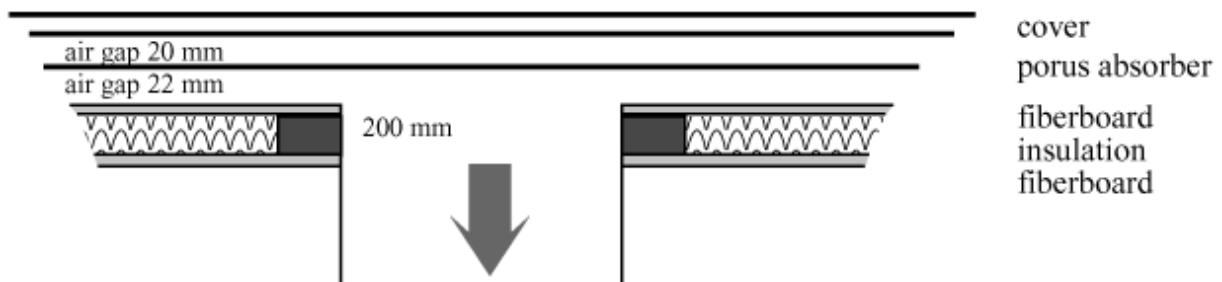


Figure 2.7. Section showing the outlet of the collector

The orientation of the collector was due south and the tilt was 30° . In Ghana the tilt will be lower due to the closer location to equator. However, in order to insure that rain may run off the collector the tilt will be 15° . The collector will in Ghana also face due south.

2.1.2. Fan

The main problem with a PV powered solar crop dryer is the fan: the fan should be inexpensive, durable and produce high flow rates at a high pressure while having a low power consumption in order to keep the price of the solar crop dryer down and at the same time ensure an efficient drying process.

In order to limit the necessary size of the PV-panel the flow rate through the crop was decreased considerably compared to conventional dryers. With the air flow in the design case of $300 \text{ m}^3/\text{h}$ per unit the air speed through the drying bed was 0.06 m/s . This is very low compared to the $0.3\text{-}0.7 \text{ m/s}$ in conventional cross flow dryers and also low compared to the 0.1 m/s in conventional platform dryers.

The data sheet for the chosen fan is shown in appendix A. The fan is type 7212N from Pabst. The characteristic of the fan is shown in figure 2.8, curve 2. The figure shows that the pressure drop of the system should be below 50 Pa at a flow rate of $300 \text{ m}^3/\text{h}$ as the flow rate else may drop to around $200 \text{ m}^3/\text{h}$.

The voltage range of the fan is between 6 and 15 V and the nominal power demand is 12 W.

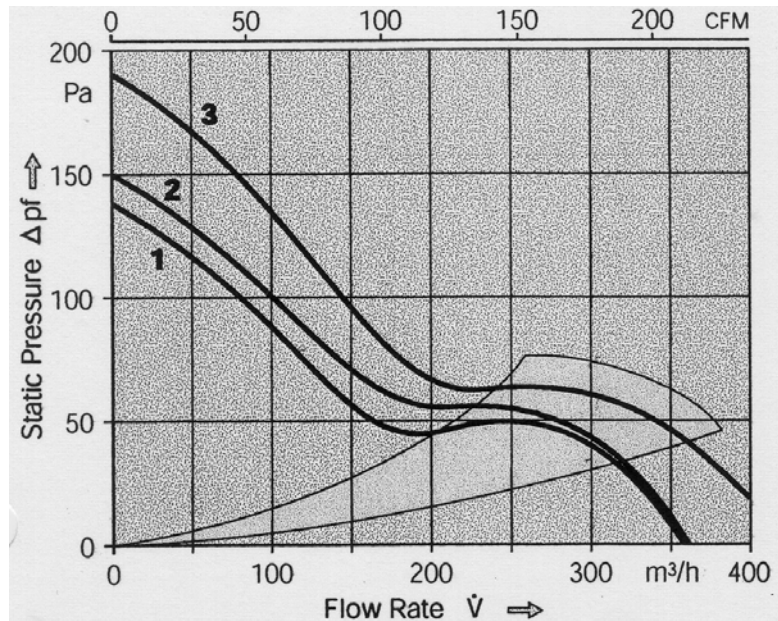


Figure 2.8. The characteristic of the applied fan.

2.1.3. PV

The chosen PV-panel is from Intersolar type Phoenix Gold. A data sheet for the PV-panel is shown in appendix B. The rated power of the panel is 14 Wp. Figure 2.2 shows the solar collector with PV-panels at each end while figure 2.9. shows a close-up of one of the PV-panels. At first the fan was only powered by one PV-panel. However, one panel was not enough to obtain the wished design flow rate of 300 m³/h.



Figure 2.9. The bottom PV-panels of the dryer.

2.1.4. Ductworks

The ductworks of the dryer were made of plywood. The ductworks consisted of a funnel shaped manifold connecting the collector to a squared duct leading to the fan. The manifold is shown in figure 2.10 while the complete ductworks is shown in figure 2.11.



Figure 2.10. The manifold connecting the collector with the duct leading to the fan.



Figure 2.11. The entire ductworks of the dryer.

2.1.5. Drying bed

The drying bed was as the ductworks made of plywood. The drying bed consists as shown in figure 2.1 of a pressure chamber with trays containing the crops on top. The pressure chamber ensures an even air distribution through the trays. The drying bed contains 6 removable drying trays which each may contain approx. 20 kg maize. The rather small removable drying trays are to ease the loading and unloading of the dryer. The drying trays are positioned in such a way that they fit tightly together and to the pressure chamber in order to avoid leakages. The initial internal dimensions of the drying trays are 826 (length) x 273 (width) x 125 (height) mm³ giving a total drying area of 1.35 m² and a total drying volume of 0.168 m³ per tray. The trays were made of 12 mm plywood (the long sides) and 32 in the ends with a plastic net with a low pressure drop in the bottom.

Figure 2.12 shows the drying bed while figure 2.13 shows a close-up of the drying trays filled with maize



Figure 2.12. The drying bed.

2.2. Measuring equipment

The aim of the tests on the prototype unit of the solar crop dryer were to determine the drying capacity and the thermal performance of the solar crop dryer. For this reason a measuring system was installed in and around the dryer. Figure 2.14 shows the location and types of the applied sensors. Solar Energy Centre Denmark was responsible for the determination of the thermal performance of the system while the Department of Agricultural Engineering dealt with the drying capacity. The black sensors in figure 2.14 were installed by Solar Energy Centre Denmark while the red sensors were installed by Department of Agricultural Engineering.



Figure 2.13. The drying trays.

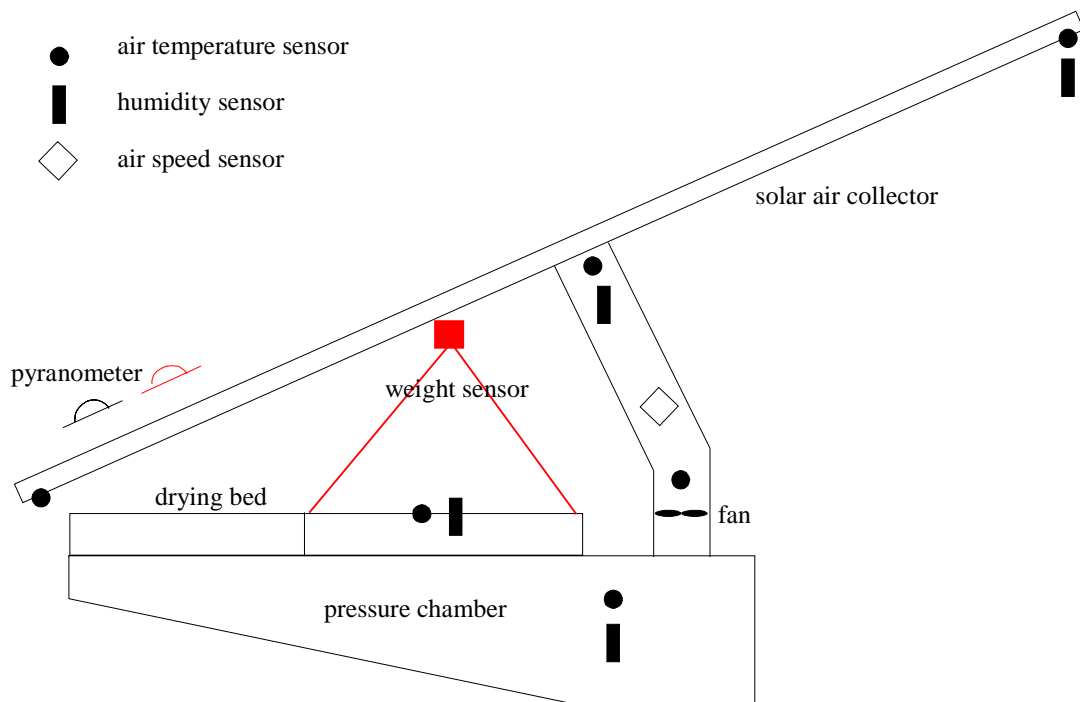


Figure 2.14. Location and type of the used sensors for the test of the solar crop dryer.

2.2.1. Sensors

Pyranometers

Both Solar Energy Centre Denmark and the Department of Agricultural Engineering had installed a pyranometer. The pyranometer from Solar Energy Centre Denmark was a calibrated pyranometer from Eppley type PSP – see figure 2.15, while the pyranometer from Department of Agricultural Engineering was a Campbell Pyranometer type SP1110. Both pyranometers were located at the same orientation and tilt as the solar collector.



Figure 2.15. The pyranometer from Solar Energy Centre Denmark. Compared to figure 2.2 the photo shows also another collector.

Temperature sensors

All temperature sensors were PT100 class A sensors. The locations of the sensors were as shown in figure 2.14.: On sensor (shielded from direct sunlight) at both inlets to the collector, on sensor (also shielded) in the outlet from the collector, one sensor before the fan, one sensor at the start of the pressure chamber and finally one sensor just above one of the drying trays.

Air humidity sensors

All air humidities were measured by calibrated DOL14 relative air humidity sensors from Skov: One sensor was located at the top inlet to the collector (see figure 2.16) and as such measuring the ambient humidity, one sensor after the collector, one sensor at the start of the pressure chamber and finally one sensor just above one of the drying trays. In order to decrease the influence of wind on the latter DOL14-sensor, an open plastic funnel was located above the DOL14-sensor and the air temperature sensor – see figure 2.17.

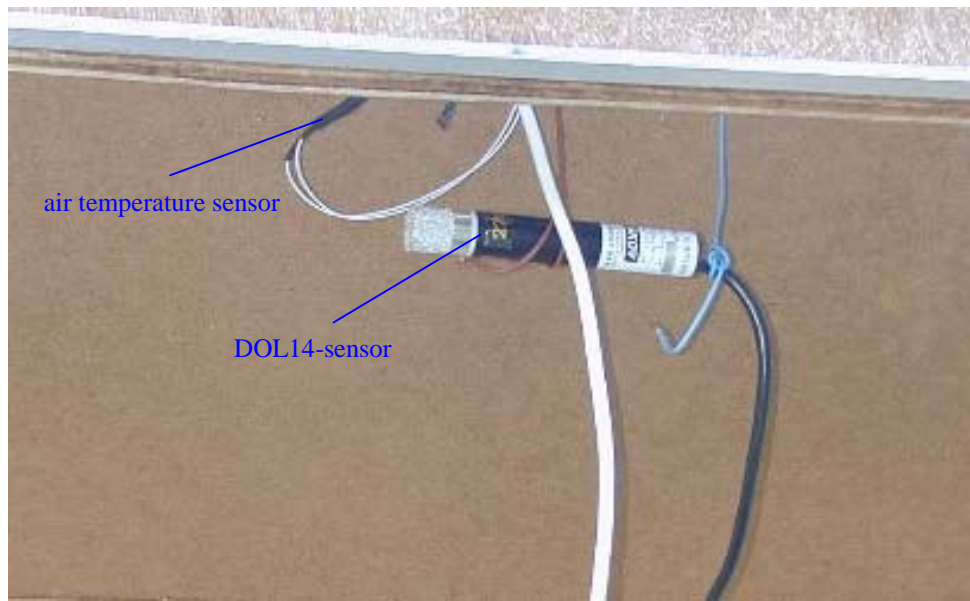


Figure 2.16. The air temperature sensor and DOL14-sensor at the top inlet to the collector.

Weight sensor

The weight sensor was a calibrated Bofors force transducer type KRG-4-TO. Figure 2.17 shows the weight sensor, which continuously measured the weight of one of the drying trays. The weight of all drying trays including maize were measured before and after the test in order to determine any difference in drying conditions across the drying bed.

Air speed sensor

The air speed in the squared duct was measured using a calibrated air speed sensor from Envic type AFC-1D as shown in figure 2.18. The air speed together with the cross section of the duct gave the air flow rate in the system.

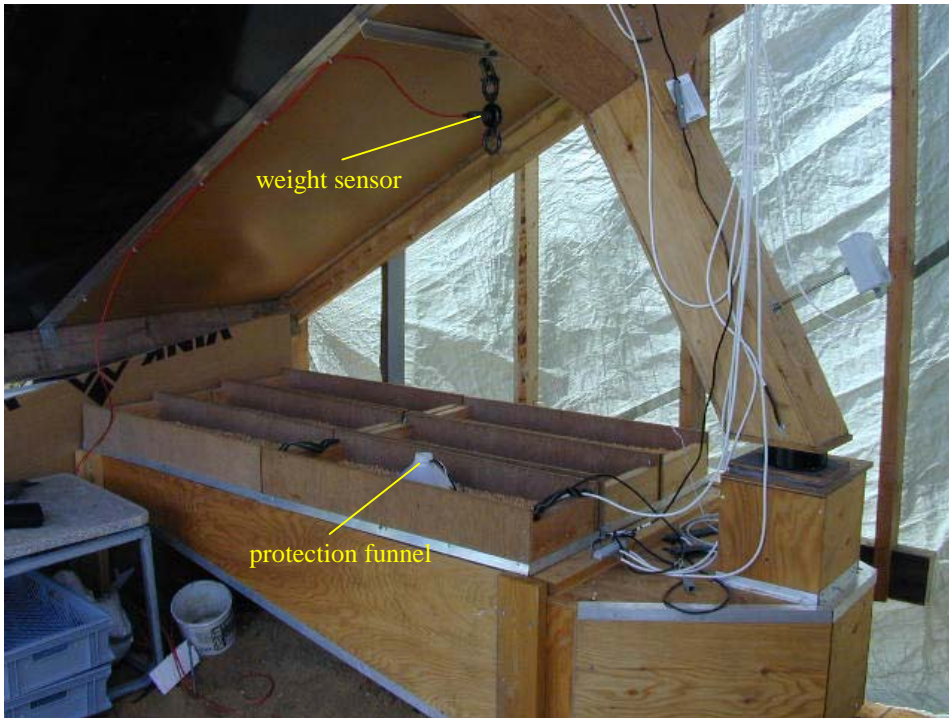


Figure 2.17. The weight sensor and the funnel protecting the air temperature sensor and the DOL14-sensor on top of one of the drying trays.



Figure 2.18. The air speed sensor.

Pressure transmitter

The pressure drop of the system is of vital importance for the operation of the system. The pressure drop over different parts of the system was measured by the Department of Agricultural Engineering using a calibrated micro manometer from ALNOR type 3KDS.

2.2.2. Data logging

The measured data from the equipment from the Solar Energy Centre Denmark were obtained using devices from Digital Devises. The data was scanned each 10th second and averaged in to 5 minutes values which were stored on the hard disk of the pc controlling the data logger.

The measured data from the equipment from the Department of Agricultural Engineering (except pressure drop) were obtained using a data logger from Campbell type CR10. The data was scanned each 10th second and averaged in to 10 minutes values. The values was stored in the data logger and by the end of the tests transmitted to a pc.

2.2.3. Processing of the data

The measured values were by the data loggers transformed into physical meaningful values like solar radiation, temperatures, humidity, air speed and weight. The data was afterwards transferred to Solar Energy Centre Denmark and the Department of Agricultural Engineering for further treatment.

2.3. Measuring results

The first test was initiated in the afternoon on May 17. Do to operation failure, however, measuring data from the data acquisition system of Solar Energy Centre Denmark are not available for the period May 18, 19:00 - May 19, 12:00. The measuring period ended at midnight May 22. The time is in the following graphs shown as day number – May 19 being 139 and May 22 144.

Figure 2.19 shows weather data for the period: Total solar radiation and ambient temperature - the latter is equal to the inlet temperature of air at the top of the collector. Figure 2.20 shows the measured solar radiation obtained from the pyranometer of the Department of Agricultural Engineering. Figure 2.19 and 2.20 show that the solar radiation was very scattered during the test period.

The ambient temperature was down to 4°C in the night and up to 18°C during the day. Figure 2.24 shows that the ambient humidity was from above 90% (the instrument cannot measure humidity higher than 90%) in the night and down to 35% as the lowest during the day.

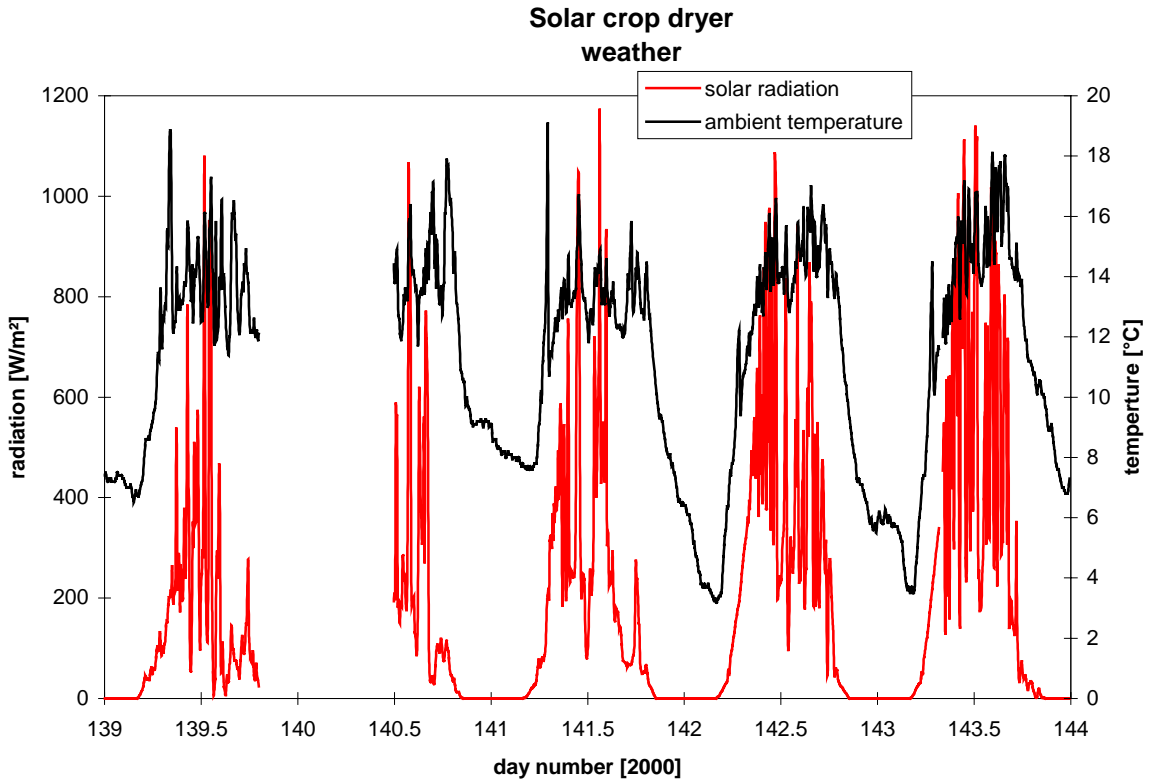


Figure 2.19. Solar radiation and ambient temperature during the test period.

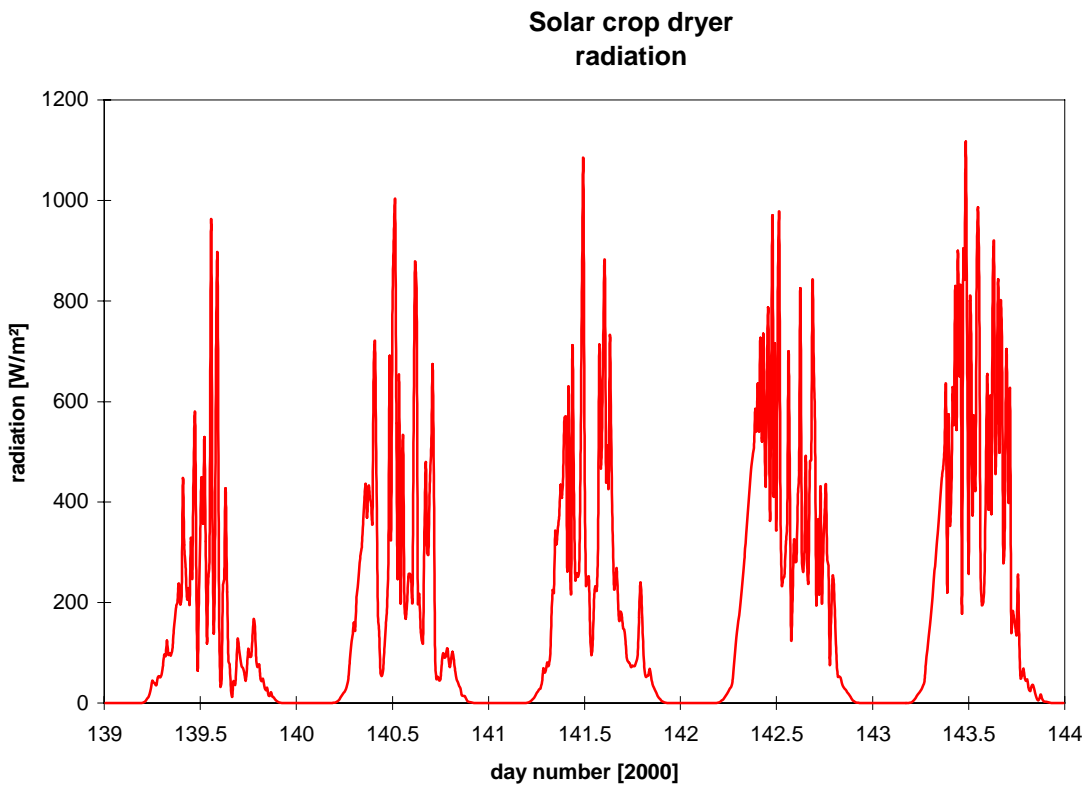


Figure 2.20. The solar radiation measured with the pyranometer of the Department of Agricultural Engineering.

Figure 2.21 shows the inlet and outlet temperatures of the collector, while figure 2.22 shows the air temperatures in the dryer: out of the collector, before the fan, under the drying bed and just above the drying bed. Figure 2.21 shows a slight difference in the two inlet temperatures to the collector. The inlet temperature at the bottom of the collector is during daytime higher than the inlet temperature at the top of the collector. This is because the bottom inlet is closer to the ground as shown in figure 2.1. The inlet temperature will, therefore, be affected by the heating of the ground in front of the dryer by the sun during the day.

Figure 2.23 is generated from figures 2.21 and 2.22 and shows the temperature differences in the system: the temperature increase over the collector, the temperature difference over the duct between the collector and the fan, the temperature difference over the fan + the first part of the pressure chamber and the temperature difference over the drying bed + the second part of the drying chamber. Figures 2.21 and 2.23 show a large temperature increase of the air when passing the collector – up to 30 K. The figure further shows a temperature drop over the ductworks and pressure chamber of up to 5 K. This is caused by the heat loss of the uninsulated ductworks and pressure chamber. In the important part of the dryer – the drying bed - is a temperature drop of up to 20 K seen. This temperature drop is partly caused by the thermal capacity of the maize but more important by the evaporation of water from the maize.

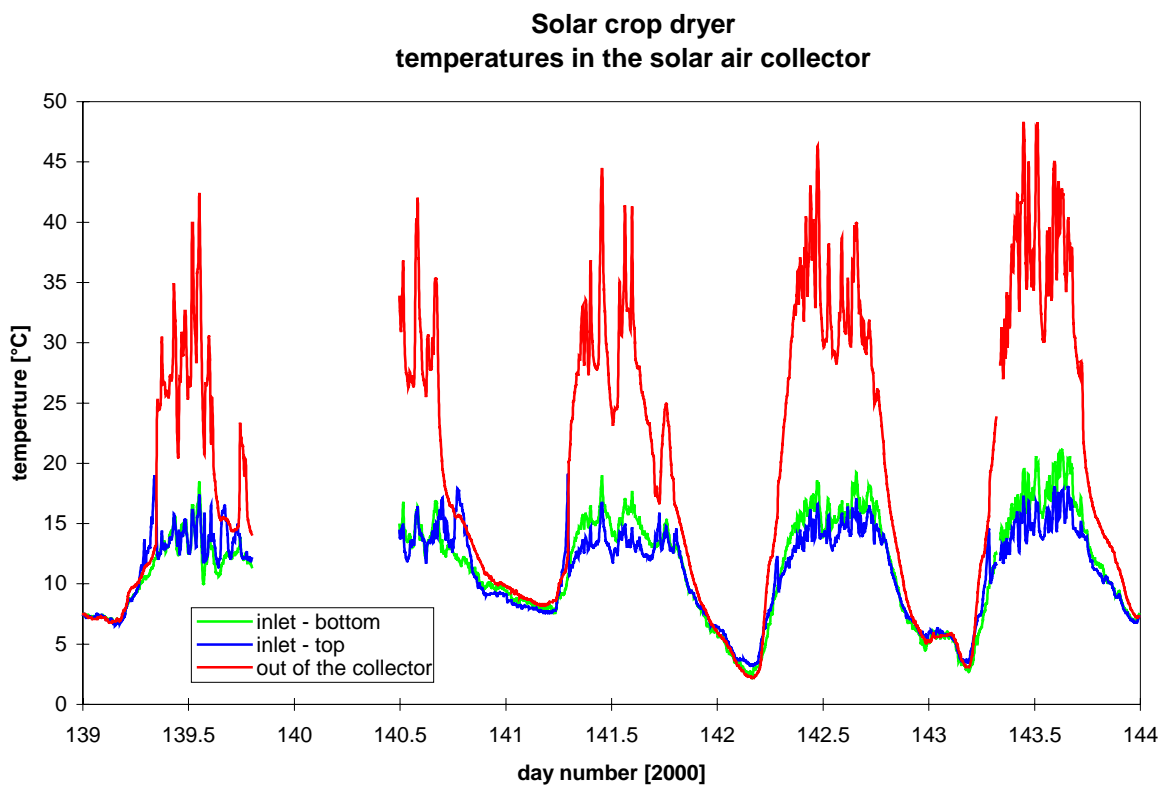


Figure 2.21. Inlet and outlet temperature of the solar collector.

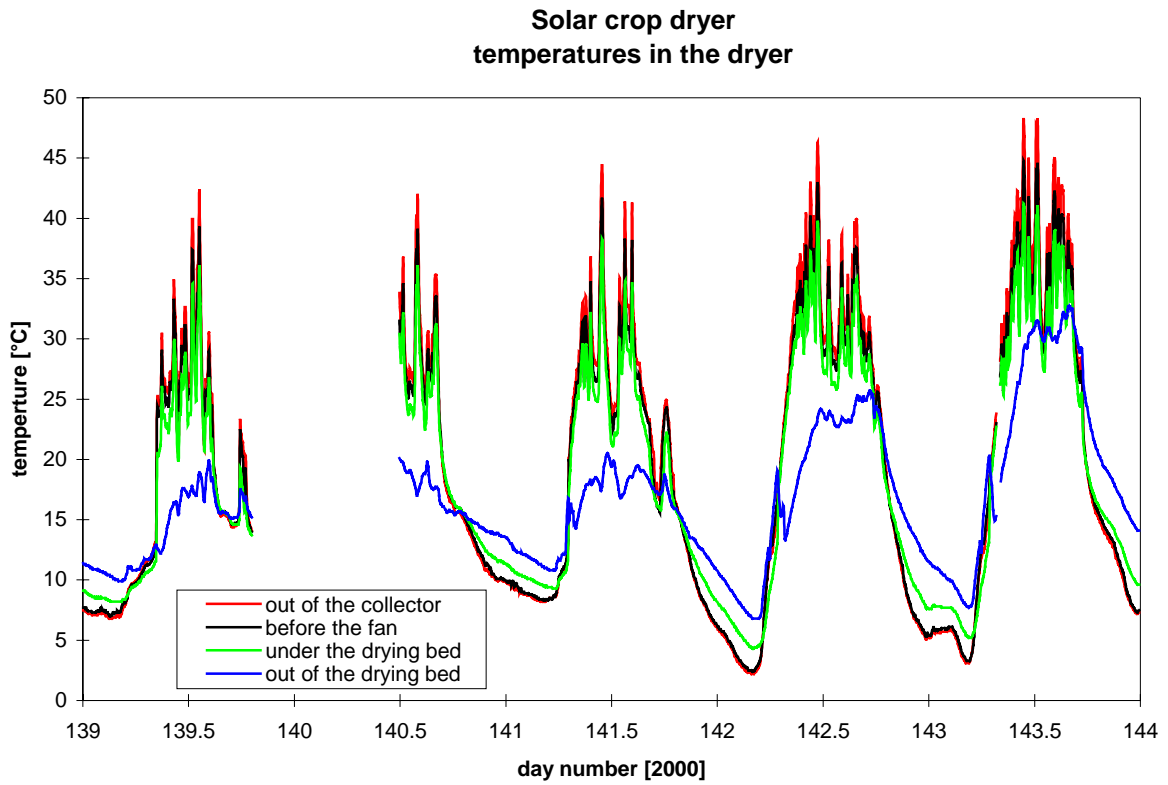


Figure 2.22. Temperatures in the system.

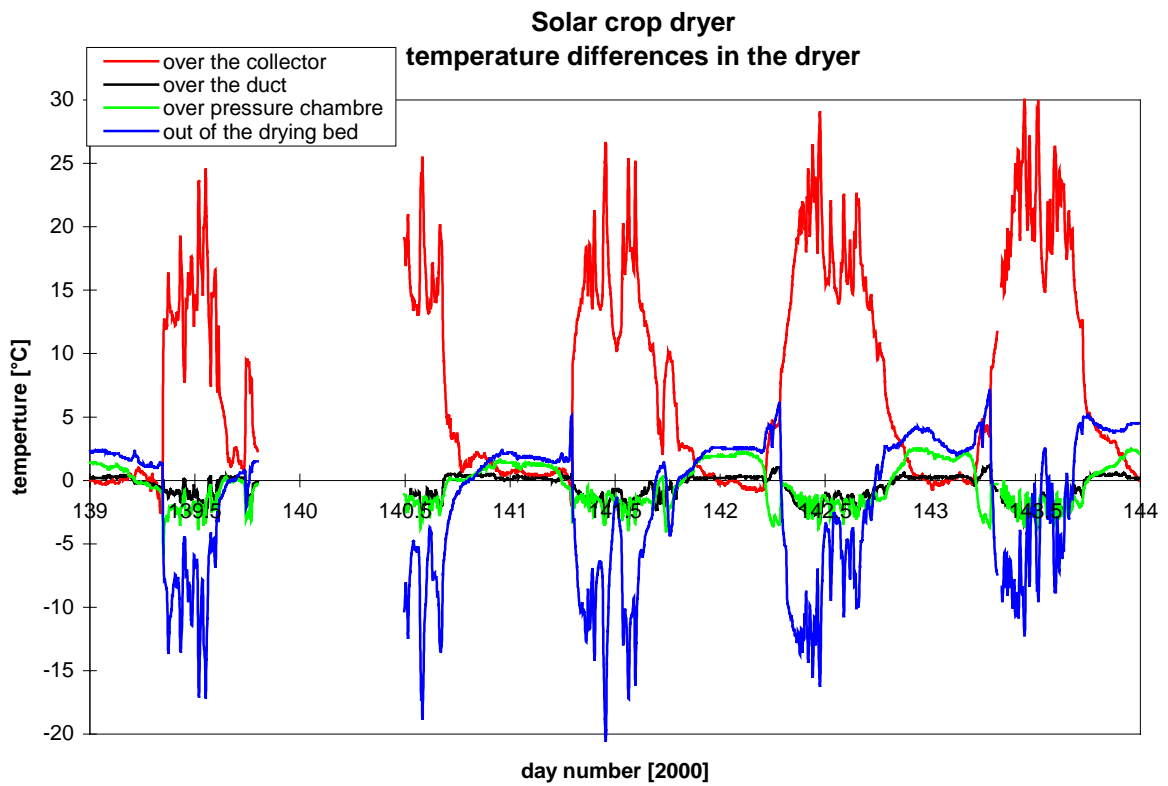


Figure 2.23. Temperature differences in the system.

Figure 2.24 shows the relative humidity in the dryer: in the top inlet (= ambient humidity), after the collector, under the drying bed and just above the drying bed. There is during solar radiation a major reduction in the humidity content of the air in the pressure chamber compared to ambient – a reduction of up to 35% point. The low humidity in the pressure chamber hardly affects the humidity of the air leaving the drying bed during the first two days. However, as the maize gets dryer and the evaporation of water from the maize decreases the humidity of the air leaving the drying bed falls to a value close to the humidity in the pressure chamber indicating that the drying process is completed. This is illustrated when comparing figure 2.24 with figure 2.25 showing the weight of a drying tray with maize.

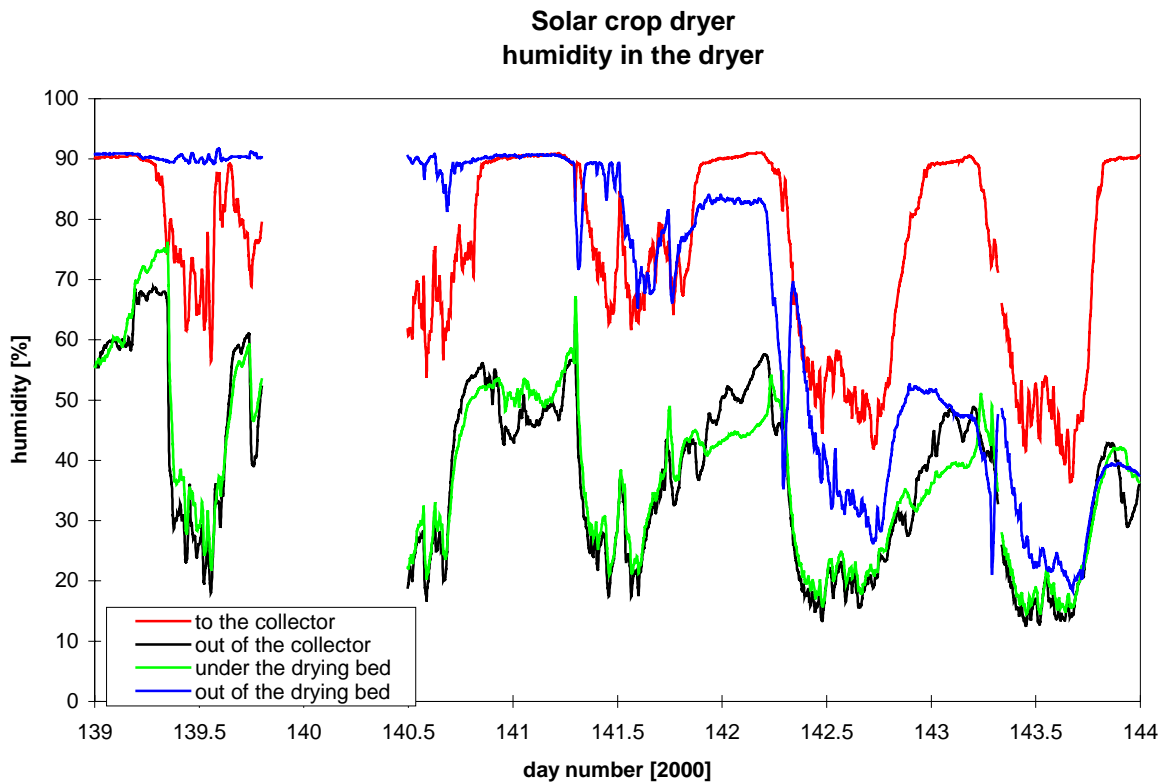


Figure 2.24. The humidity of the air to and in the dryer.

Figure 2.25 shows the measured weight of one of the drying trays with maize. The curve shows a strange phenomenon: the weight increases by approx. a pound in the morning. This is explained by a temperature dependency of the weight sensor. The sensor is black and the sun was able to hit the sensor in the morning and heat it up. Control measurements by hand do not show this increase in the weight in the morning. During the succeeding tests the temperature of the sensor was measured continuously and the weight output were corrected for the temperature according to the data sheet for the sensor. No increase of importance in the weight in the morning was hereafter seen.

The weight of the tray started at 24.3 kg (of which the maize was 20 kg) and ended at 21.3 kg. The moisture content was at the start of the test 22% and ended at 10.2%, which is the need at Silkwood Farms. Figure 2.26 shows the end moisture content of the maize in the 6 trays – the start moisture content was identical for all the trays. The standard deviation is 0.68.

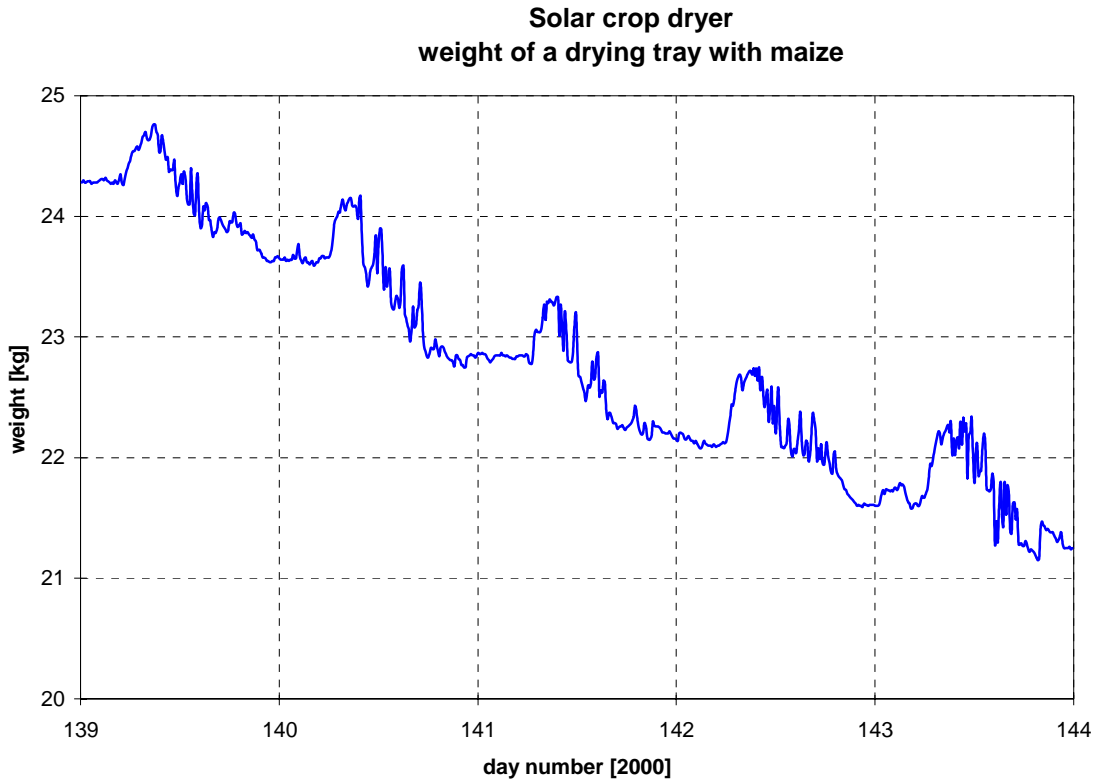


Figure 2.25. The weight of one of the drying trays during the test.

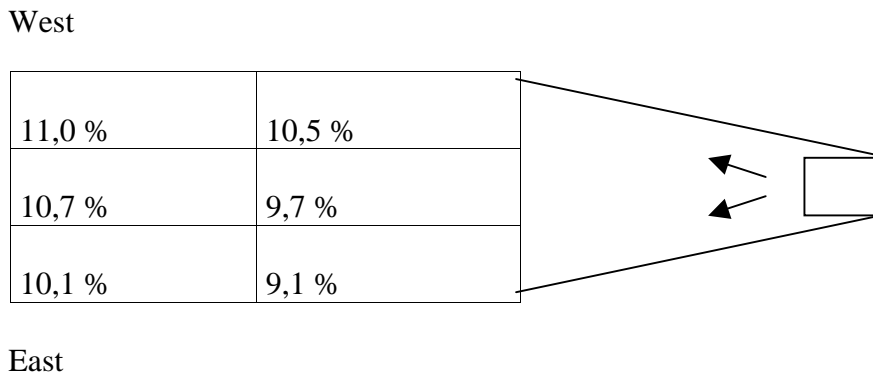


Figure 2.26. The moisture content of the maize in the 6 drying trays at the end of the test.

Figure 2.26 shows that the drying process was somewhat uneven – i.e. a difference of nearly 2% point between the tray with the highest and lowest water content.

Figure 2.27 shows the air flow rate in the system, while figure 2.28 shows the power transferred to the air in the solar air collector. Figure 2.27 shows that the design flow rate of 300 m³/h is only reached at very high radiation levels. The collector supplies the air with up to 2,500 W at high radiation levels.

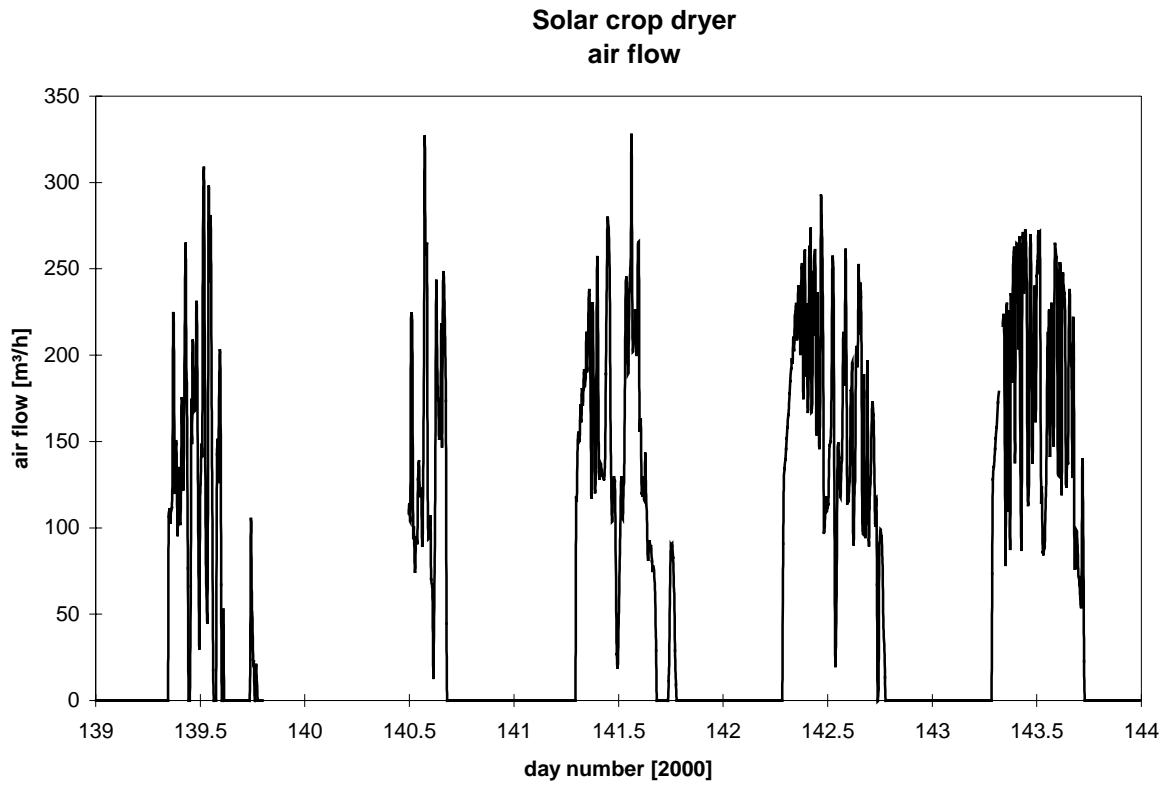


Figure 2.27. Air flow in the system.

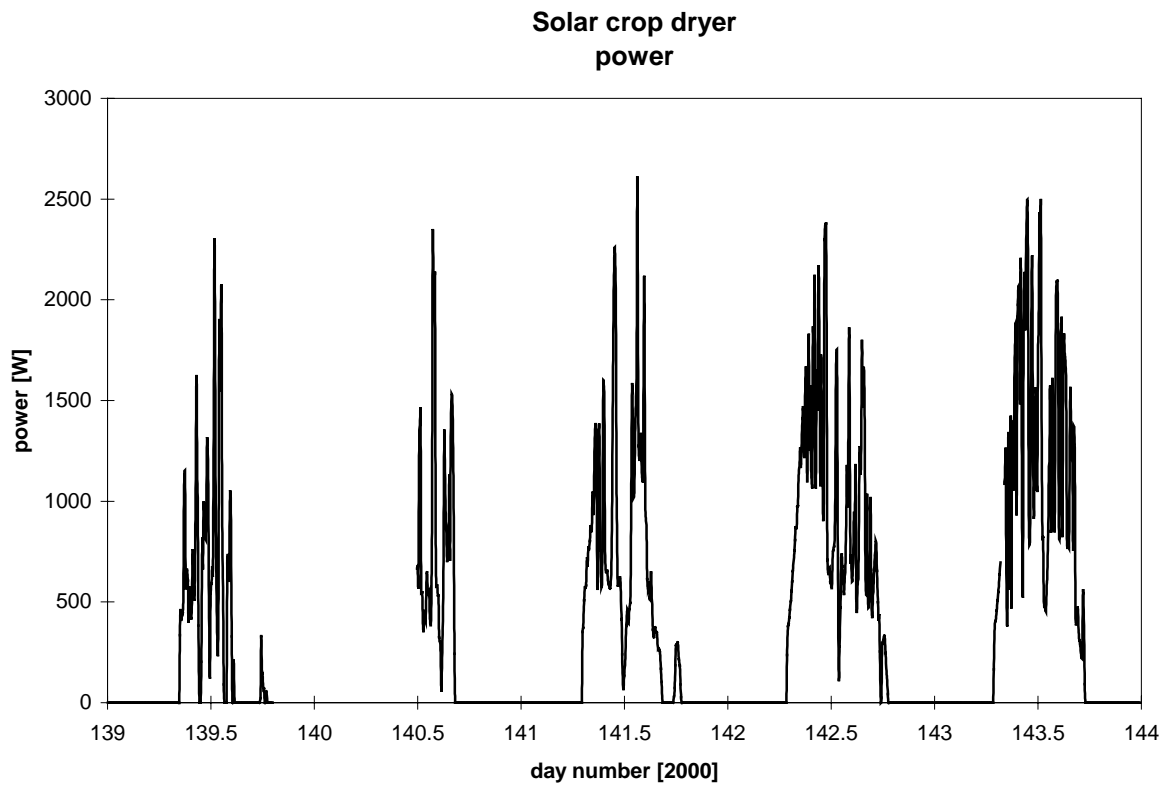


Figure 2.28. Power transferred to the air in the collector.

2.3.1. Drying capacity

The need at Silkwood Farms is to dry the maize down from a water content of 22% to 10%. A theoretical calculation has been carried out on the following conditions: ambient relative humidity: 70%, air speed through the drying bed: 0.06 m/s and temperature of the air to the drying bed: 45°C. Under these conditions the duration of the drying process is calculated to be 30 hours, where the drying from 22 to 12% takes 15 hours and from 12 to 10% also takes 15 hours. The last 2% point water is thus the hardest to dry out.

It took 5 days to dry the maize down from a water content of 22% to 10%. This is longer than the above 30 hours. However, before making any firm statements about the drying capacity it is necessary to compare the weather conditions during the test with the weather conditions in Ghana during the three periods where the drying of maize occurs – August, September and January with August/September being the main period. Weather data for Accra is shown in appendix C.

The irradiation during the five days of the test is shown in table 2.1. The measured irradiation from both pyranometers is shown in the table.

Day	Solar Energy Centre Denmark W/m ² /day	Department of Agri- cultural Engineering W/m ² /day
May 18	-	2690
May 19	-	4050
May 20	3840	3940
May 21	5060	5330
May 22	5470	5790

Table 2.1. Measured irradiation during the test period. Values for May 18-19 are partly missing for the pyranometer of Solar Energy Centre Denmark and are, therefore, not shown. There is a difference of the values between the two pyranometers of 6% which is acceptable.

From appendix C the daily mean irradiation for Accra is found to:

Month	Accra W/m ² /day
January	4300
August	4100
September	4900

Table 2.2. Monthly mean daily radiation in Accra.

The two tables show that the irradiation during the test period for most of the days was only a little less or higher than the mean irradiation in Accra.

The humidity level of the ambient air was during the first three days similar to the conditions in Accra where 60-70% may be expected during daytime. However, during the last two days of the test the humidity level dropped to 40-60%.

Based on this it must be stated that the duration of the drying process is too long. It should preferably only be 2-3 days during mean weather conditions.

The longer drying time than expected is due to the low air flow rate and not due to a poor collector as may be seen in the next section. The temperature out of the collector may actually be too high during sunny conditions. In order to keep the germination capacity of the maize the air to the drying bed should only exceed 45° during short periods. Figure 2.29 shows that the temperature difference between the air to the drying bed and the ambient temperature may be 20 K for longer periods and 23 K for shorter periods.

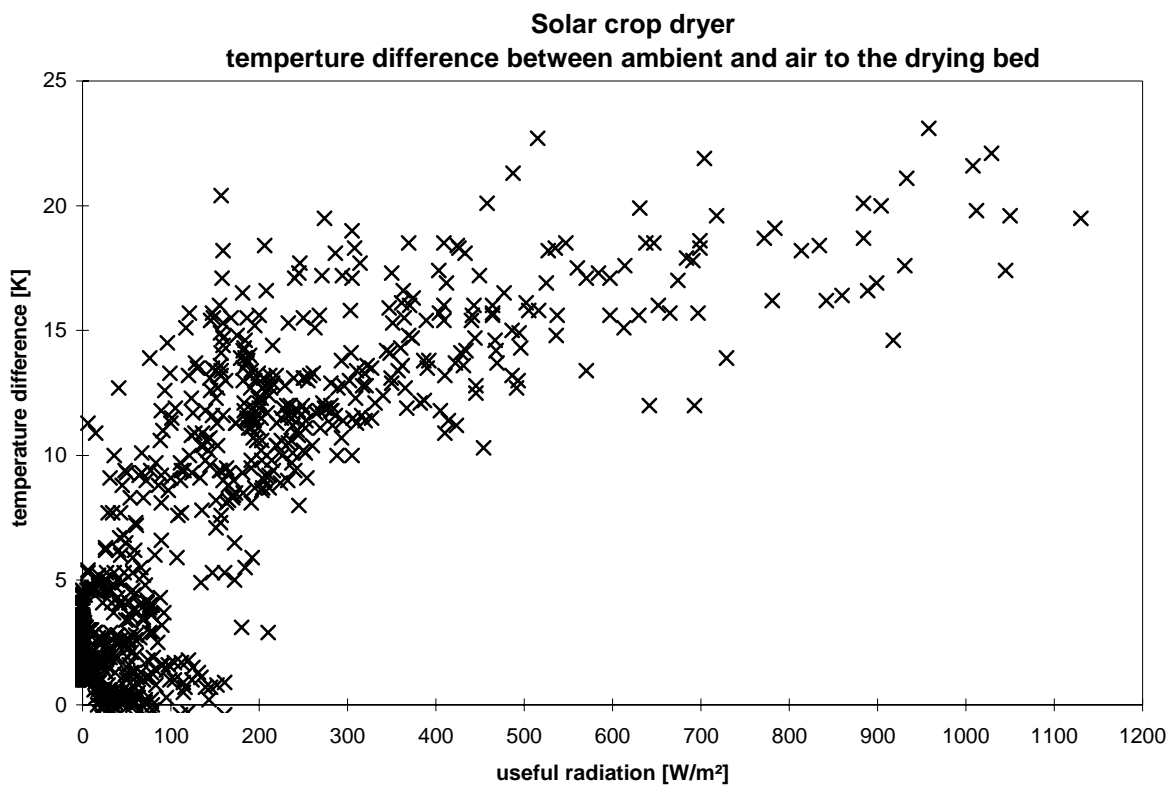


Figure 2.29. The difference between the air temperature to the drying bed and the ambient temperature dependent on the useful radiation.

The mean ambient temperature in Accra will during August/September be up to 27°C and in January up to 32°C. This means that the temperature of the air to the drying bed may go up to 50-55°C during short period and for longer periods between 47 and 52°C. This is close to what can be accepted but should be reduced in order to make sure that the germination capacity of the maize is not decreased.

This can be done by increasing the air flow through the system. The air speed through the system is lower than the design values of 300 m³/h as seen in the following section 2.3.3. If the air flow rate is increased the drying process will also speed up. How to achieve this is discussed in section 2.3.4.

2.3.2. Collector efficiency

Figure 2.30 shows the efficiency of the solar air collector calculated in two ways: the black curve is based on the total (measured) solar radiation, while the red curve is based on the useful radiation - i.e. corrected for the reflection in the cover of the solar air collector at incidence angles above 0° in such a way, that the efficiency may be compared with standard efficiency tests with an incidence angle of zero. The latter method of calculating the efficiency gives, therefore, the most correct picture of the efficiency of the collector. In order to correct for the reflections it is necessary to calculate the split between direct and diffuse radiation based on the measured total radiation. This was done using the equations in (Duffie and Beckman, 1991). The calculated split introduces an uncertainty compared to a case where both total and diffuse radiation are measured. The following equation has been applied to account for the reflection in the cover:

$$k = 1 - \tan^a(\theta/2)$$

where θ is the incidence angle for the radiation: the actual incidence angle for the direct radiation and 60° for the diffuse radiation. a is 3.2 for the cover of the collector and 3.7 for the PV-panel (Nielsen, 1995).

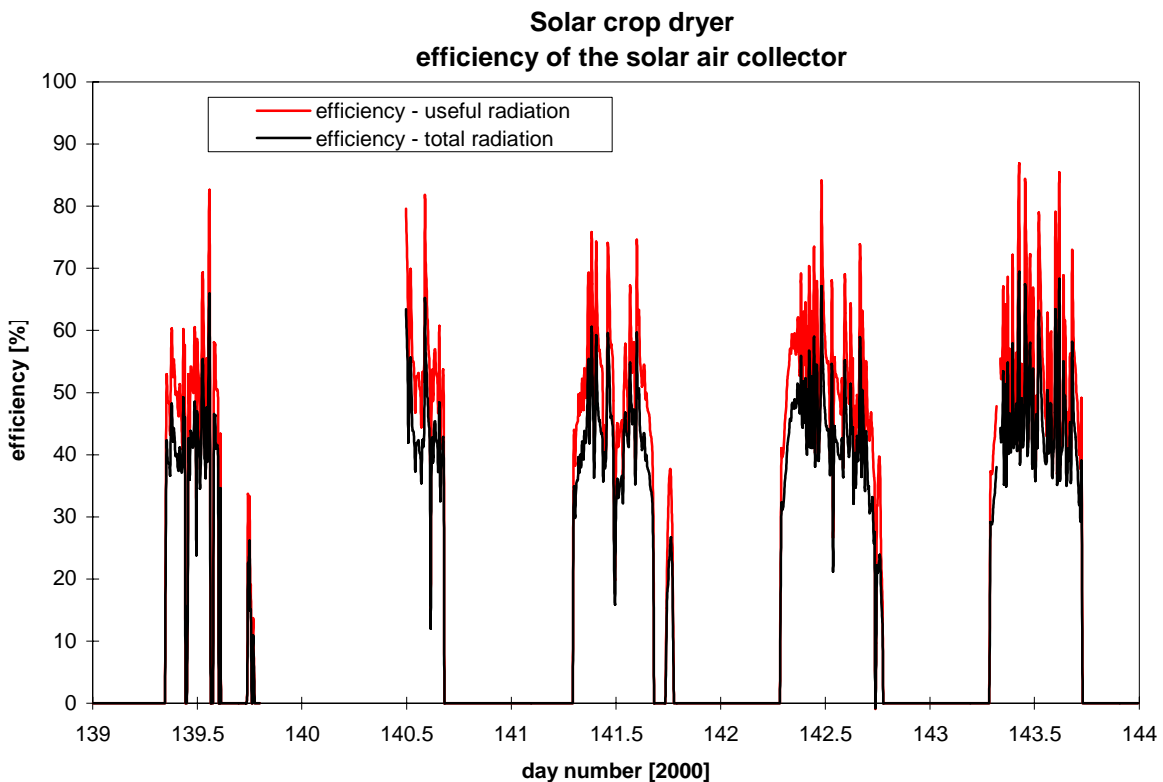


Figure 2.30. The efficiency of the collector calculated in the two above described ways.

Figure 2.31 shows the efficiencies dependent on the total air flow rate through the system. Figure 2.32 shows the efficiencies dependent on the air flow rate per m^2 collector area (normalized flow rate). In figure 2.32 is the efficiency of the solar air collector of the Summer House Package (Jensen, 1994 and Fechner, 1999) also shown. The green curve is the efficiency from IEA Task 19 (Fechner, 1999), while the blue curve is the efficiency from (Jensen, 1994). The collector of the Summer House Package is a small solar air collector utilizing the

same principle and cloth absorber as the collector in the dryer. The Summer House Package collector was in (Fechner, 1999) found to have the second highest efficiency of the 8 investigated commercial solar air collectors. The figure shows that the collector of the solar crop dryer is very efficient as the efficiency of the collector of the dryer most of the time is above the efficiency of the collector of the Summer House Package. However, the graph shows a strange bulge at low air flow rates and a drop at higher air flow rates which cannot be explained based on the present data.

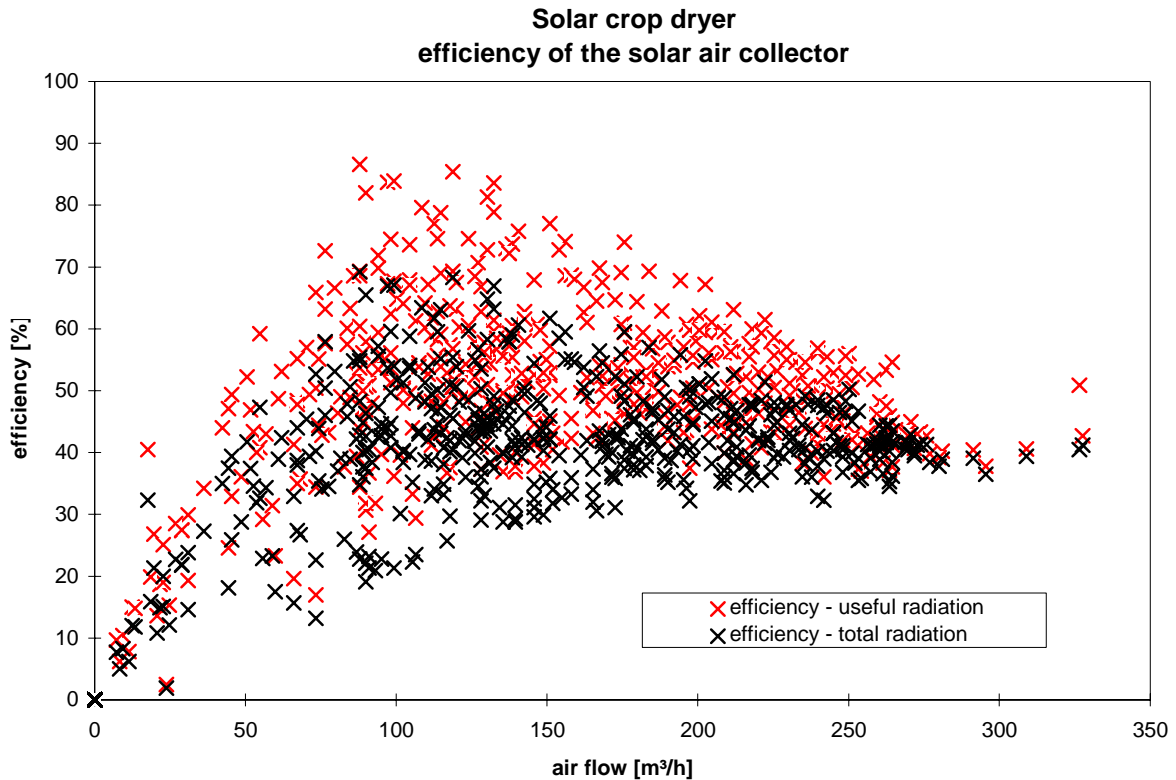


Figure 2.31. The efficiency of the collector dependent on the total flow rate trough the system.

Figures 2.33 and 2.34 show the two ways of calculating the efficiency (2.33 based on useful solar radiation, 2.34 on total radiation) dependent on the air flow rate and changes in the radiation level. Efficiencies with at black x are where the level of solar radiation has decreased compared to the former 5 minutes period. A red Δ indicate that the radiation level has increased, while a blue \square is for efficiencies where the radiation level within $\pm 3\%$ is identical to the radiation level of the former 5 minutes period. Figures 2.33 and 2.34 show that the scattering in the efficiency mainly is due to the heat capacity of the collector. The high efficiencies occur mainly during cooling down - i.e. during a decrease in radiation level, while the low efficiencies occur during warming up - i.e. during an increase in radiation level.

The impression from the first test is, that the efficiency of the collector is higher than the Summer House Package at low flow rates but lower at higher flow rates. Further measurements are necessary to in order to more precisely define the efficiency of the collector – especially measurements obtained during periods with clear sky conditions is important.

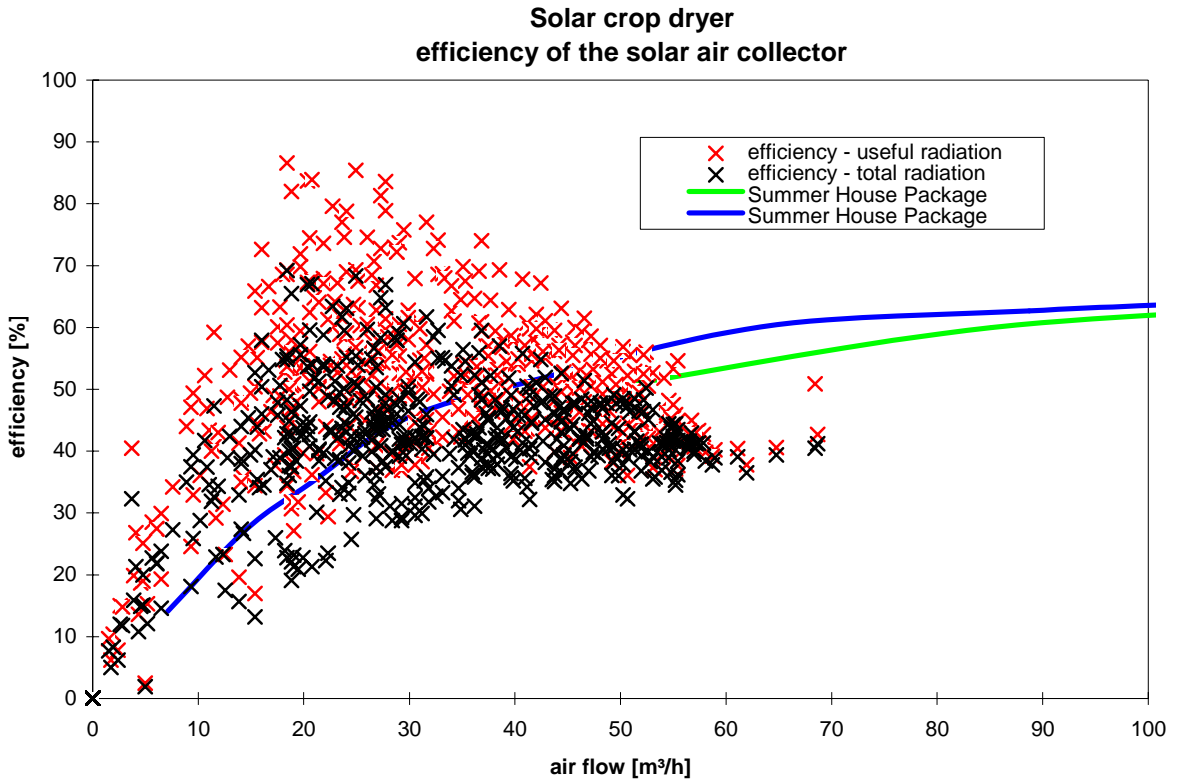


Figure 2.32. The efficiency of the collector dependent on the normalised flow rate through the collector together with the efficiency of the Summer House collector.

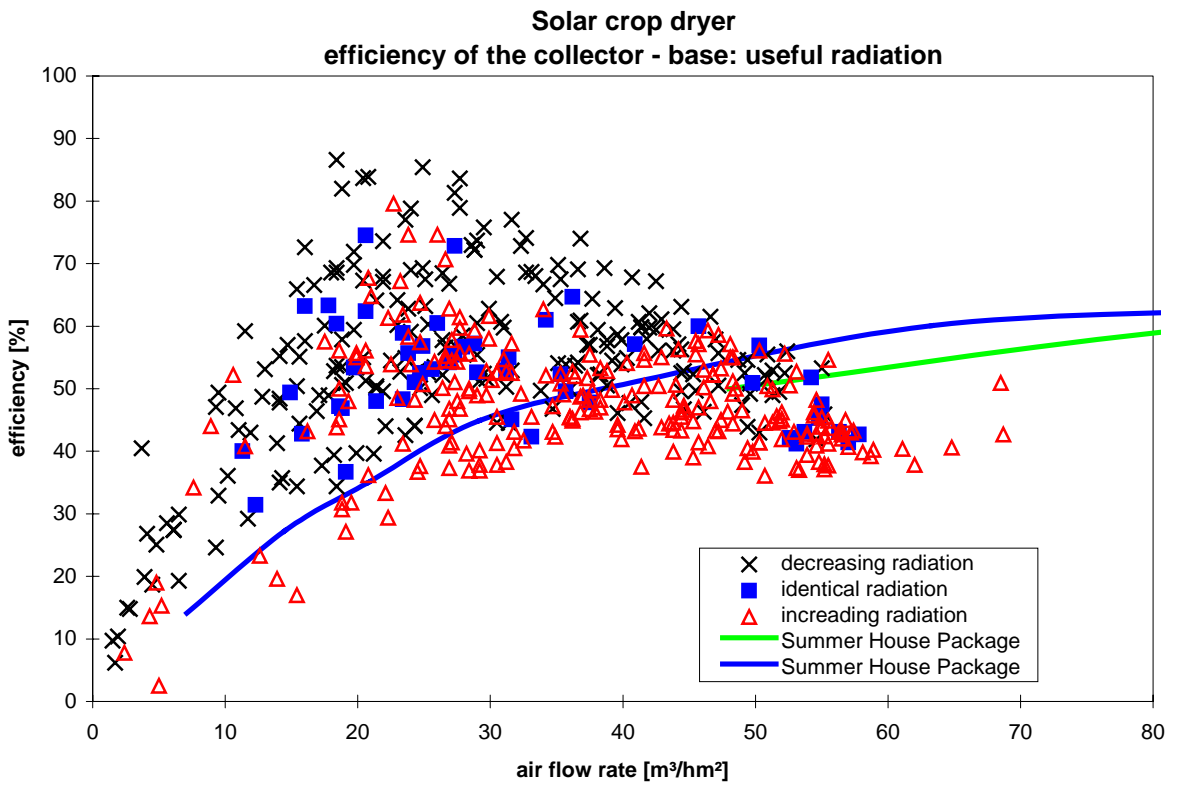


Figure 2.33. The efficiency of the collector dependent on the normalised flow rate through the collector and if changes in the radiation level has occurred.

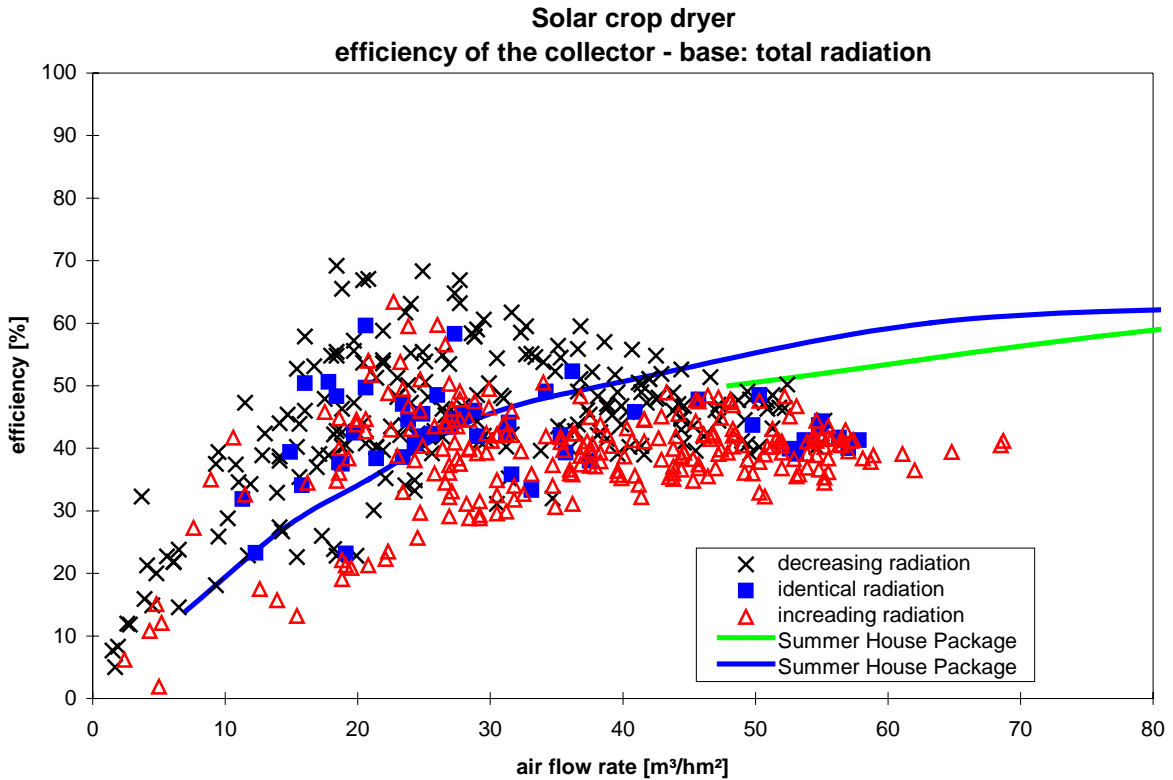


Figure 2.34. The efficiency of the collector dependent on the normalised flow rate through the collector and if changes in the radiation level has occurred.

2.3.3. Flow rate

Figures 2.35 and 2.36 show the total flow rate of air through the system dependent on the radiation level – figure 2.35 dependent on the level of the total radiation while figure 2.36 shows the same situation dependent on the usable radiation level on the PV-panel. The figures show that although the design flow rate of 300 m³/h is met at some point the general picture is, that the flow rate is too low – except for few peak values only up to 275 m³/h.

2.3.4. Pressure drop

The static pressure in different part of the system was measured in order to determine which parts mainly were responsible for the total pressure drop across the system. Figure 2.37 shows where the static pressures were measured. Based on the measured static pressures five pressure drops could be determined:

- lower half part of the collector = pressure drop across inlet + absorber
- upper half part of the collector = pressure drop across inlet + absorber
- collector = as above + the outlet of the collector
- collector + ductworks until fan = as for collector + the ductworks until the fan = the total pressure drop over the system
- drying bed = pressure drop across the drying trays including maize

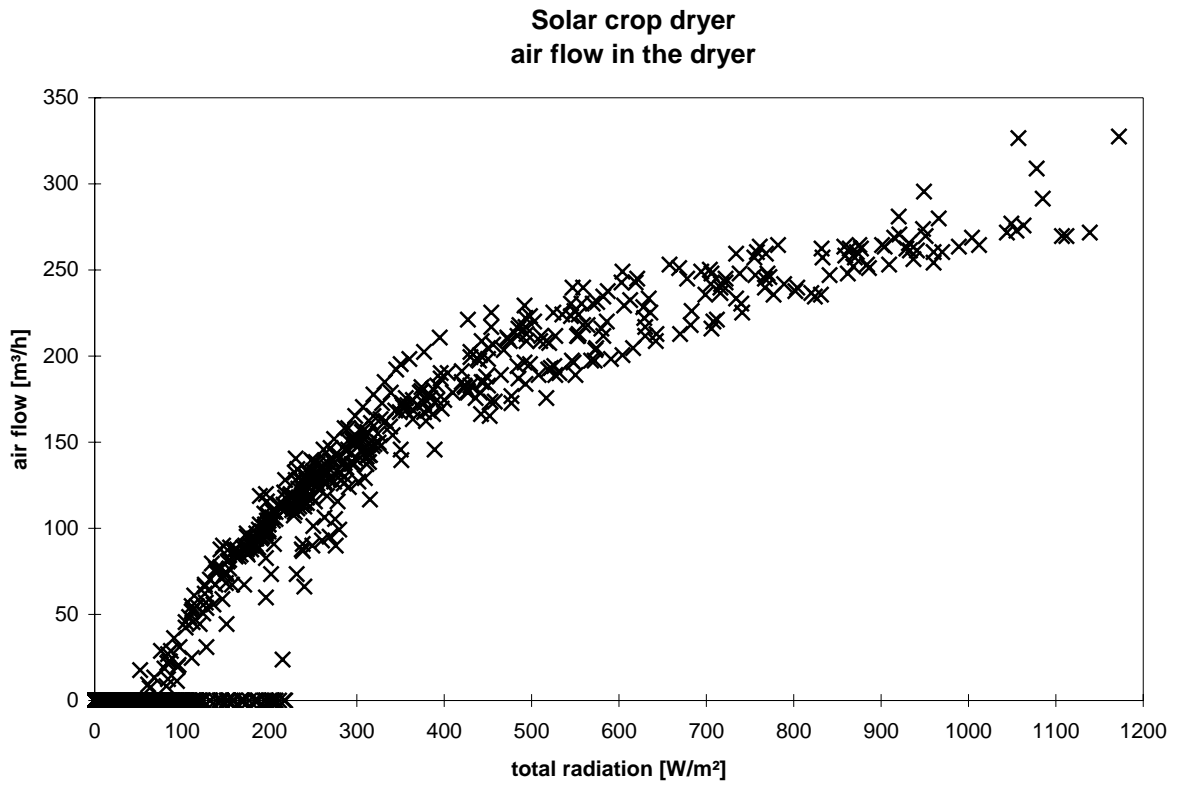


Figure 2.35. The air flow rate dependent on the total radiation.

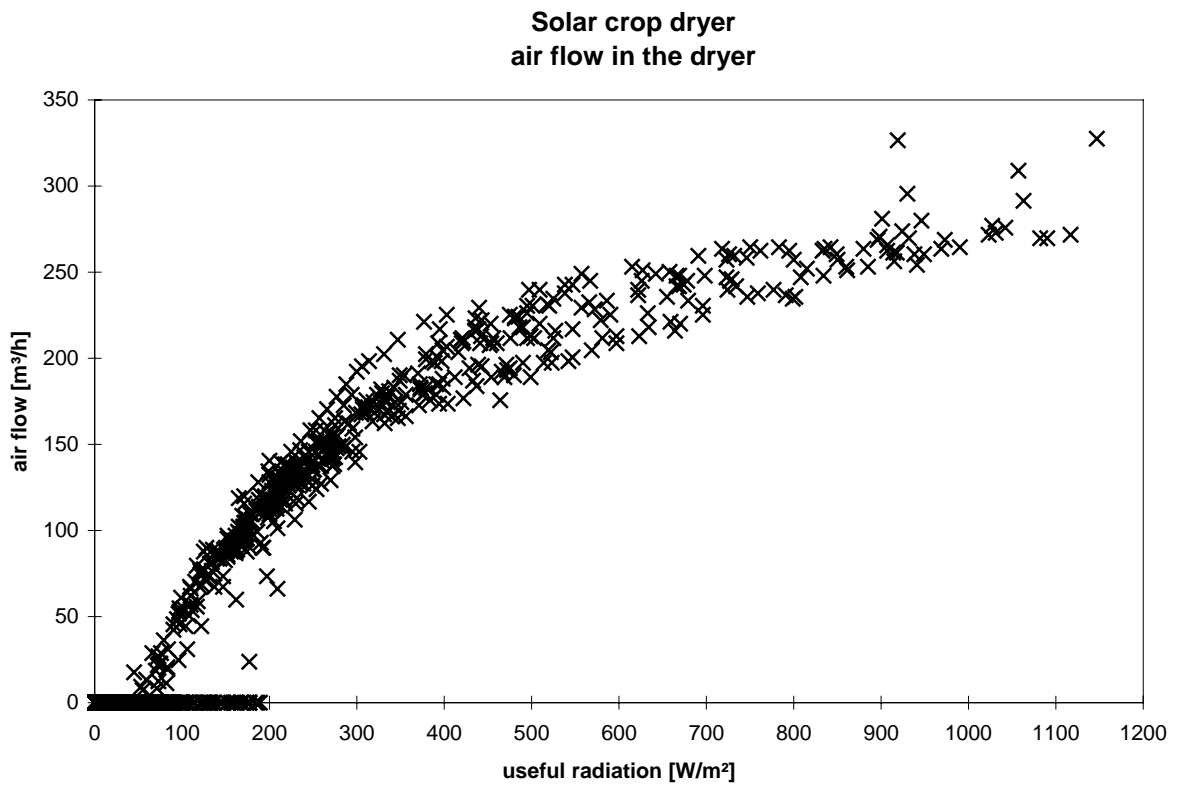


Figure 2.36. The air flow rate dependent on the useful radiation on the PV-panel.

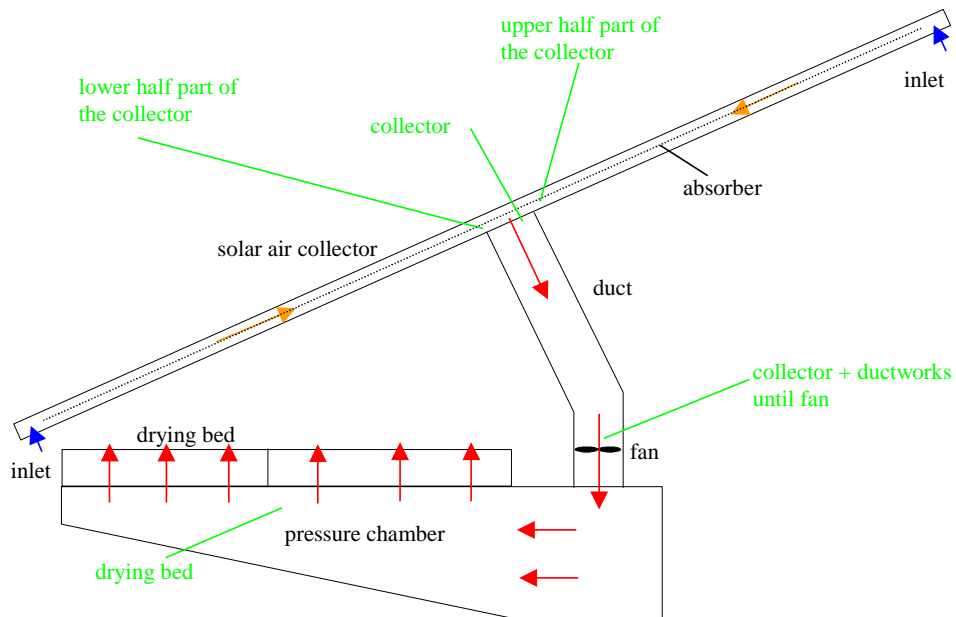


Figure 2.37. Illustration of where the static pressures were measured in the system.

Figure 2.38 shows the measured static pressures (equal to the above mentioned pressure drops) as a function of the flow rate in the system. The figure shows that the pressure drop of the system at flow rates above 300 m³/h exceeds the critical value of 50 Pa where the flow rate suddenly may drop to around 200 m³/h – see figure 2.8. The pressure drop of the system is thus too high. Main responsible for the high pressure drop is the outlet of the collector. There is also a high pressure drop across the inlet + absorber. As a certain pressure drop over the absorber is necessary to create an even air distribution the pressure drop over the absorber should, therefore, not be reduced. The pressure drop across the ductworks may also be lowered using more smooth connections. The pressure drop across the drying bed should, however, not be decreased as this may lead to an uneven distribution of the air flow across the drying bed.

A reduced overall pressure drop in the system will lead to a higher air flow rate through the system.

Solar crop dryer static pressure in the dryer

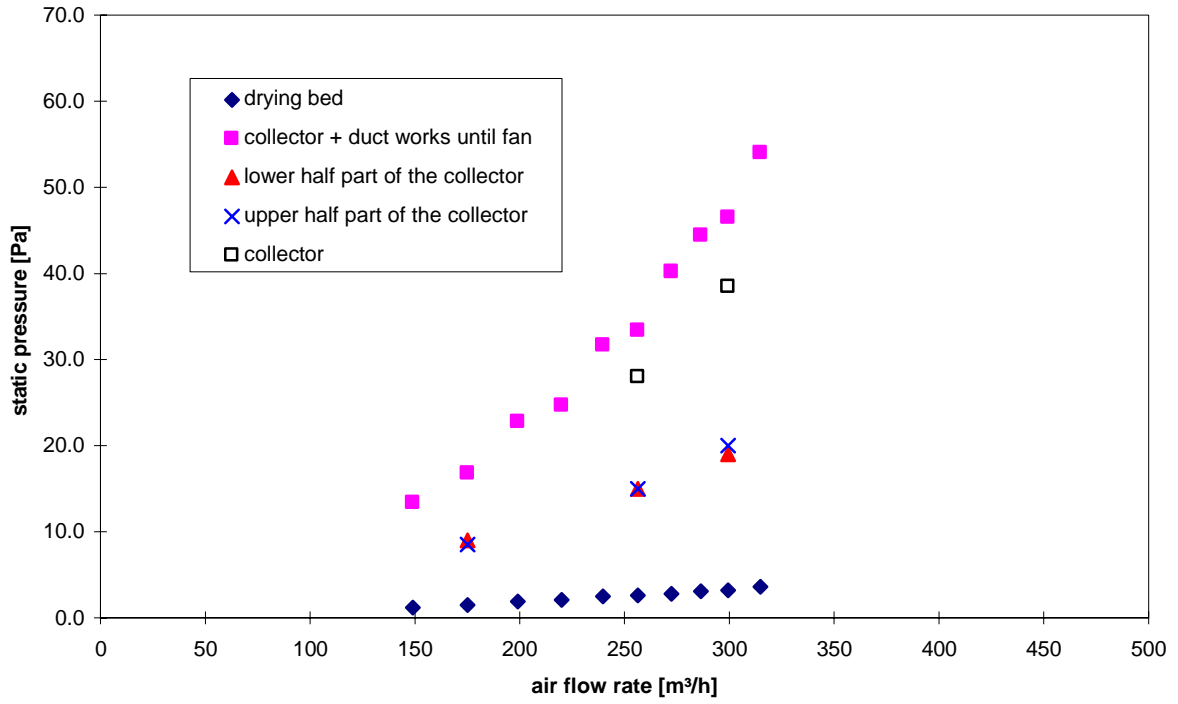


Figure 2.38. Measured static pressure/pressure drop in the dryer.

3. Modified design

Based on the test of the initial design the solar crop dryer was modified on several points: the collector, the ductworks and the drying bed.

3.2. Collector

A new collector was build, where the inlet to the collector was changed from being at the back to being at the end. This will reduce the pressure drop as the air no more has to change direction. A section of the new inlet is shown in figure 3.1. The new location of the inlet further has the benefit that the air to the collector will flow behind the PV-panels and thereby cool these. This is necessary as it was realized that the temperature of PV-panels in Ghana often gets so high that the production of electricity is decreased considerably if the panels are not cooled actively.

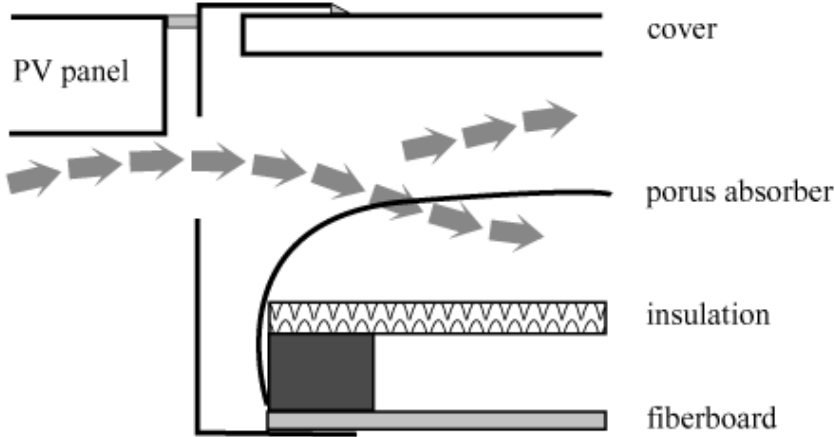


Figure 3.1. Section of the inlet of the modified collector.

The thickness of the insulation was decreased from 33 mm to 10 mm and the fibre board on top of the insulation (see figure 2.5) was also removed in order to increase air gap on each side of the absorber to 27 mm. This will decrease the pressure drop.

Finally the outlet from the collector was modified as shown in figure 3.2 as the largest pressure drop was located here.

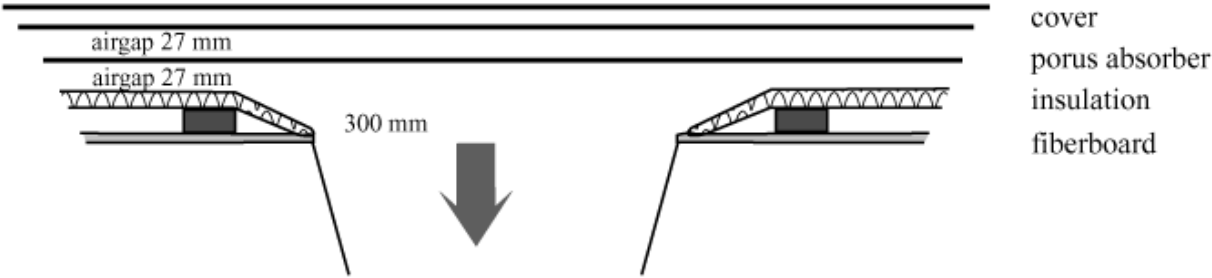


Figure 3.2. Section of the outlet of the modified collector.

3.2. Ductworks

The ductworks of the system was changed from being only made of plywood (see figure 2.11) to mainly being made of metal. The squared duct on each side of the fan was changed to circular ducts with a cross section 5% larger than the squared duct. The sudden changes in cross section areas of the original ductworks were changed to more smooth connections on each side of the fan. This will reduce the turbulence in the air and thus reduce the pressure losses and, therefore, lead to an increased air flow rate. Figure 3.3 shows the modified ductworks. The air temperature sensor originally located just before the fan was moved to right after the fan.



Figure 3.3. The modified ductworks.

3.3. Drying bed

The drying trays were changed from being made of plywood to being made of plastic - polypropylen. The reason for this was that it is easier to clean plastic than plywood and that the stability and strength of the plastic net seams to be sufficient.

The number of trays was not changed. The outer dimension of the plastic boxes were (length, width and depth) 600 x 400 x 278 mm³, while the internal dimension were 558 x 358 x 262 mm³ leading to a drying area of 1.2 m². Figure 3.4 shows the plastic boxes



Figure 3.4. The new drying trays made of plastic.

3.4. Pressure drop

The pressure drops in the system were again measured at the same locations as shown in figure 3.1 – except for the pressure drop over the lower part of the collector as this is identical to the pressure drop over the upper part of the collector. Figure 3.5 shows the measured pressure drops.

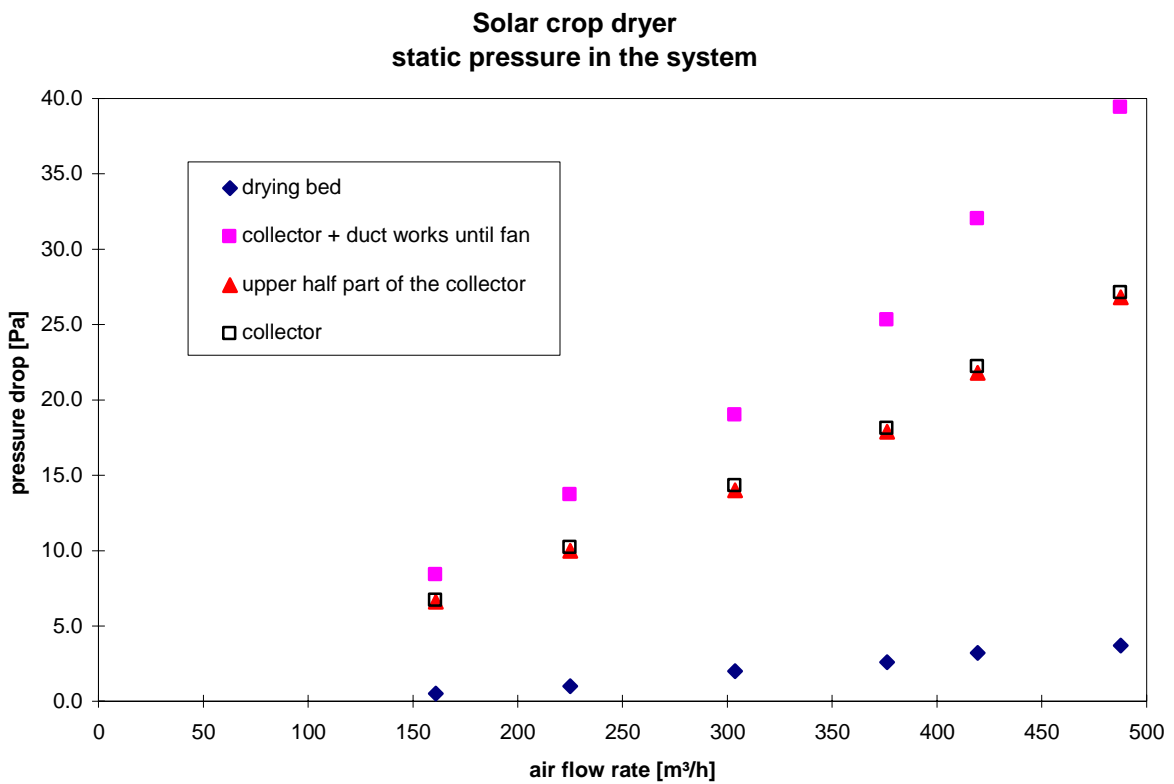


Figure 3.5. Measured static pressure/pressure drop in the modified dryer.

When comparing figure 3.5 with figure 2.38 it is seen that the total pressure drop (collector + ductworks until fan) at the design flow rate of 300 m³/h has been decreased by more than 50%. The total pressure drop over the collector is now only half of the initial design, which is caused by the new design of the outlet – the pressure drop over the upper half for the collector is unchanged while the pressure drop over the outlet is almost eliminated. The pressure drop over the ductworks from the collector to the fan has been reduced to one third.

Figure 3.6 shows the air flow rate through the initial design and the modified design dependent on the power to the fan. The figure further shows the increase in air flow rate due to decrease in pressure drop across the dryer. The increase in flow rate is highest for high air flow rates – up to 60% while lower at low air flow rates – down to 30%. The decrease in pressure drop has thus led to a high increase in the air flow.

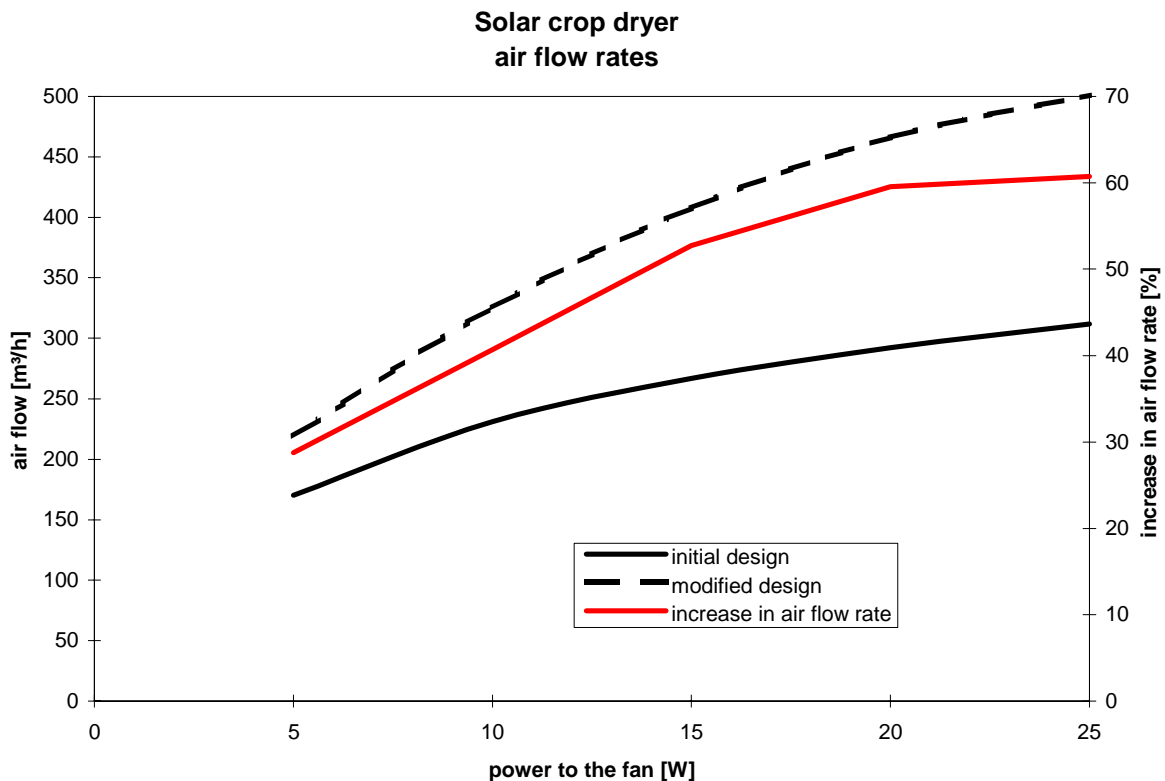


Figure 3.6. Air flow rated in the initial and modified design of the dryer.

3.5. Measuring results

The following graphs show the measurements from June 15 until June 18 (both days inclusive) – day number 167-170.

Figure 3.7 shows the weather conditions during the test. Although still scattered the daily radiation was higher than during the first test as seen when comparing the below table 3.1 with table 2.1. The ambient temperature was also during daytime higher than during the first test – up to 25 °C. The humidity level (figure 3.11) was due to the higher temperatures lower in the second test period.

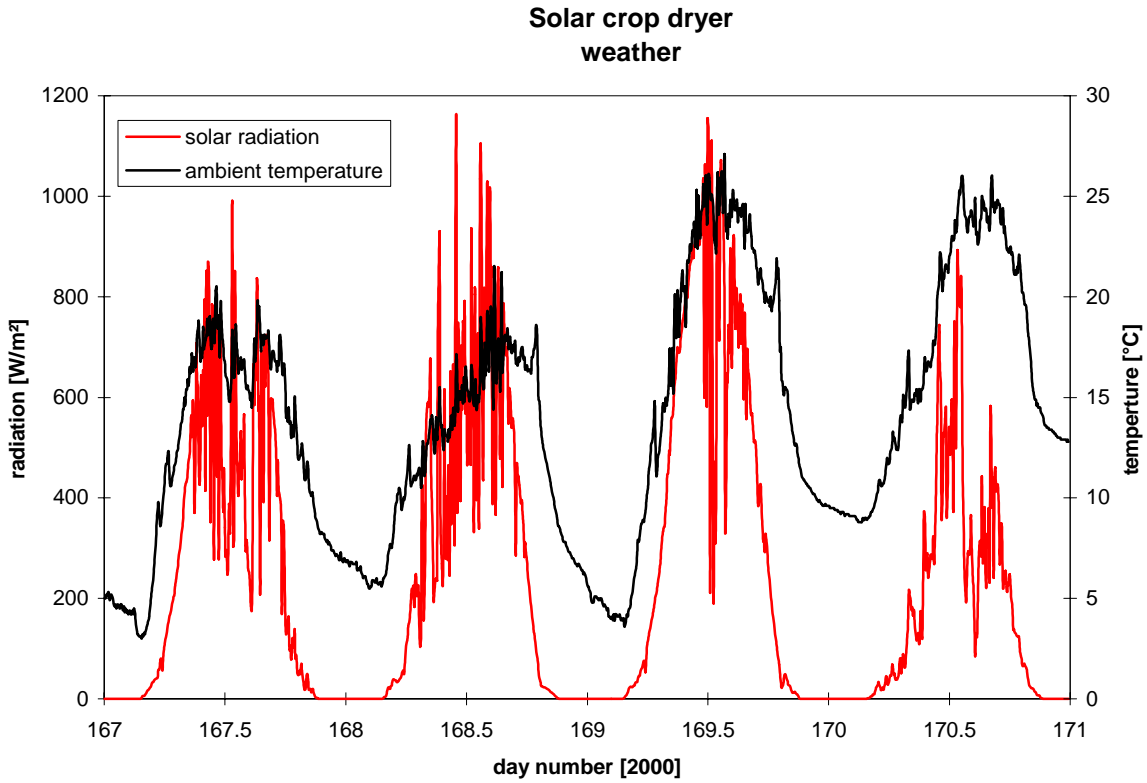


Figure 3.7. Solar radiation and ambient temperature during the second test.

Day	Daily irradiation W/m ²
June 15	5790
June 16	6360
June 17	7750
June 18	3980

Table 3.1. Measured irradiation during the second test period.

Figures 3.8-10 show the temperature and temperature differences in the system, while figure 3.11 shows the humidity level to and in the dryer.

Although a higher ambient temperature the outlet temperature of the collector is similar to the outlet temperature of the initial collector as seen when comparing with figure 2.21. The temperature increase over the collector reached in the first test 30 K while in the second test this temperature difference only reaches 25 K (figures 2.23 and 3.10). This indicates that the air flow in the system has been increased.

Figure 3.11 shows that the humidity of the air to the drying bed is similar to the first test – see also figure 2.24 – although the ambient humidity was lower during the second test. This is due to the lower increase in the temperature across the collector.

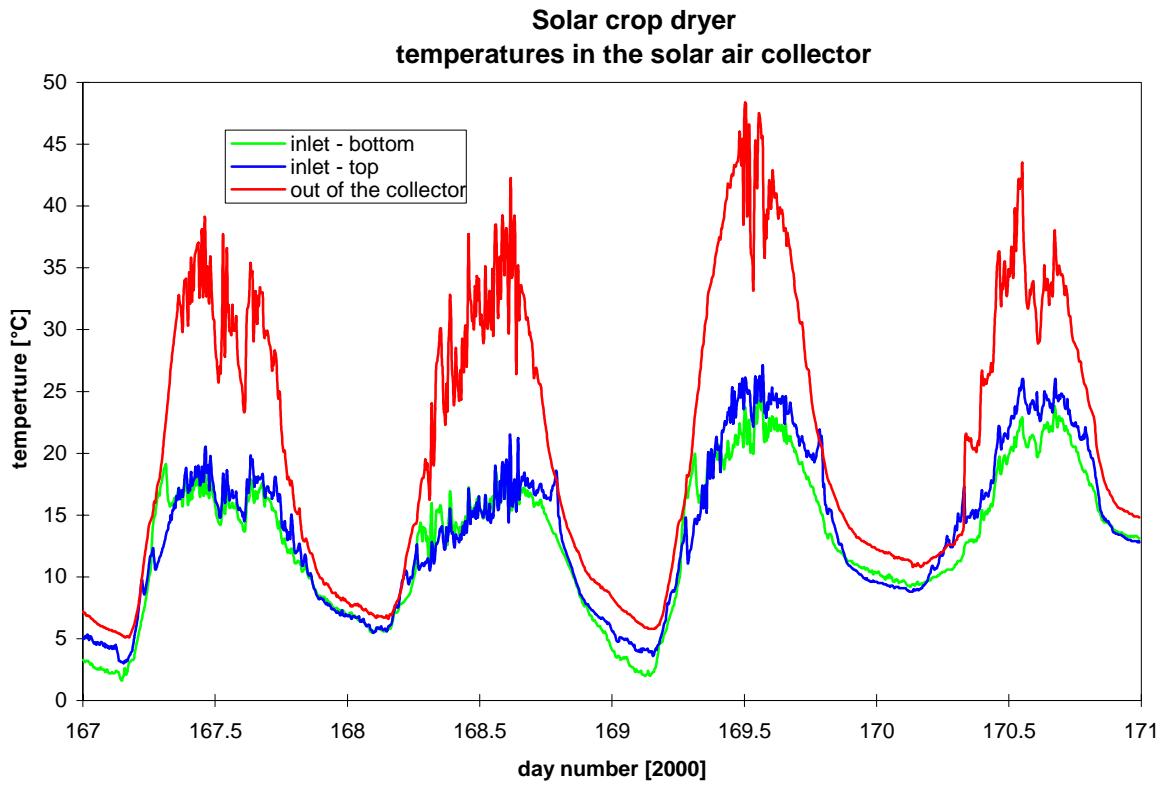


Figure 3.8. Inlet and outlet temperature of the solar air collector

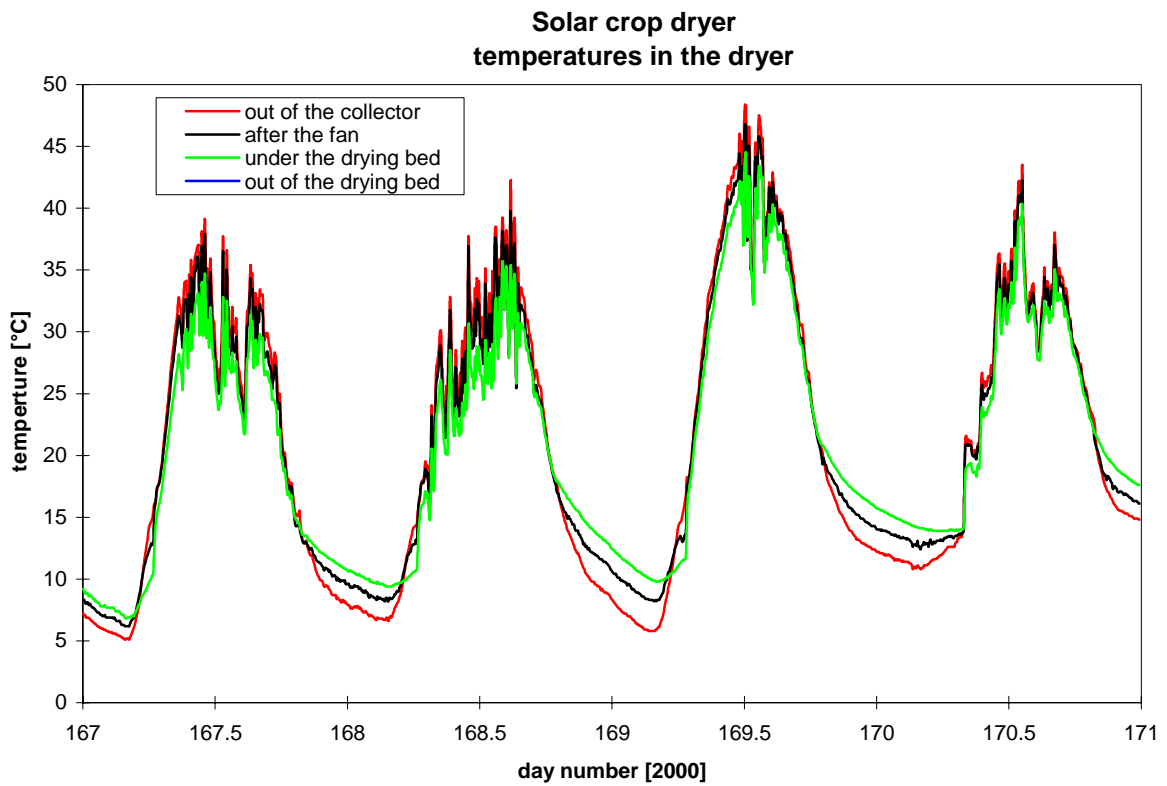


Figure 3.9. Temperatures in the system.

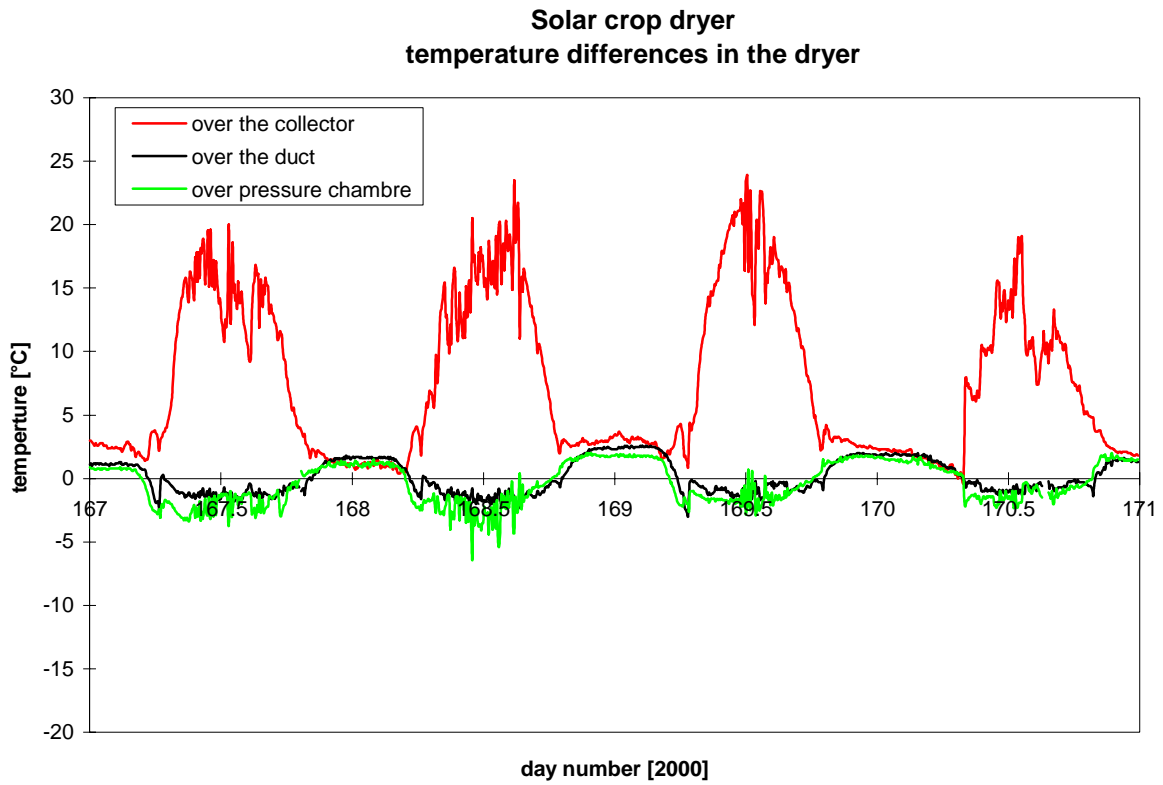


Figure 3.10. Temperature differences in the system.

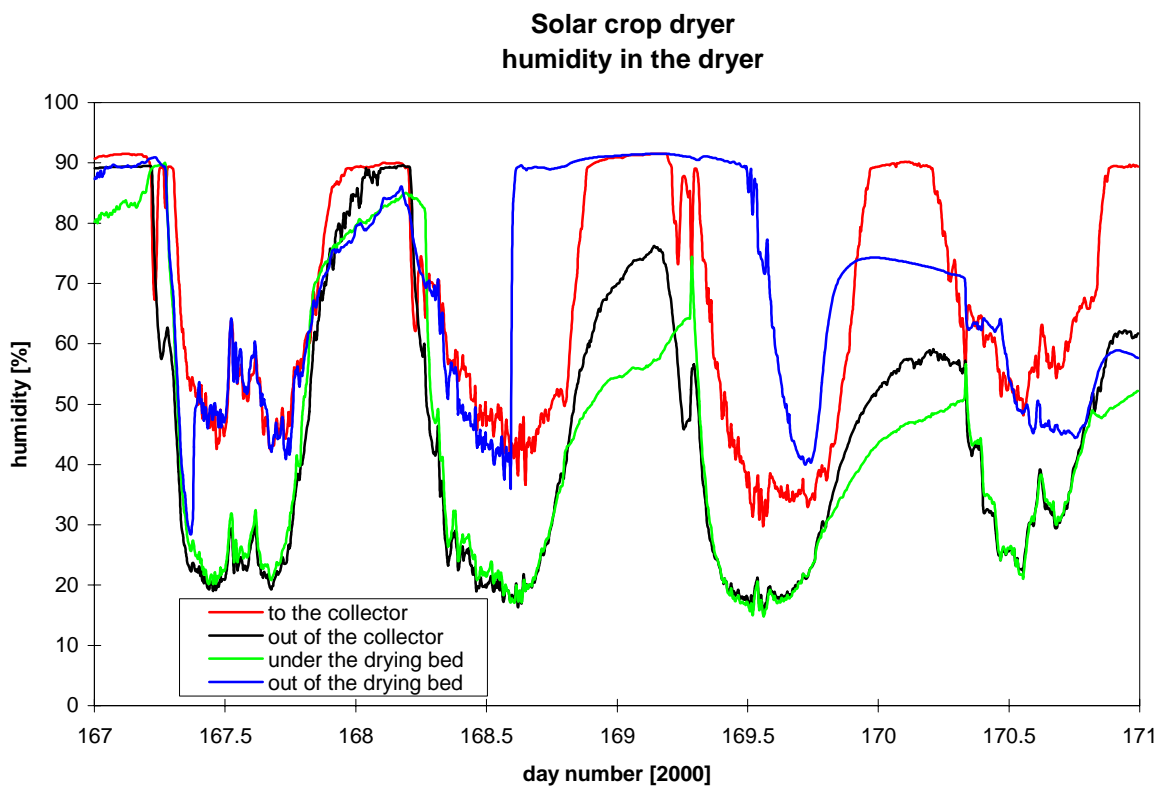


Figure 3.11. The humidity of the air to and in the dryer.

Figure 3.12 shows the air flow in the system. The air flow is as expected from the previous graphs higher than during the first test. Figure 3.12 shows that the air flow got so high that it got out of the range of the air speed sensor. Figures 3.13-14 show the air speed as a function of the solar radiation (total and useful radiation). While the air flow in the first test only occasionally exceeded 275 m³/k, figures 3.12-14 indicates that the max air flow rate in the second test was in the order of 375 m³/h which means an increase by one third.

Figure 3.15 shows the power transferred to the air in the solar air collector. The max power is increased compared to the first test – see figure 2.28. If the air speed sensor could have measured the right air speed the shown power may have reached 3000 W, while it during the first test was 2500 W. This is due to a higher efficiency of the collector because of a higher flow rate as seen later.

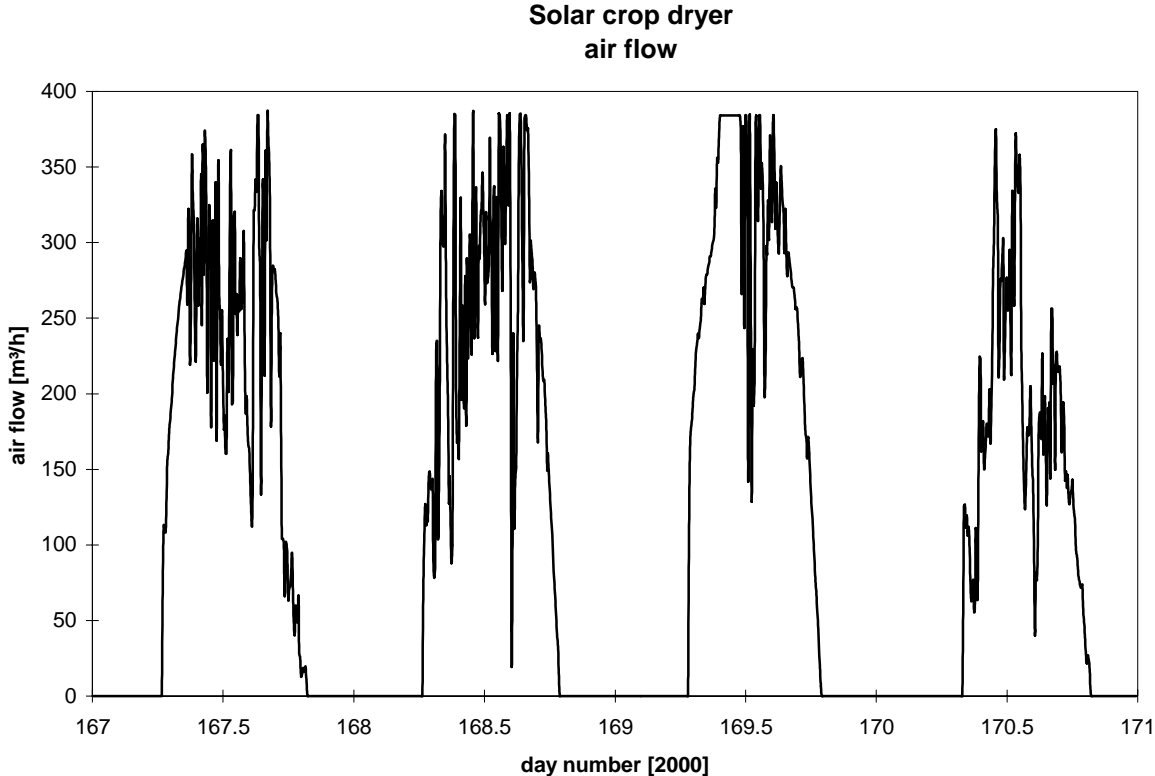


Figure 3.12. Air flow in the system.

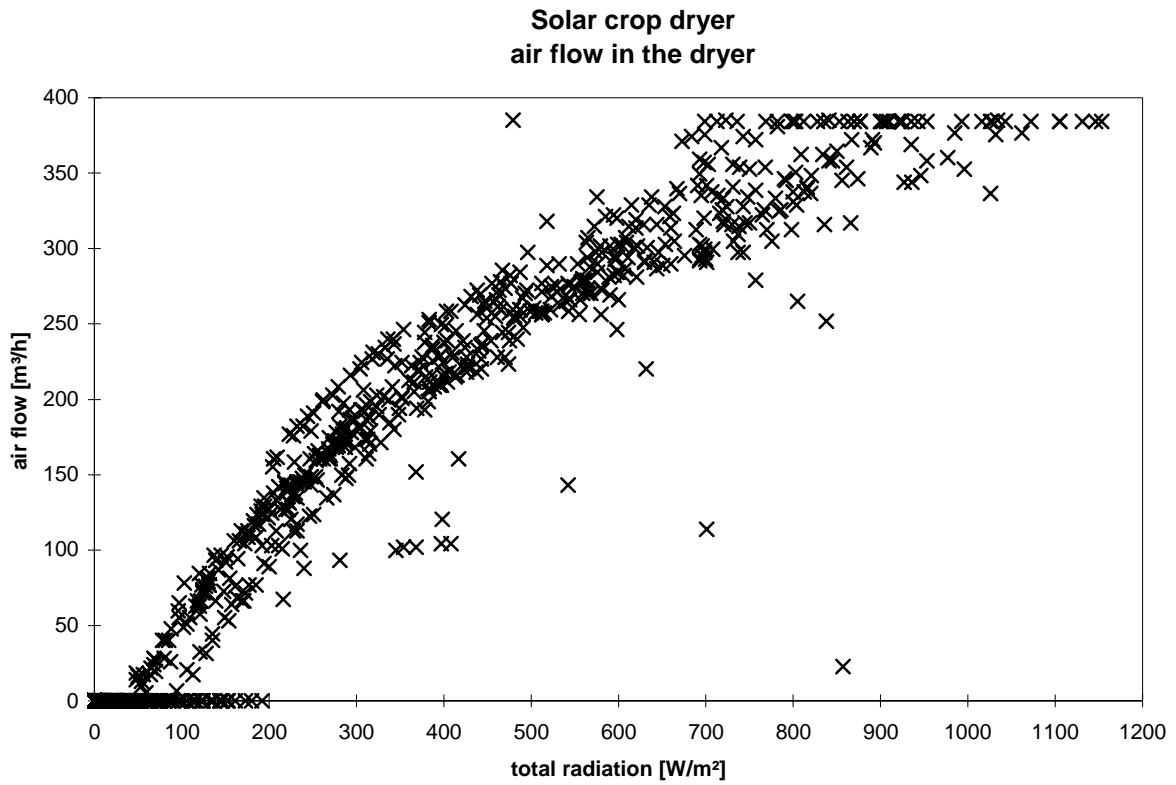


Figure 3.13. The air flow rate dependent on the total radiation.

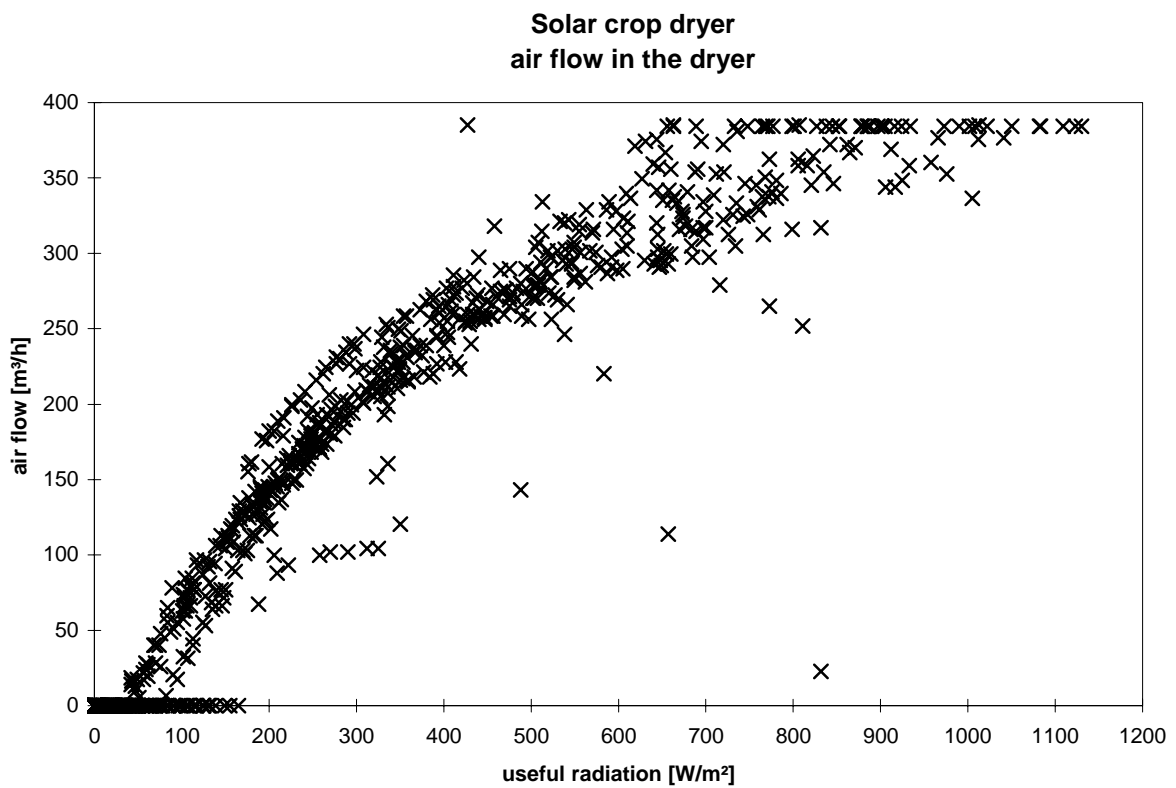


Figure 3.14. The air flow rate dependent on the useful radiation on the PV-panel.

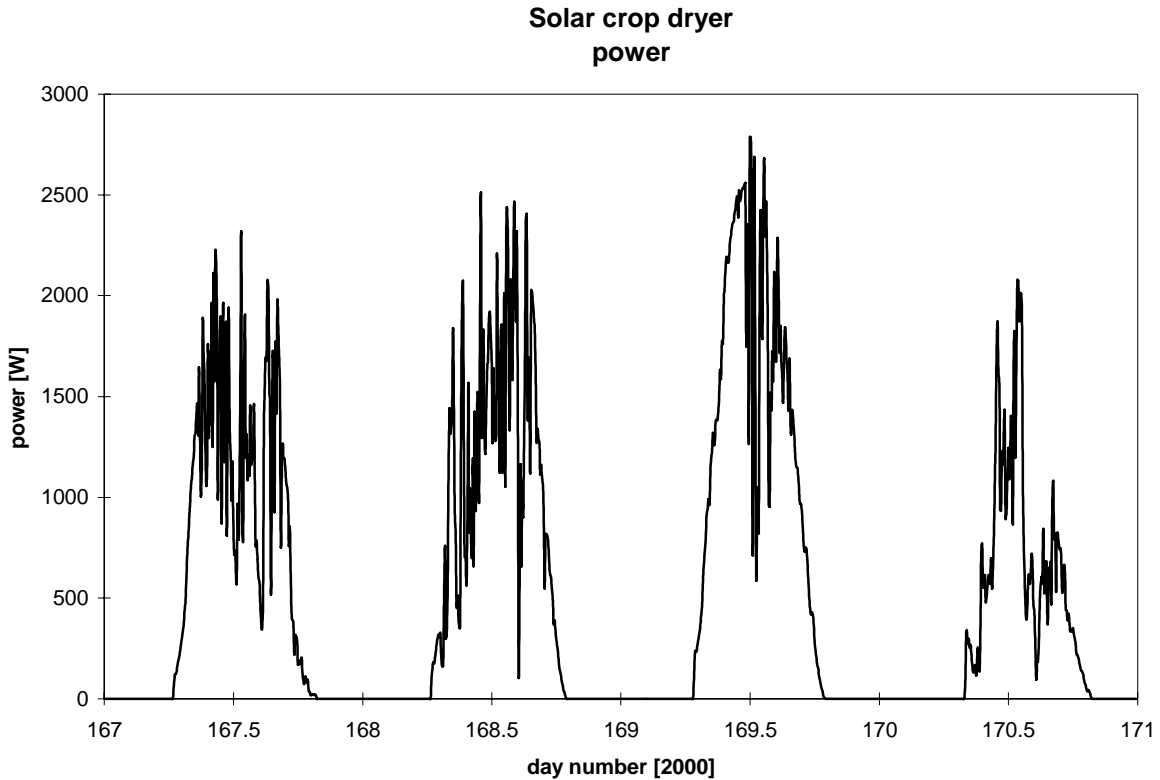


Figure 3.15. Power transferred to the air in the collector.

3.5.1. Drying capacity

Figure 3.16 shows the measured weight and calculated moisture content of the maize in one of the drying trays. The values are obtained for the period June 16 – June 19 – i.e. a phase shift compared to the other graphs in this section of 1 day. Due to this the solar radiation measured by the department of Agricultural Engineering is shown in figure 3.17. From figures 3.16-17 it is seen that the first and the second day were sunny, while it was overcast during the second day.

Figure 3.16 shows that the moisture content is decreased from 22% to close to 12% during the first 1½ day. Hardly any drying occurs during the second day due to a low radiation level. The third day brings the moisture content close to the desired value – 10%. The pattern shown in figure 3.16 fits very well with the theory on the duration of the drying – see section 2.3.1.

Figure 3.18 shows the moisture content of the maize in the drying trays based on weighing of all the trays after the finalization of the test. Figure 3.18 shows for unexplained reasons lower moisture contents than indicated in figure 3.16.

The test shows that it is possible to obtain a duration of the drying time of down to two days. Further reduction of the drying time demands a higher air flow rate and a larger collector area - both for the solar air collector and the PV-panels. This, however, will increase the price of the dryer considerably.

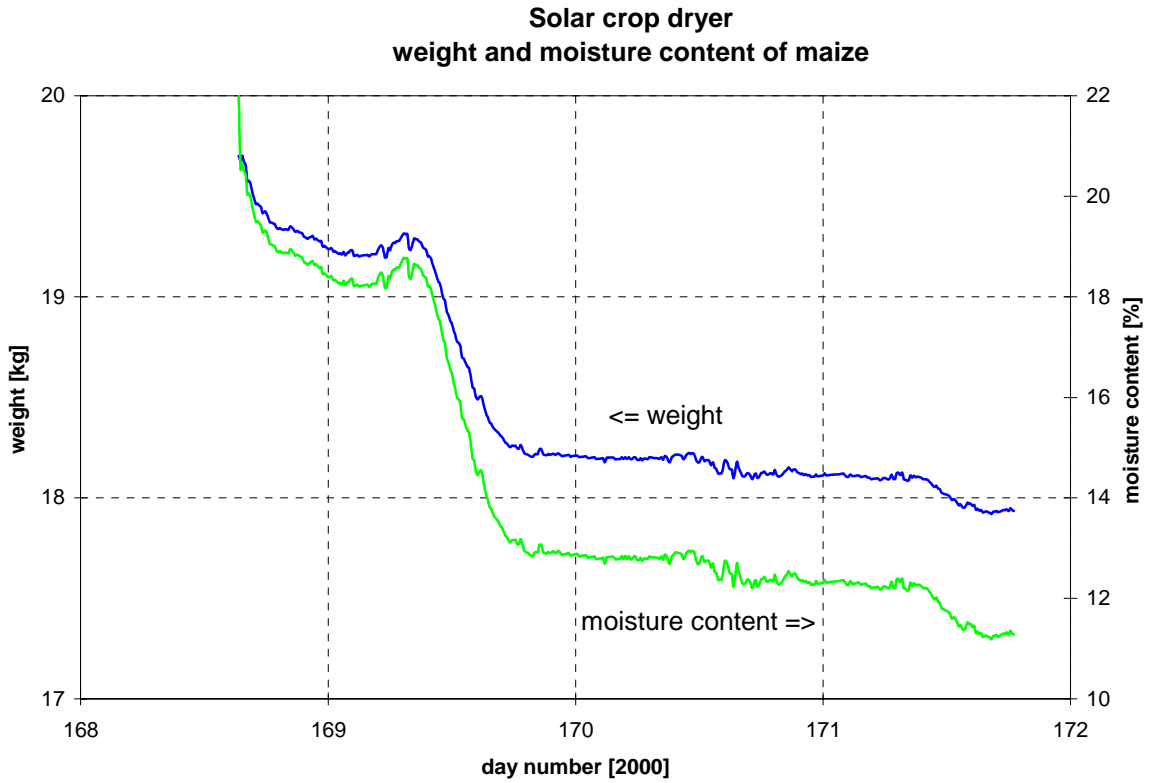


Figure 3.16. The weight and moisture content of one of the drying trays during the second test.

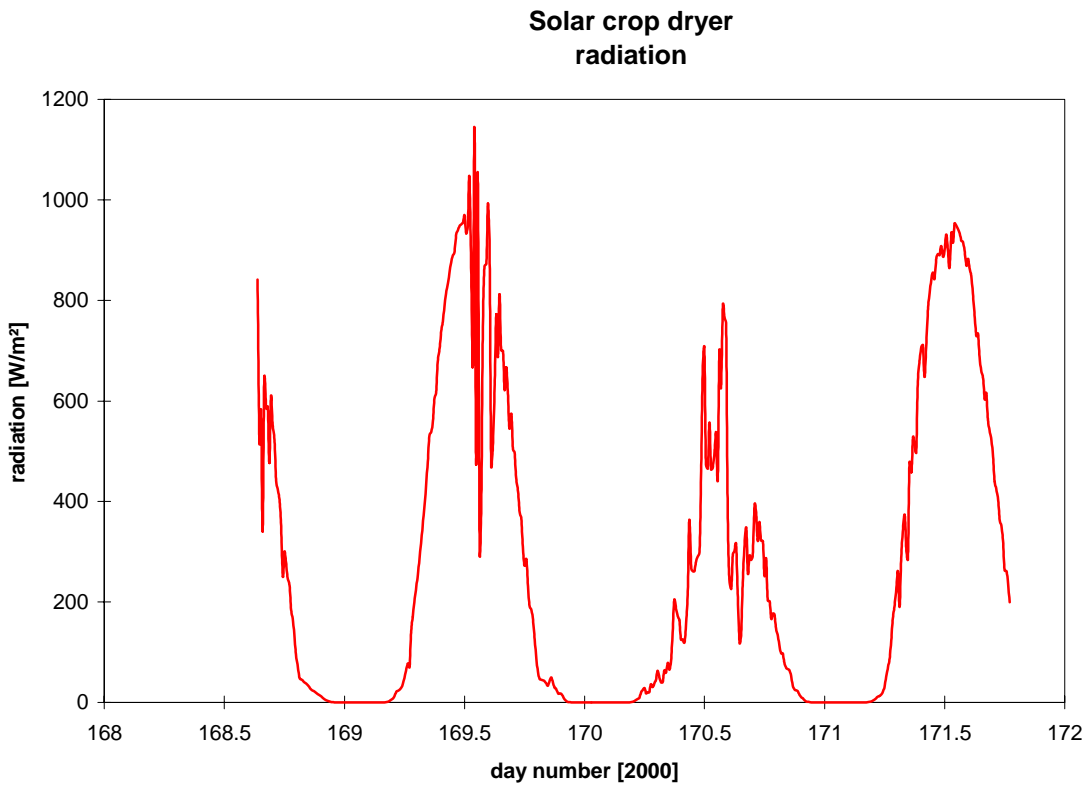


Figure 3.17. The solar radiation measured with the pyranometer of the Department of Agricultural Engineering.

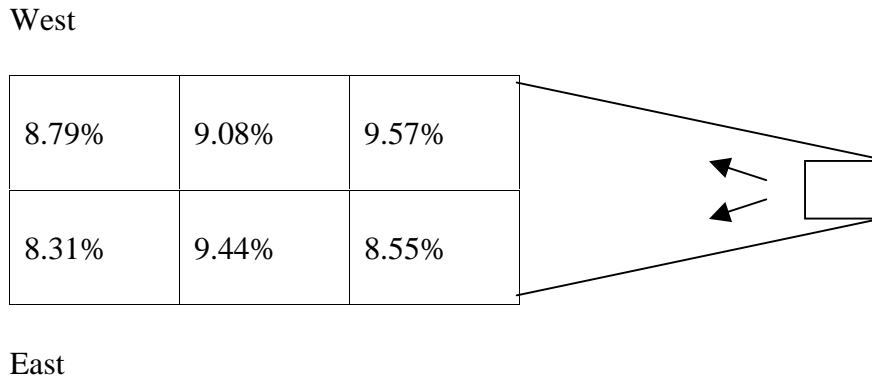


Figure 3.18. The end moisture content of the maize in the 6 drying trays.

Figure 3.18 shows a much more even drying process than shown in 2.26. The difference in moisture content between the tray with the highest and lowest moisture content is here only about 1% point.

3.5.2. Temperature of the air to the drying bed

Figure 3.19 shows the temperature increase of the air to the drying bed dependent on the useful radiation. The figure shows that the temperature increase due to the higher air flow rate has decreased compared to the first test. The temperature increase at an useful radiation of 900 W/m^2 has decreased from around 20 to around 16 K. This gives a mean temperature of the air to the drying bed in the modified dryer of $43\text{-}48^\circ\text{C}$ in Ghana. The increase in air flow has thus reduced the risk of damaging the maize. However, if the performance of the solar cell decrease due to higher ambient air temperatures in Ghana compared to the tests or the ambient temperature exceeds 32°C there will still be a risk of damaging the seed.

3.5.3. Collector efficiency

The following five graphs showing the efficiency are generated in the same way as the graphs in section 2.3.2.

The pattern of the graphs 3.21-24 looks different from the graphs in section 2.3.2. The shape formed by the values look here as could be expected – i.e. no bulge as in the first test. However, the values at a flow rate of $384 \text{ m}^3/\text{h}$ ($80.5 \text{ m}^3/\text{hm}^2$) should not be considered as these are for flow rates above what could be measured with the present air speed sensor – i.e. both flow rate and efficiency are wrong for these points.

The impression from figure 3.22-23 is that the collector is a bit less efficient than the collector in the Summer House Package – around 10% less efficient. However, the loss in efficiency is well paid back by the increase in air flow rate. And when comparing figure 3.15 with figure 2.28 it is seen that more power out of the collector has been gained – max power increase from 2500 to 3000 W = an increase of 20%.

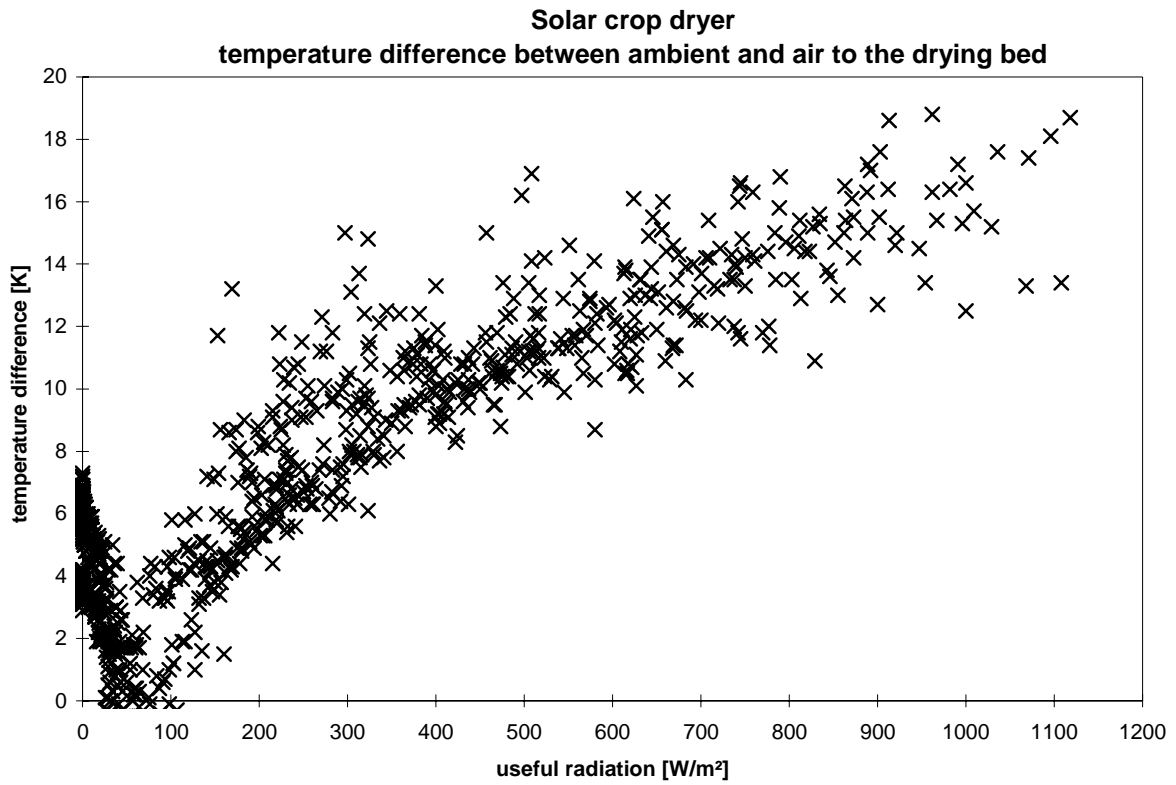


Figure 3.19. The difference between the air temperature to the drying bed and the ambient temperature dependent on the useful radiation.

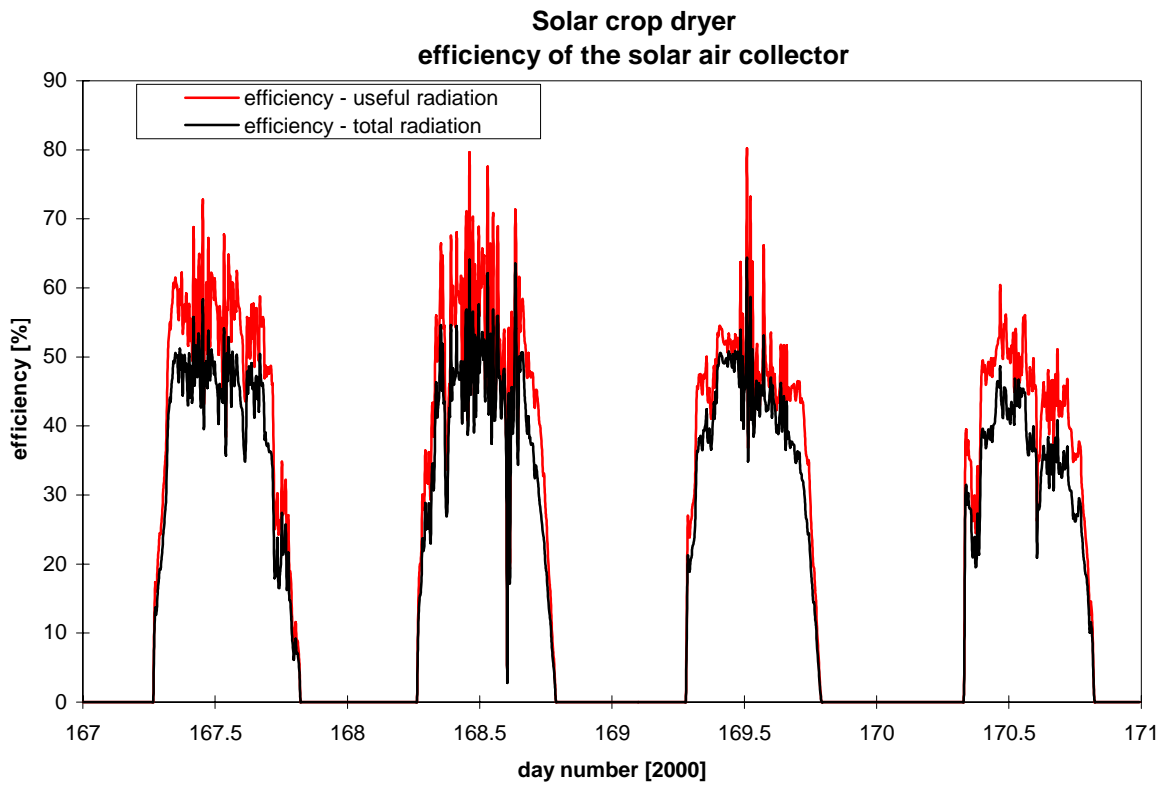


Figure 3.20. The efficiency of the collector dependent on either total or useful radiation.

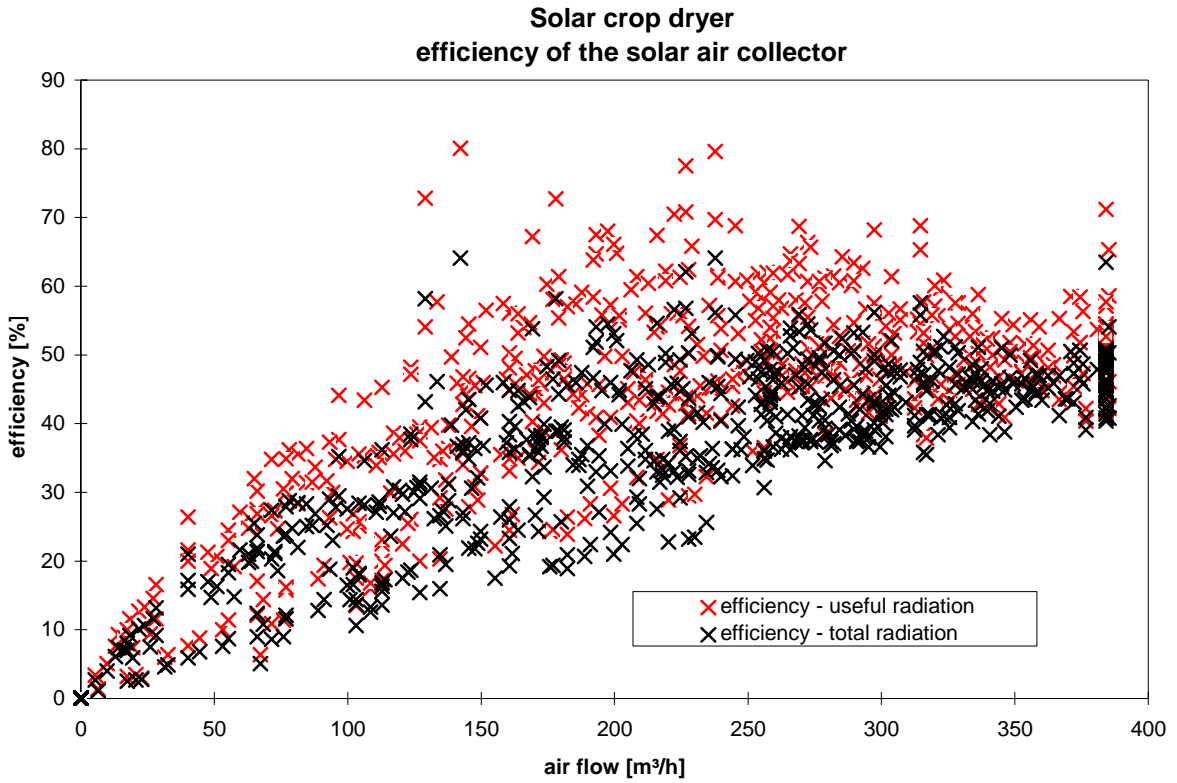


Figure 3.21. The efficiency of the collector dependent on the total flow rate through the system.

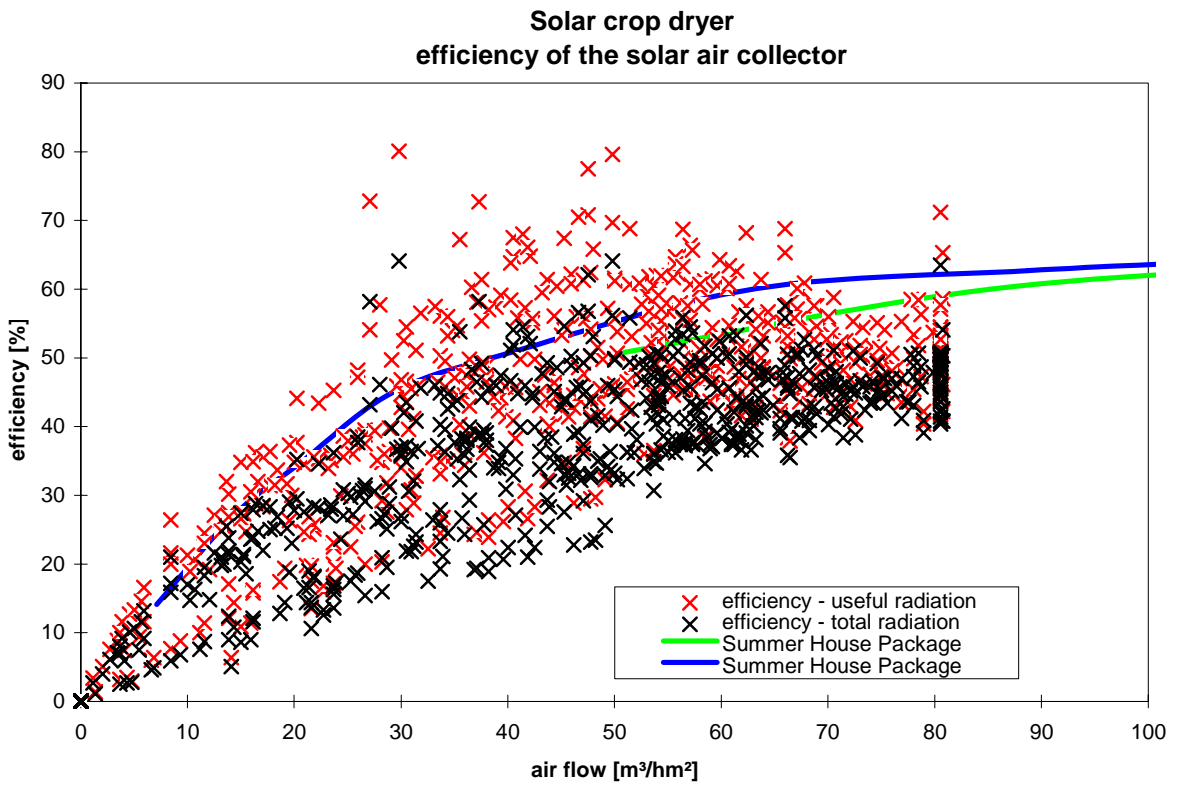


Figure 3.22. The efficiency of the collector dependent on the normalized flow rate through the system together with the efficiency of the Summer House package.

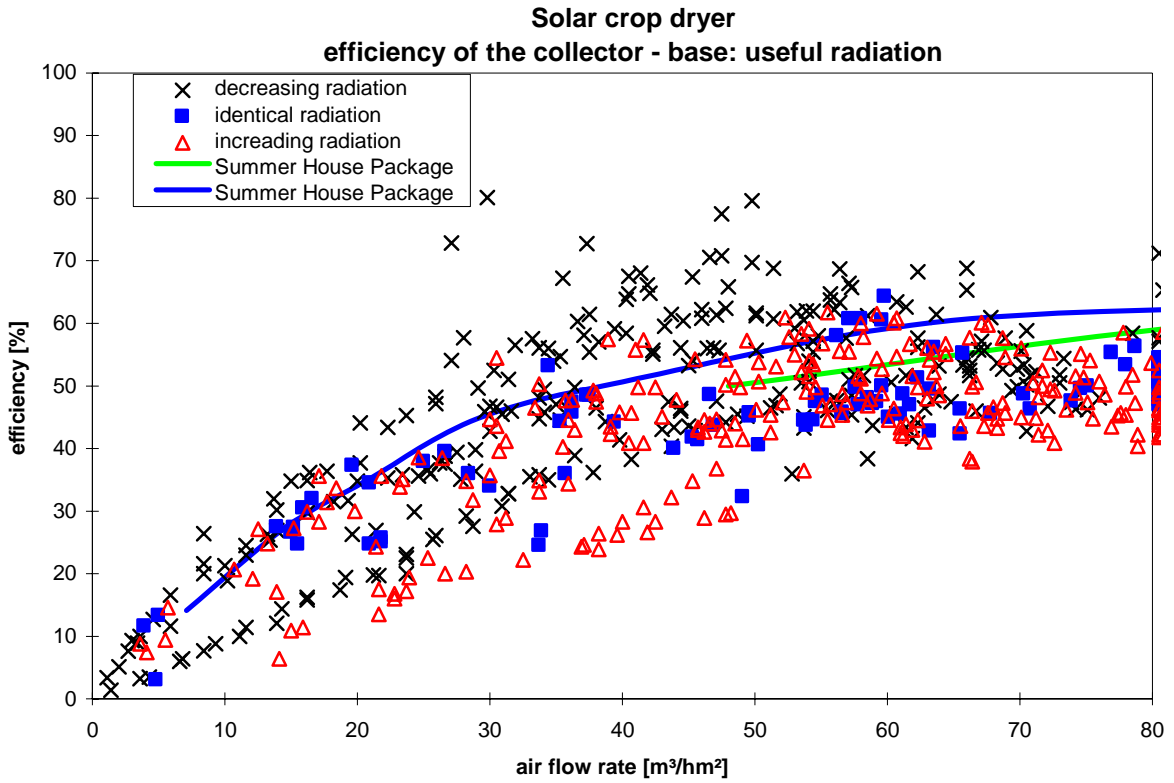


Figure 3.23. The efficiency of the collector dependent on the normalized flow rate through the system and if changes in the radiation level has occurred.

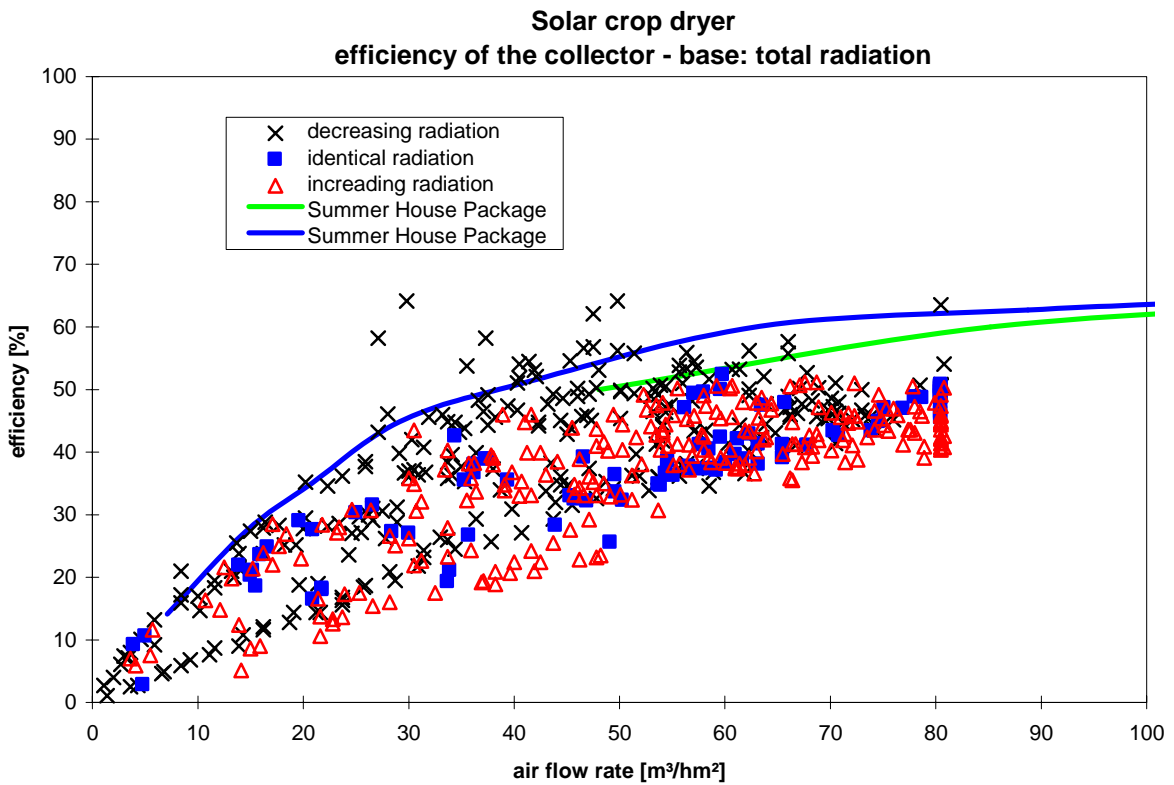


Figure 3.24. The efficiency of the collector dependent on the normalized flow rate through the system and if changes in the radiation level has occurred.

3.6. Measurements with a new air speed sensor

The air speed sensor was replaced with another sensor with a larger measuring range. The measurements were started again with the new air speed sensor on June 20. The following graphs will concentrate on the air flow rate through the system and the efficiency of the collector. No wet maize was dried during this test. The dry maize from the former test was left in the drying bed in order to create the right pressure drop over the drying bed.

Figure 3.25 shows the radiation and ambient air temperature during the period June 20 – June 25 (both inclusive). The weather was characterized by two very hot days in the beginning of the period – comparable to Ghanaian conditions, and rather stable solar radiation. The four last days of the period showed more normal Danish weather conditions: ambient temperatures below 20°C and a high degree of scattering of the solar radiation.

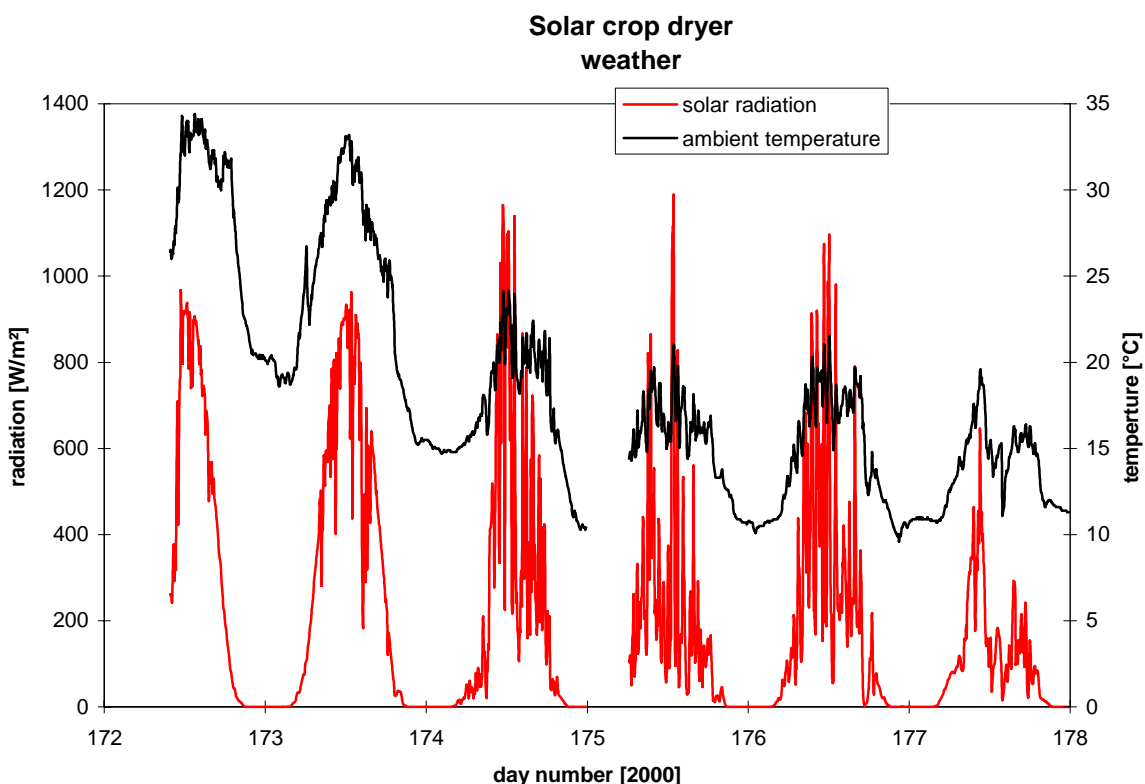


Figure 3.25. Solar radiation and ambient temperature during the period June 20 – June 25.

Figure 3.26 shows the air flow rate through the system. When comparing with 2.27 it is seen that the max air flow rates has increased from 325 to 500 m³/h – i.e. an increase of 54% which is close to the expected increase shown in figure 3.6 – especially if it is considered that the ambient temperature was lower during the period shown in figure 2.27 than in figure 3.26 leading of a bit higher air flow rate in figure 2.27 as discussed in the next paragraphs.

Figure 3.26 indicate that the air flow rate is lower during the two first days than during the last four days. Figure 3.27 shows the air flow rate dependent on the ambient temperature where a black x is values from the first two days while a red Δ is values from the last four days. The graph shows a clear dependency on the ambient temperature. This dependency hides the real dependency on the temperature of the solar cells, which has not been measured. However, if it

is assumed that the difference in ambient temperature between the two periods is more or less identical to the difference in cell temperature between the two periods it is seen from figure 3.27 that the mean temperature difference between the two periods is 10 K. The efficiency of a PV-panel will normally change by 0.5% for each 1 K change in the temperature level. Based on this it would have been expected that the air flow rate would have increased by 5% from the first period to the second period. However, the air flow rate changed from max 400 to max 500 m³/h which means an increase of 25%.

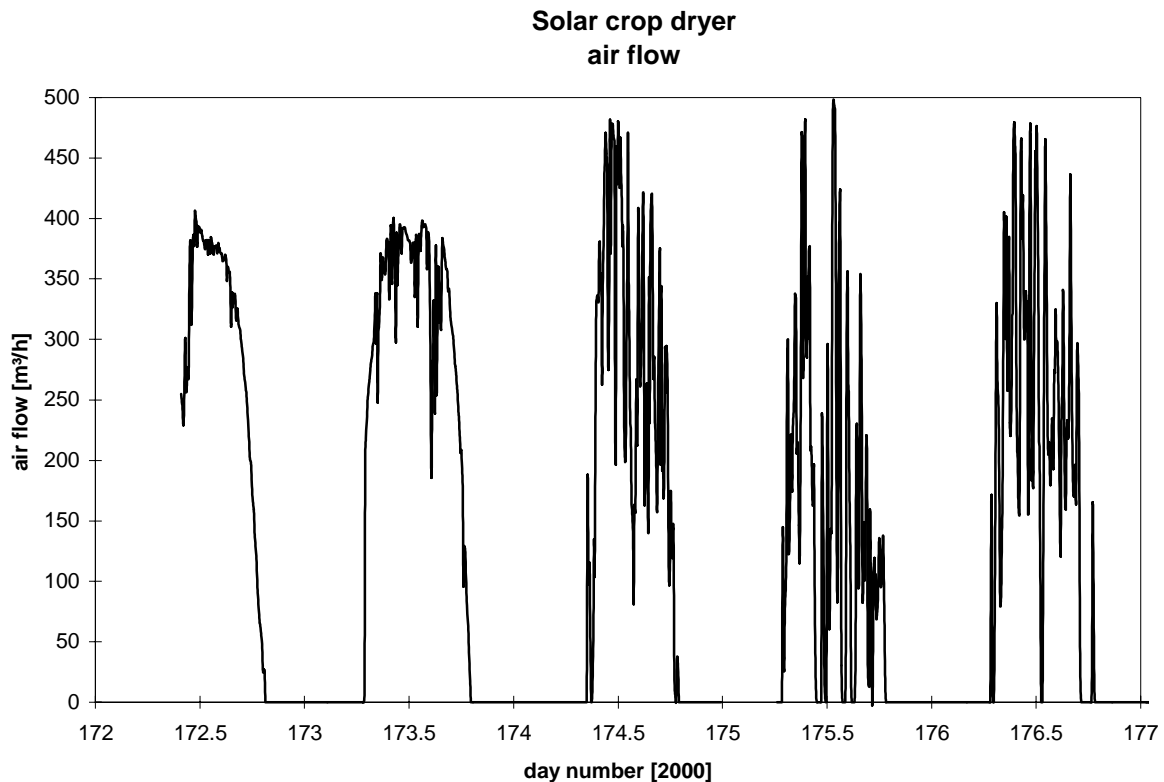


Figure 3.26. The air flow rate in the system.

This larger increase in air flow rate compared to the expected increase in the power from the PV-panels can only be explained by the fact that the characteristics of the fan and the PV-panels do not match. It is expected that this can be solved by putting a maximum power point tracker in between the fan and the PV-panels. A maximum power point tracker ensures that the working point (relationship between voltage and current) for the PV-panels always gives the max power out of the PV-panels. It is necessary to ensure a high power production from the PV-panels under all conditions in order to ensure max air flow rate in the dryer and thereby ensure low drying time, high efficiency of the collector and prevent too high temperatures of the air to the drying bed. An alternative to a maximum power point tracker is additional PV-panels. The choice between the two solutions should be based on an economical evaluation.

3.6.1. Efficiency

Figure 3.28 shows the power transferred to the air stream in the collector. The max power is now above 3500 W.

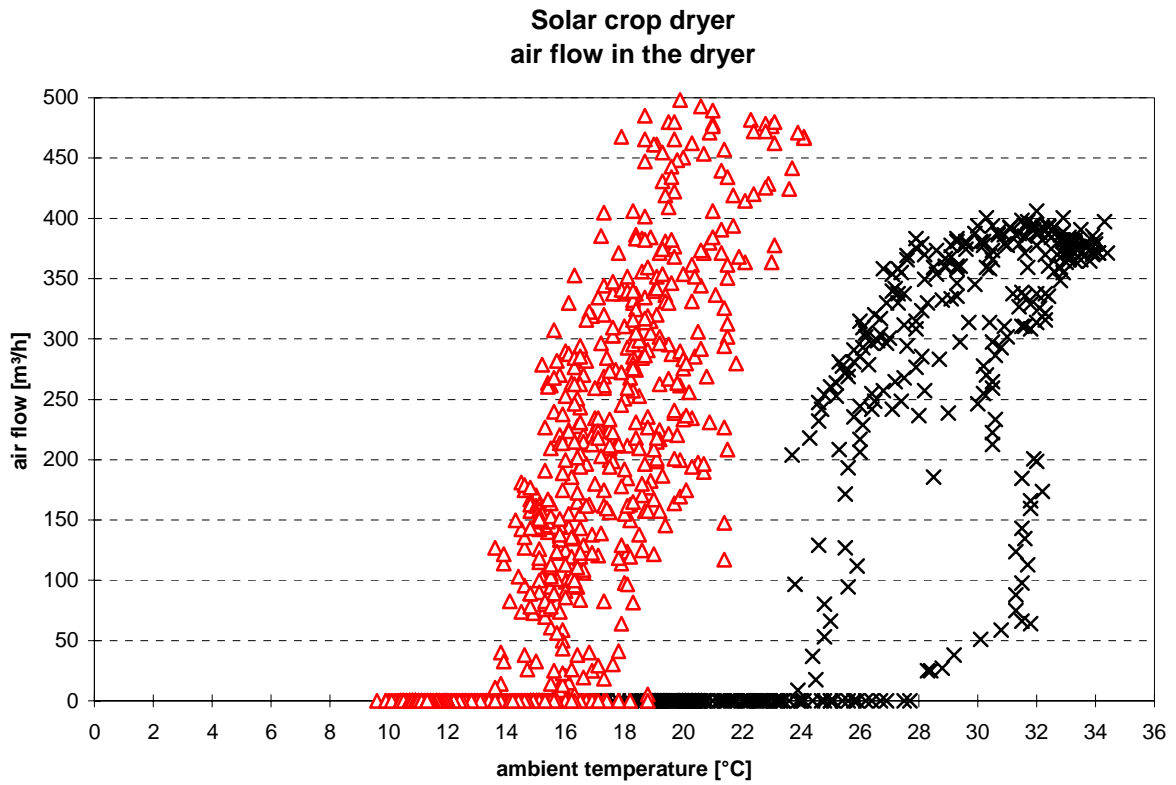


Figure 3.27. The air flow rate dependent on the ambient temperature.

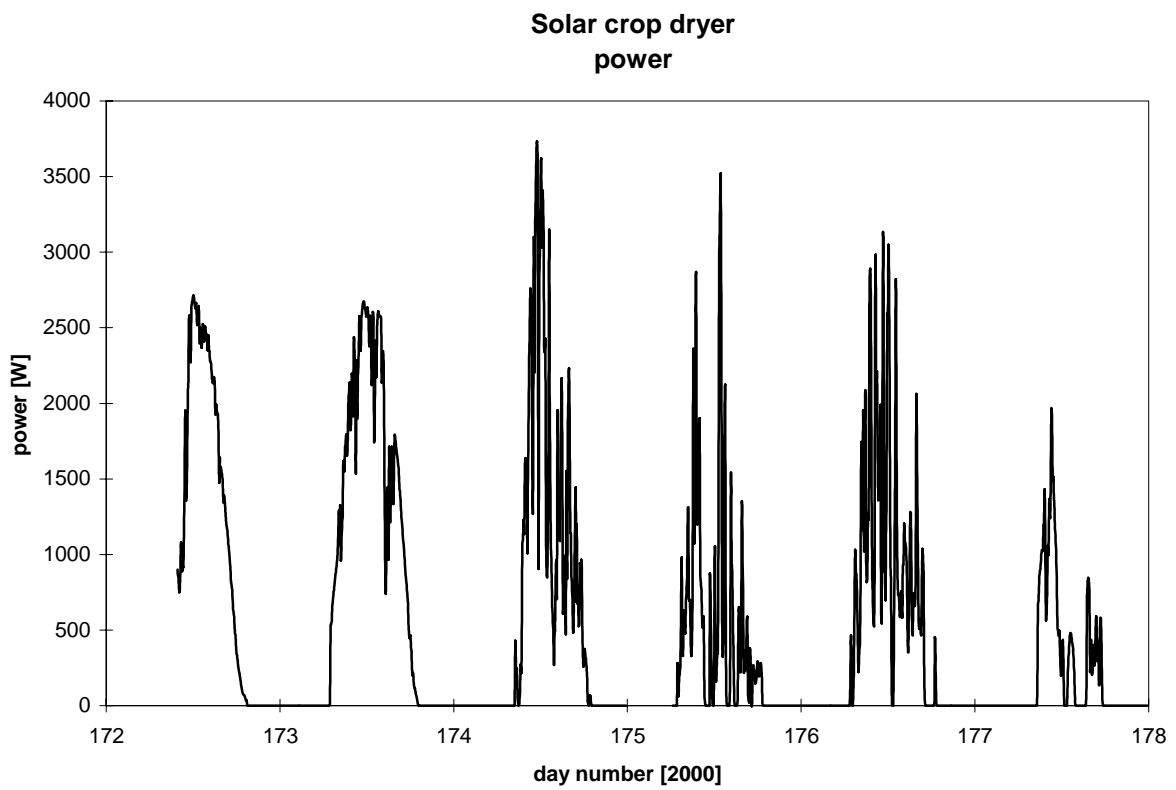


Figure 3.28. Power transferred to the air in the collector.

Figure 3.29 shows the efficiency of the collector in chronological order calculated based on total and useful radiation, while figures 3.30 and 3.31 shows the efficiency dependent on the normalized air flow rate.

Figure 3.30 show that the efficiency now is higher than the efficiency of the Summer House Package.

Figure 3.32 shows the temperature increase of the air to the drying bed. The temperature increase of the air to the drying bed is a bit higher than in figure 3.19 - around 18°C. Figures 3.19 and 3.32 shows that the increase in temperature will stay below 20°C with the shown dependency of the air flow rate on the radiation – see figure 3.13 and 3.33. This means that it is important that the high ambient temperatures in Ghana do not decrease the flow rate more than the reduction of the obtainable power from the PV-panels.

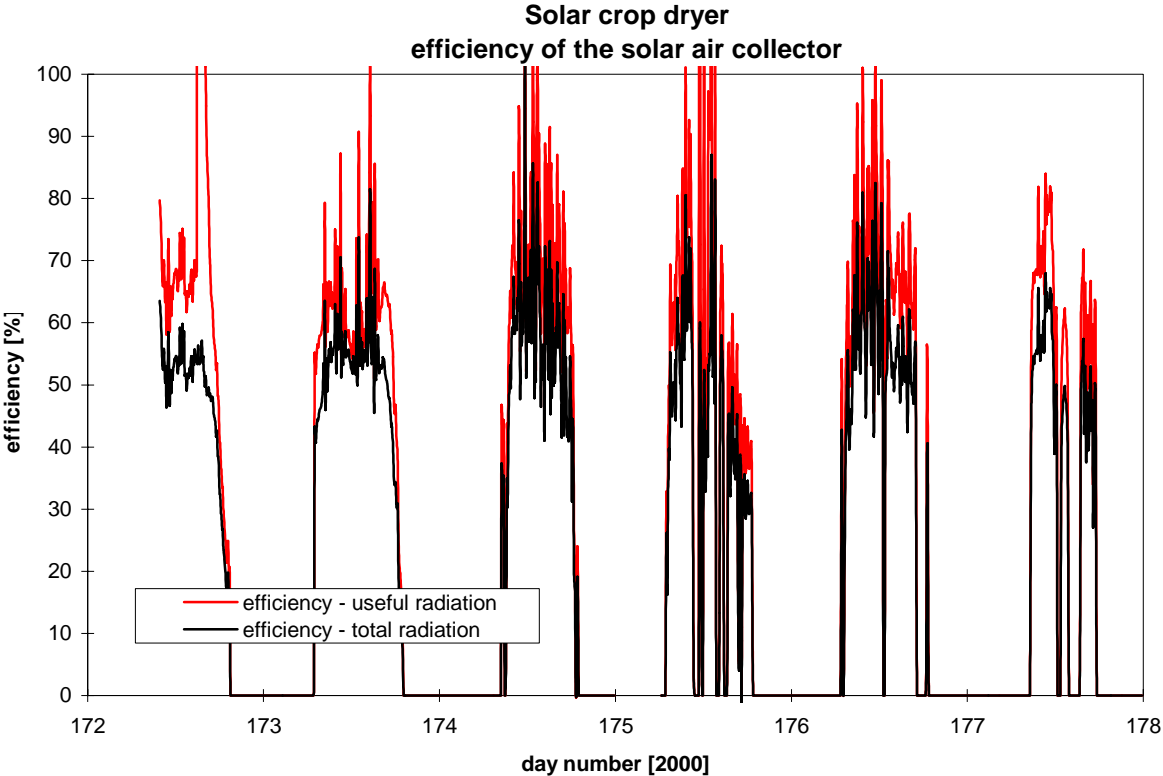


Figure 3.29. The efficiency of the collector dependent on either total or useful radiation.

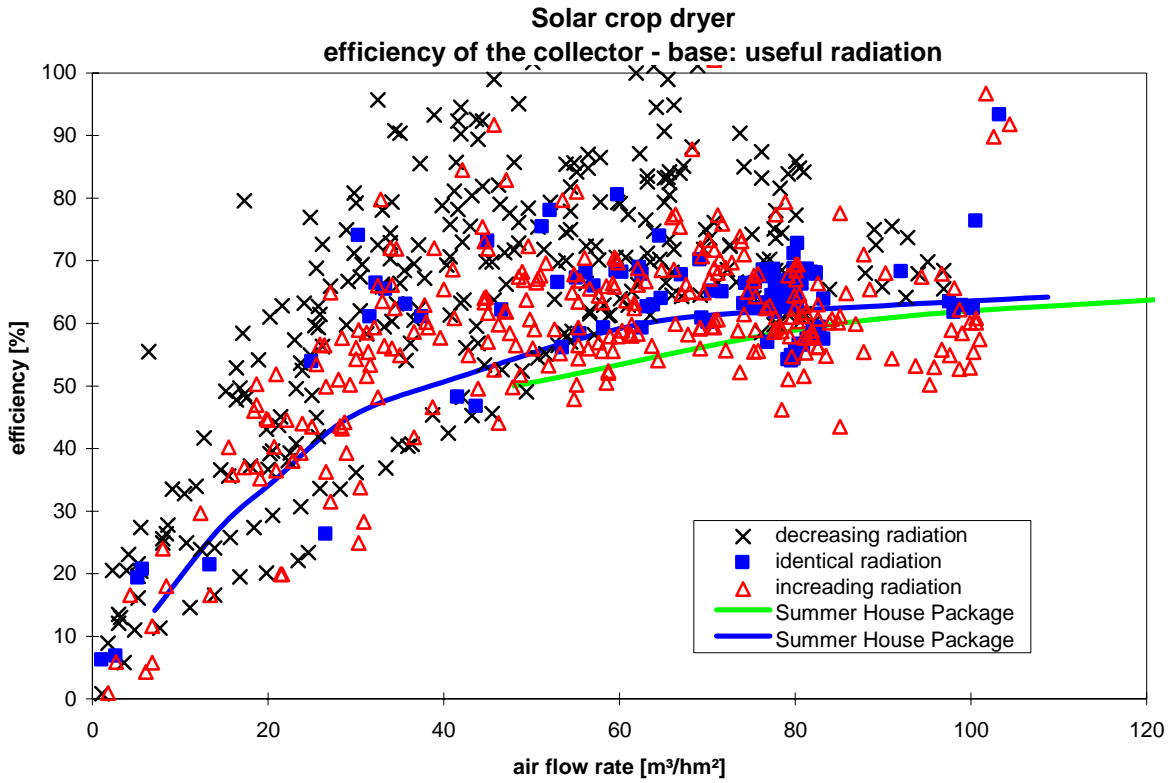


Figure 3.30. The efficiency of the collector dependent on the normalized flow rate through the system and if changes in the radiation level has occurred.

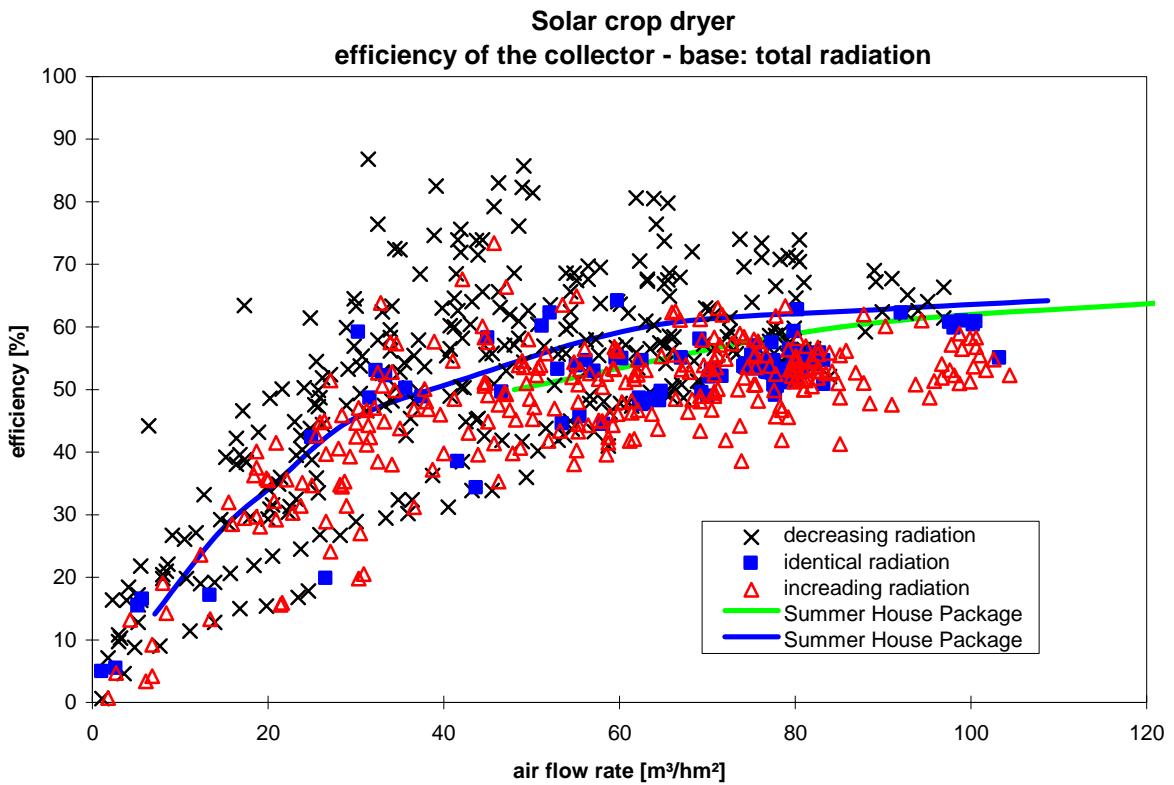


Figure 3.31. The efficiency of the collector dependent on the normalized flow rate through the system and if changes in the radiation level has occurred.

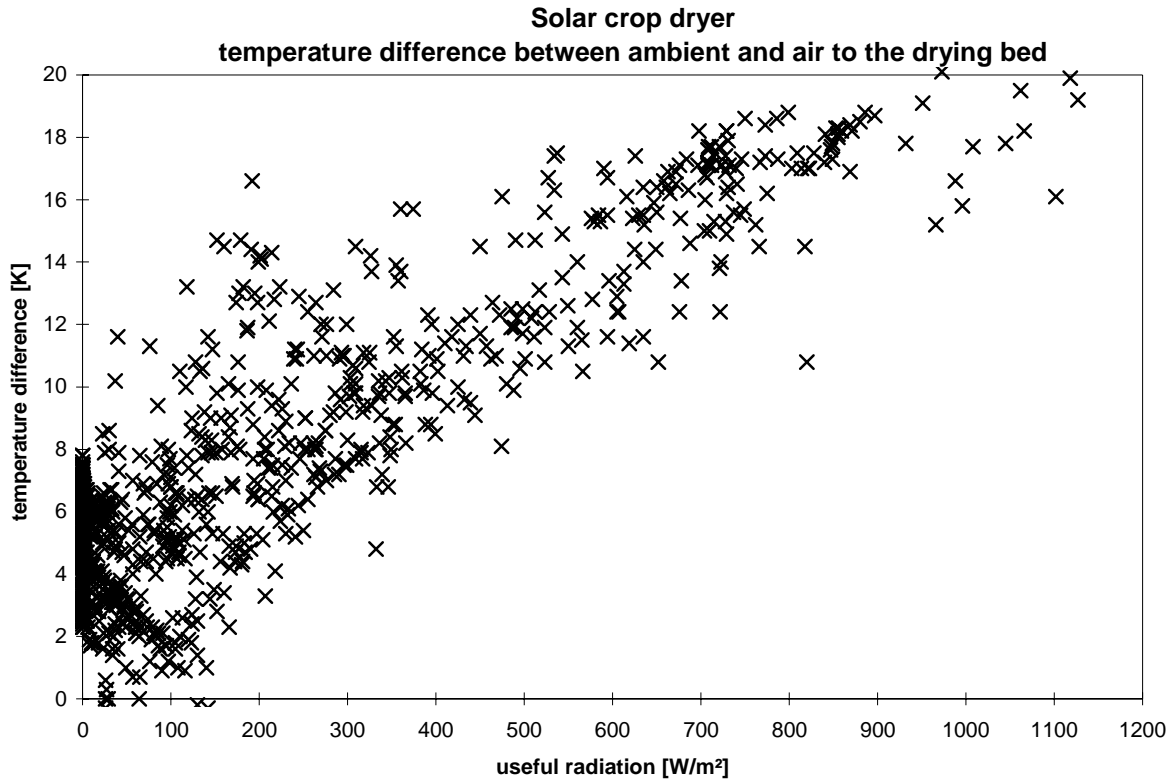


Figure 3.32. The difference between the air temperature to the drying bed and the ambient temperature dependent on the useful radiation.

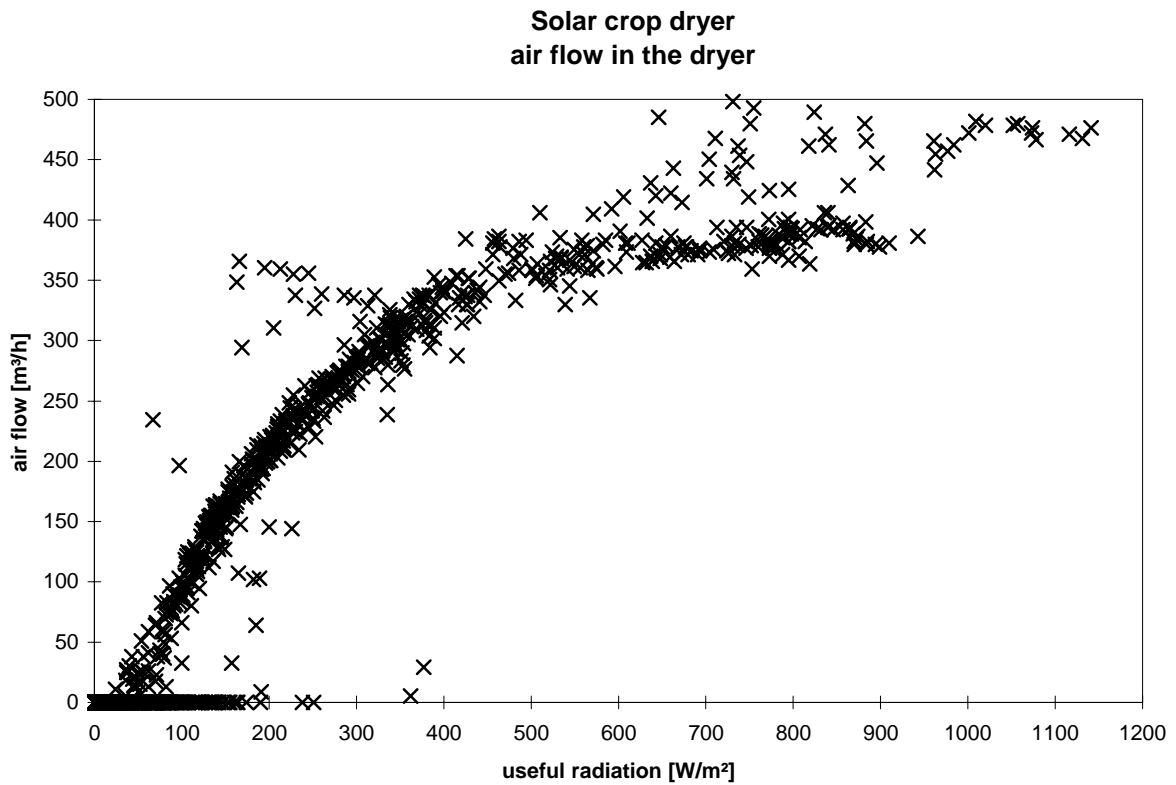


Figure 3.33. The air flow rate dependent on the useful radiation on the PV-panel.

4. Test including measuring of the power to the fan

The only modification made before this test was to include continuously measurement of the voltage and current to the fan from the PV-panels. This was done by the Department of Agricultural Engineering with their Campell data logger, which was calibrated for this purpose.

The test was carried out with wet maize in the drying bed.

4.1. Measureing results

The test was initiated in the morning of July 3 and ended at midnight July 4. Figure 4.1 shows the total radiation on the collector and the ambient temperature while figure 4.2 shows the humidity of the air to and in dryer. The period was as seen characterised by sunny conditions, rather high ambient temperatures (up to 28°C during the day and down to 10°C during the night) and a low ambient humidity level during daytime – down to 30%.

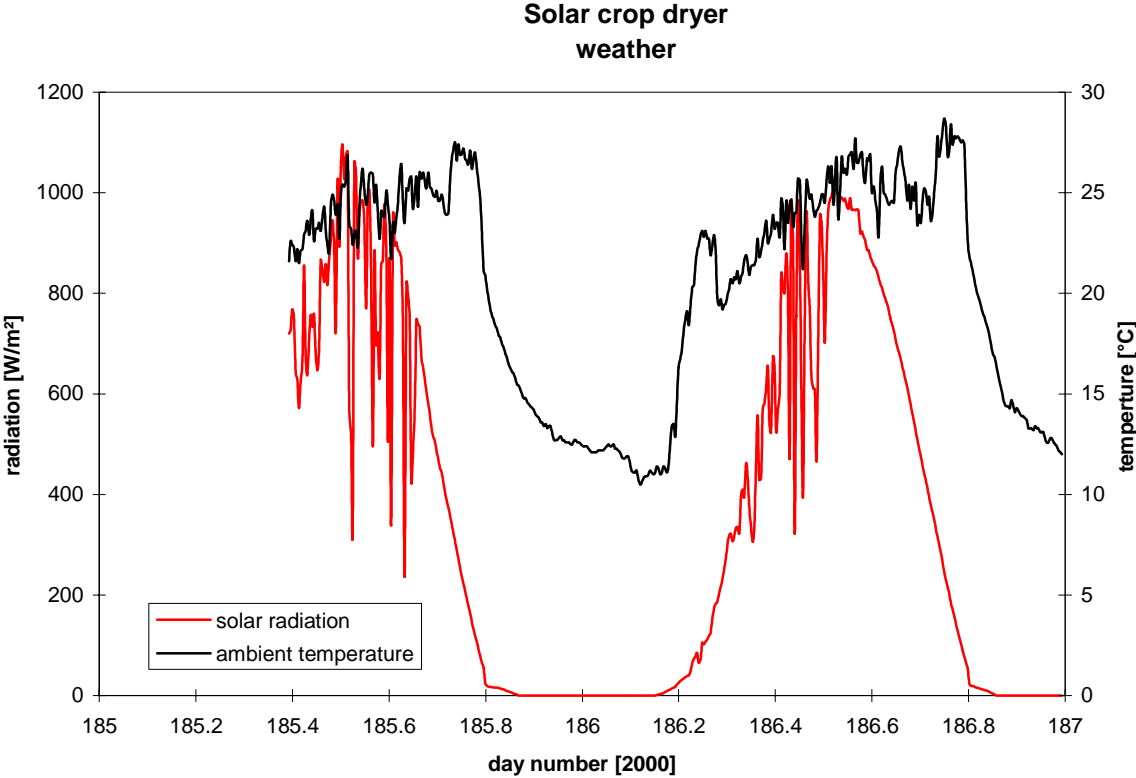


Figure 4.1. Solar radiation and ambient temperature during the third test.

4.1.2. Drying capacity

Figure 4.3 shows the measured weight and calculated moisture content of the maize in one of the drying trays. From the figure it is seen that the drying of the maize from at moisture content of 20% down to 10% took about on day. The very short drying time is due to the sunny conditions and the very low humidity level of the ambient air.

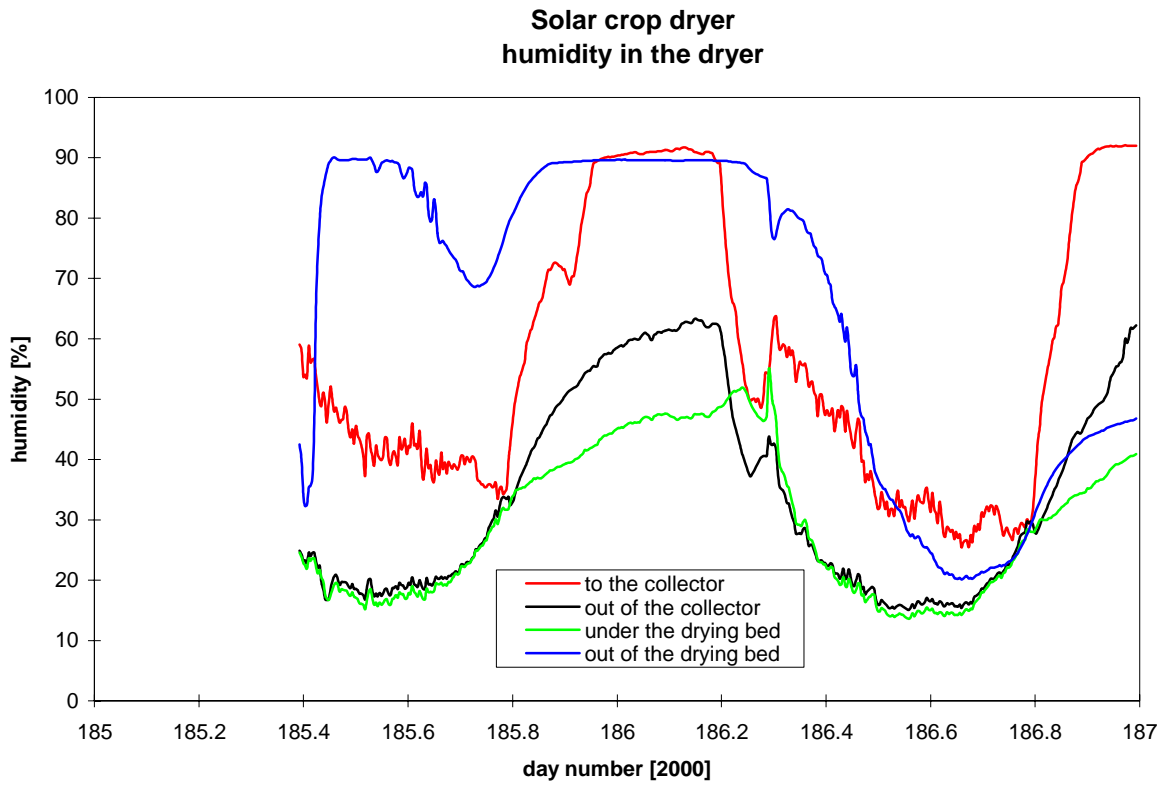


Figure 4.2. The humidity of the air to and in the dryer.

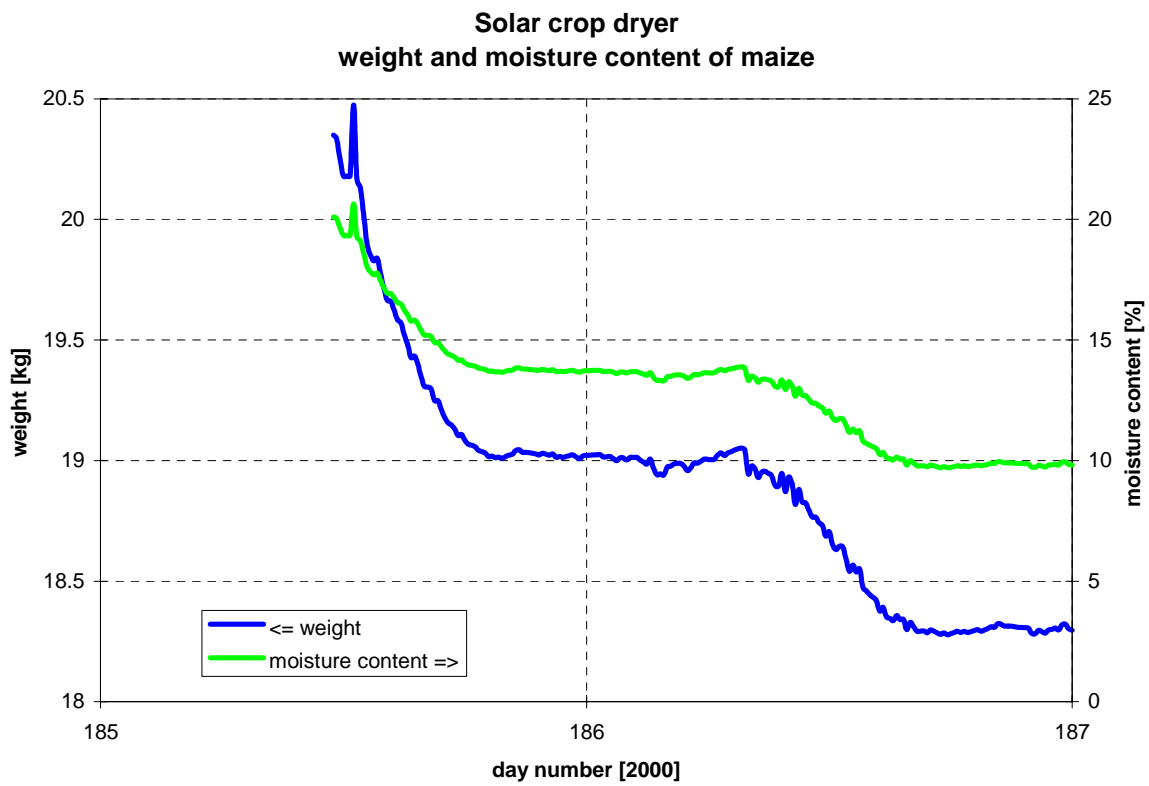


Figure 4.3. The weight and moisture content of one of the drying trays during the second test.

Figure 4.4 shows the end moisture content of the maize in the drying trays based on weighing of all the trays the day after the finalization of the test (July 5). The end moisture content of the trays was 9.65% ±10%.

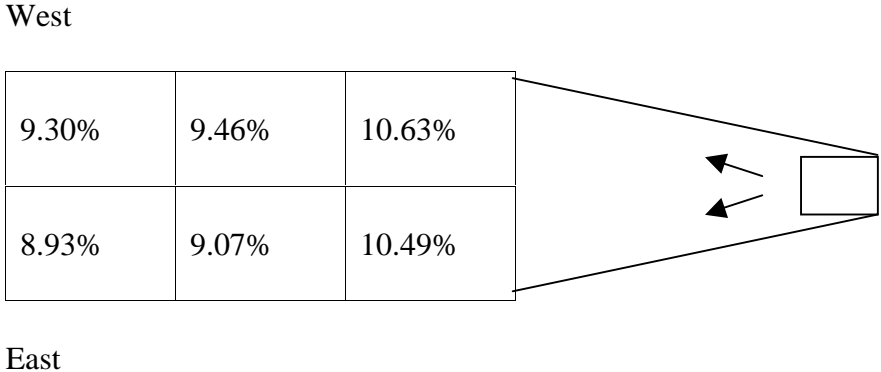


Figure 4.4. The end moisture content of the maize in the 6 drying trays.

4.1.2. Air flow rate

Figure 4.5 shows the air flow rate during the test, while figure 4.6 shows the air flow rate dependent on the ambient temperature. Based on figure 4.6 together with 3.27 the relationship in figure 4.7 between max air flow rate and ambient temperature has been established. However, please be aware that figure 4.7 has been generated based on a limited number of data – so only the indication of the trend may be used – not the absolute values.

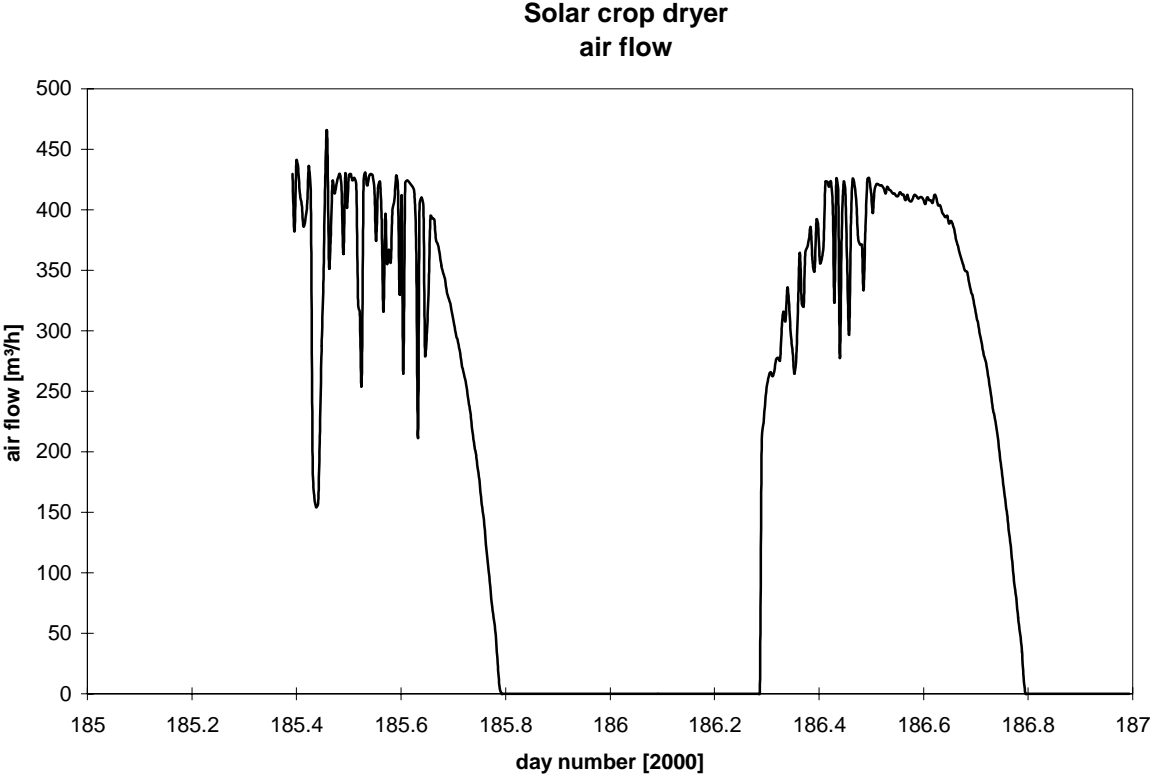


Figure 4.5. The air flow in the dryer.

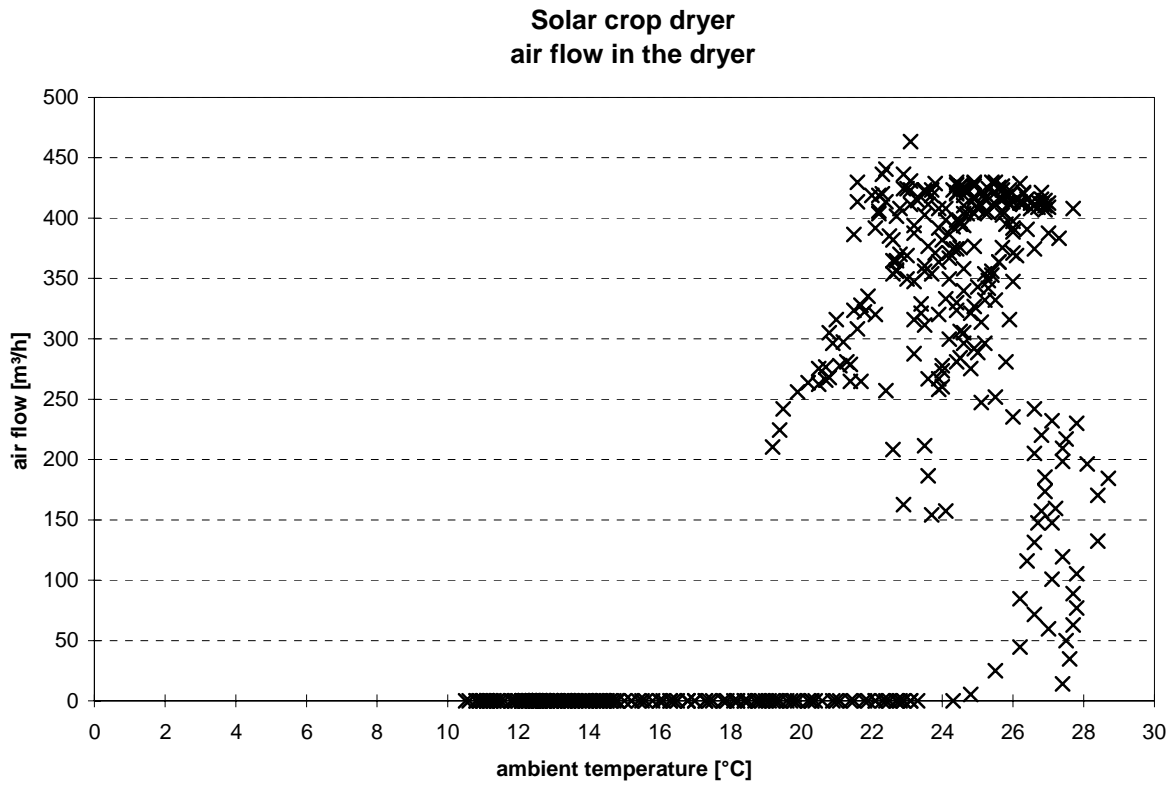


Figure 4.6. The air flow rate dependent on the ambient temperature.

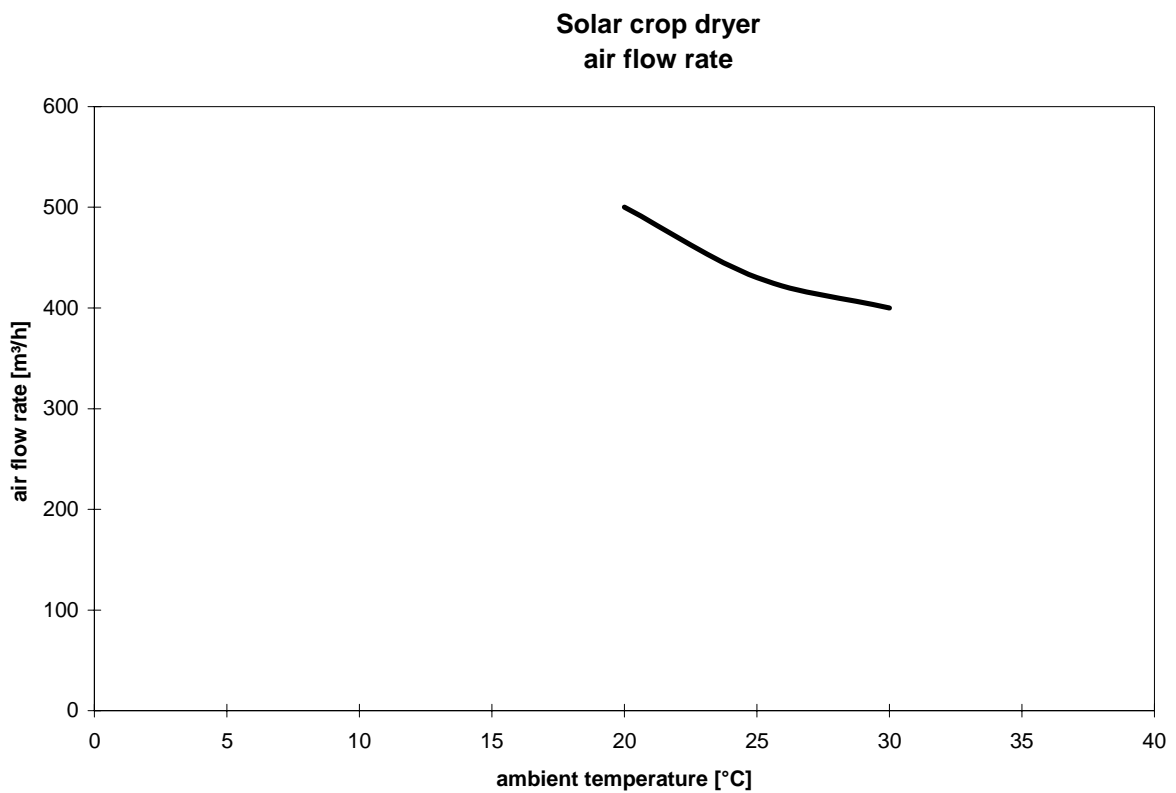


Figure 4.7. The max air flow rate dependent on the ambient temperature. Please be careful when using this figure as it is established based on a very limited number of values.

4.1.3. Voltage and current from the PV-panels

During this test the current and voltage and thereby the power from the PV-panels to the fan was measured. Figure 4.8 shows the dependency of the current and power on the voltages. The pattern of the curves is identical to the pattern of the measured current, voltage and power during the measuring of the static pressure shown in figure 3.5 where a power generator was used to create the voltage and current to the fan. This shows that the voltage delivered to the fan controls the speed of the fan. Figure 4.8 shows that for a particular voltage there will be one and only one matching current and thereby one power consumption of the fan. This means that if the voltage to the fan is e.g. 14 V the power consumption of the fan will be 17-18 W no matter if the PV-panels are able to deliver more power. The fan will thus not utilize any excess power of the PV-panels.

On the other hand – if the PV-panels are able to deliver a voltage of 14 V but only an power of 10 W the electronic in the fan will adjust the voltage until a matching current is found – in this case a voltage of 11 V and a current of 0.9 A – se figure 4.8.

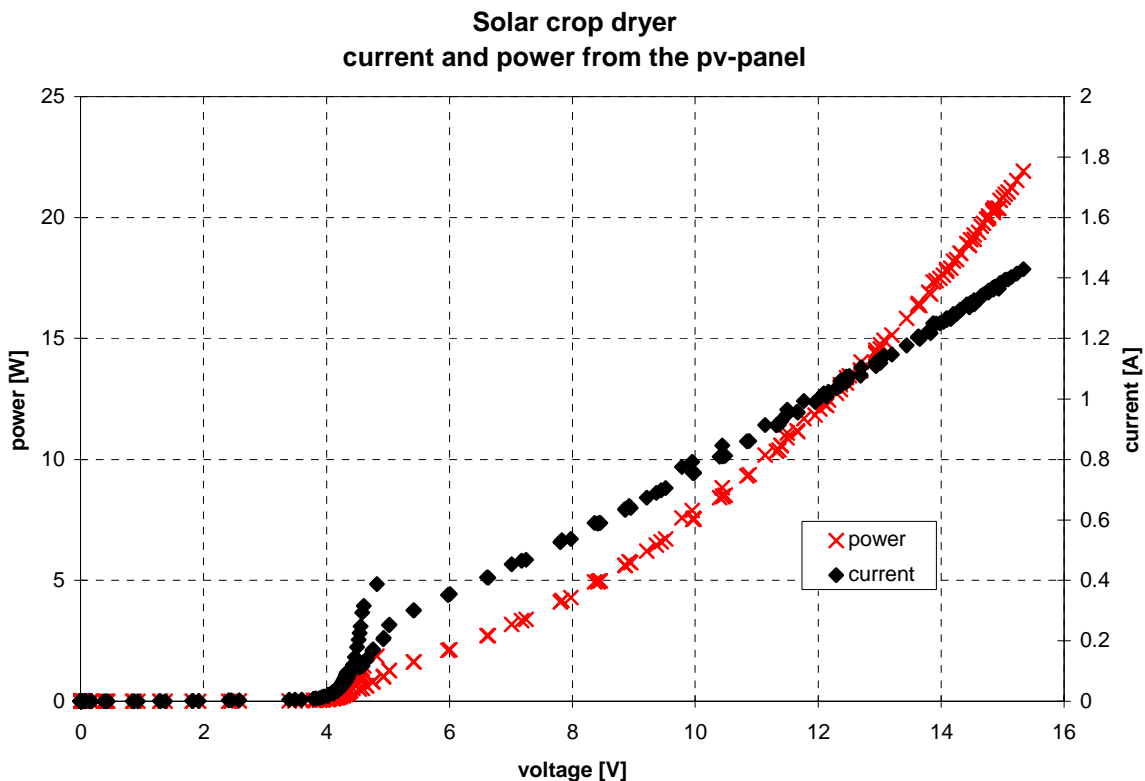


Figure 4.8. The relationship between voltage to the fan and the resulting current and power.

This means that the electronic control of the fan will overrule a traditional maximum power point tracker, which as mentioned earlier is used to maximise the energy production of PV-panels.

The problem with decreasing flow rate due to increasing ambient temperature shown in figure 4.7 is due to the fact that the max voltage from the PV-panels decrease with increasing cell temperature while the max current remain the same. This cannot (as explained) above be solved by adding more panels in parallel as this only will increase the available power but not

the voltage. A maximum power point tracker should, therefore, if excess power is available from the PV-panels be able to boost the voltage level up to a certain max level determined by what the fan is able to withstand (15 V). Or the control of the fan should be based on current rather than voltage, as this will give a more direct dependency on the radiation level.

4.1.4. Efficiency

Figures 4.1 and 4.5 shows rather stable conditions regarding the solar radiation and the air flow rate just after noon day 186 (July 4). Figure 4.9 further show that the efficiency of the collector also was rather stable during this period. The efficiency and flow rate from this stable period is in figure 4.10 compared with the two efficiency curves for the collector of the Summer House Package.

Figure 4.10 shows that the solar air collector of the dryer is as efficient as the collector of the Summer House Package for that particular air flow rate.

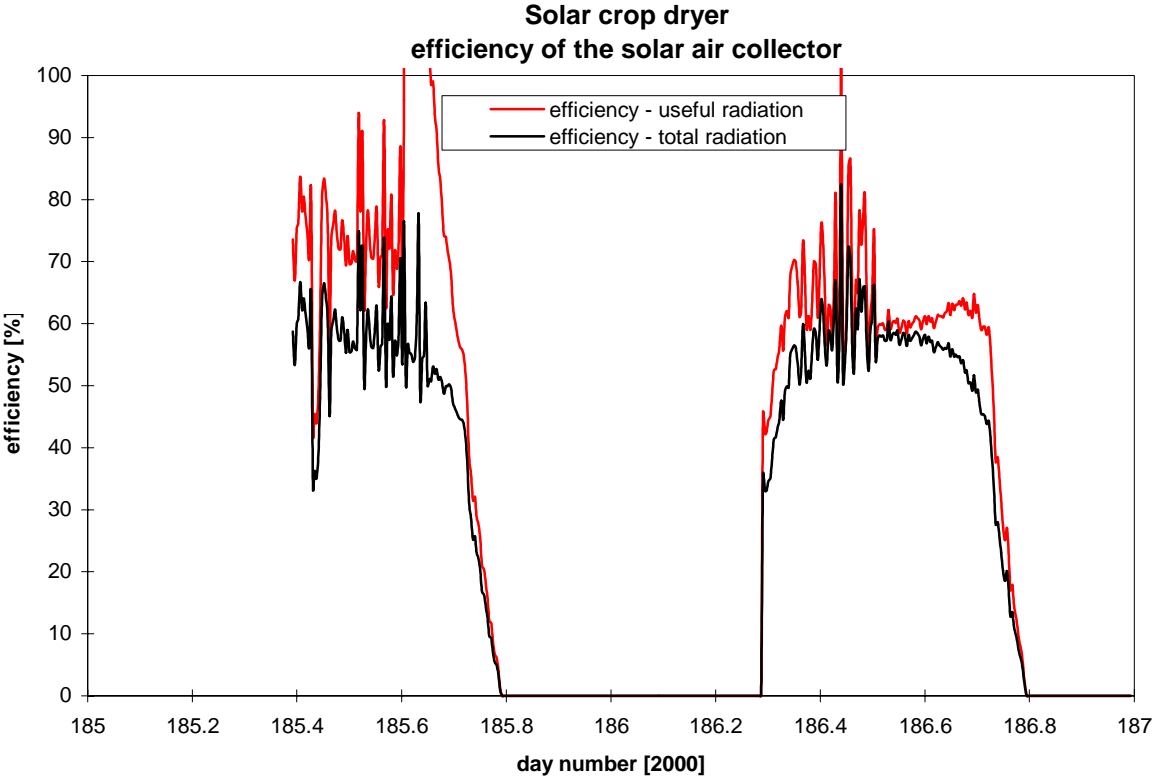


Figure 4.9. The efficiency of the collector dependent on either total or useful radiation.

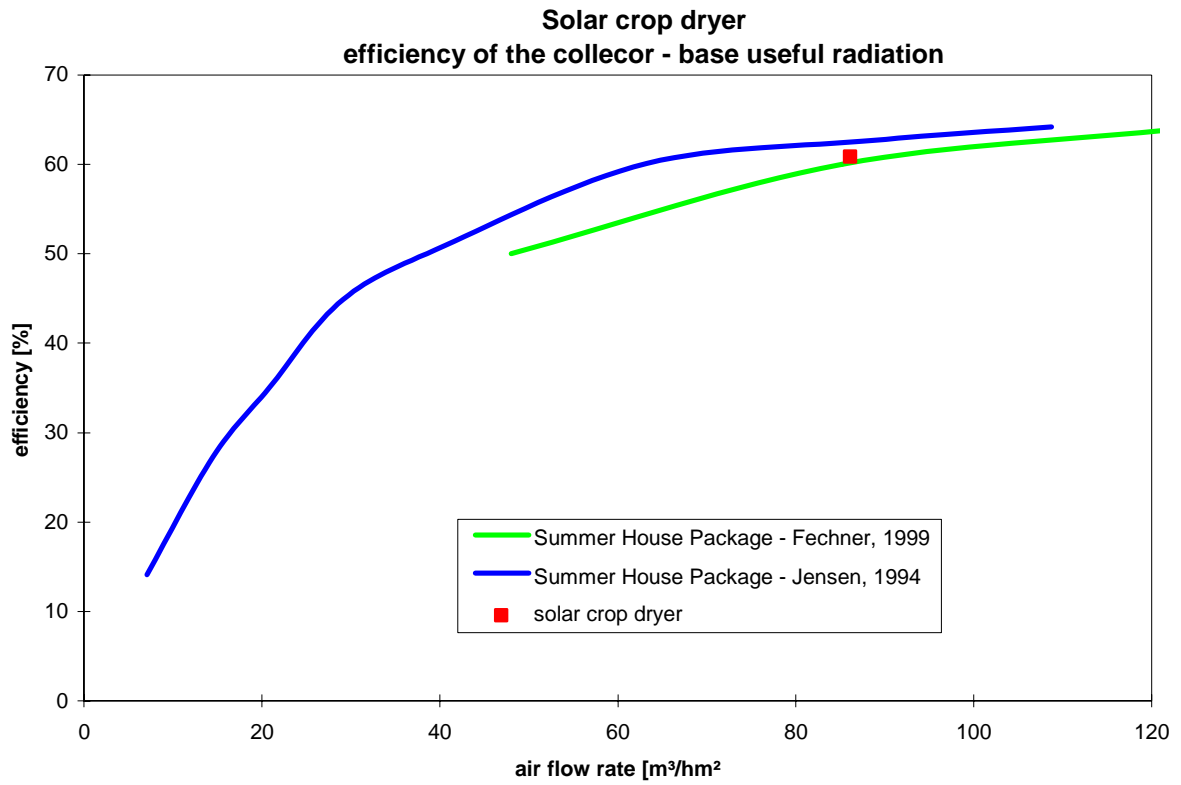


Figure 4.10. The efficiency based on the useful radiation during stable conditions compared with the efficiency of the collector of the Summer House Package.

5. Test with a filter in the inlets to the collector and with/without a maximum power point tracker

Two modifications were applied to the system prior to this test: a filter was mounted at both inlets to the collector and a maximum power point tracker was installed in-between the PV-panels and the fan.

No maize was dried during this test. The dry maize from the former test was left in the drying bed to create the right pressure drop across drying bed.

5.1. Filter

During the period December – February very fine dust is blown to Ghana from Sahara by the wind called the Hamatan. This very fine dust may by time totally block the absorber of the collector in the dryer. For this reason a filter system was constructed and installed on the solar air collector. The filters may easily be taken down and put up again in order to allow for the filters to be washed. The filters are as the absorber a fibre cloth.

Figure 5.1 shows the principle in the filter arrangement, while figure 5.2 shows a photo of the filter box. Figure 5.1 shows that the area of the filter is identical to the area of the PV-panels. However, in order to ensure a max cooling of the PV-panels by the incoming air, a baffle plate is located between the filter and the PV-panel, which forces the air to flush over the entire area of the PV-panel with a higher air speed.

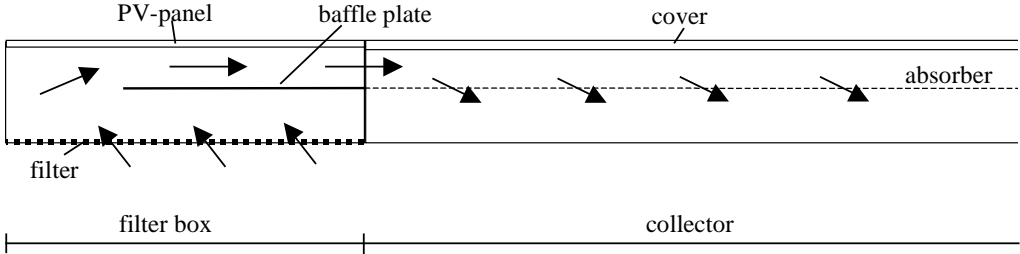


Figure 5.1. Principle drawing of the filter arrangement at both ends of the collector.

The filter boxes introduces an additional pressure drop in the system which will lead to a reduction in the air flow rate through the system. This is evaluated in the following.

5.2. Maximum power point tracker

During the first period July 18-28 no maximum power point tracker was installed while during the second period - July 29-August 8 - a maximum power point tracker (discussed in the previous chapter) was installed in-between the PV-panels and the fan. The maximum power point tracker was a traditional maximum power point tracker without the ability to boost the voltage to the fan if excess energy is available. The effect of the maximum power point tracker is evaluated in the following section.



Figure 5.2. Photo of one of the filter boxes.

5.3. Measuring results

The measuring data are in the following graphs divided in two series of graphs: one series for the period July 18-28 (day number 200-210) without the maximum power point tracker and another series for the period July 29-August 8 (day number 211-221) with the maximum power point tracker.

Figures 5.3-4 show the solar radiation and ambient temperature for the two periods. The weather condition was as shown in the two graphs rather similar

Figures 5.5-6 show the air flow rate through the system dependent on the ambient temperature while figures 5.7-8 show the air flow rate dependent on the useful solar radiation. Figures 5.5-6 shows as 5.3-4 a similar pattern for the two periods showing that the measuring results for the two periods may be compared directly.

In figures 5.5-6 it is seen that the max air flow rate of 410 m³/h is reached at an ambient temperature of about 23°C. When combining this with figure 4.7 figure 5.9 is obtained. It should be remembered that the result in figure 4.7 is rather uncertain due to the limited numbers of values it is based on – the same goes of the new value in figure 5.9 obtained with a filter in the inlets to the collector. However, figure 5.9 indicates that the filters reduce the air flow rate with about 10%. This of course increase the risk of over heating the crops, but the filters are necessary in order to prevent malfunction of the dryer due to blocking of the absorber by dust.

Figures 5.7-8 show the effect of the maximum power point tracker. The two graphs seem rather identical. An identical max air flow rate is reached for both periods as also see in figures 5.5-6. However, at start/stop (i.e. low radiation levels) differences are seen. The start/stop occurs around a radiation level of 50 W/m² without the maximum power point tracker but already around 35 W/m² with the maximum power point tracker.

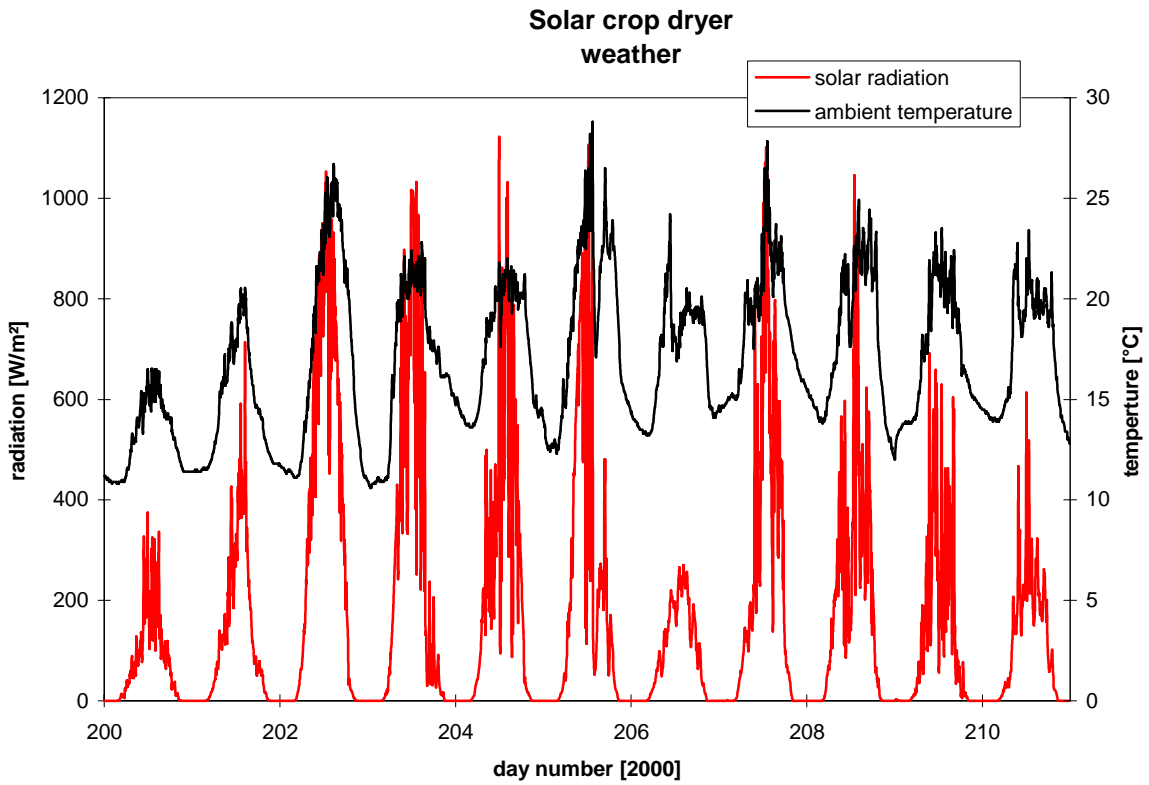


Figure 5.3. Solar radiation and ambient temperature during the period July 18-28.

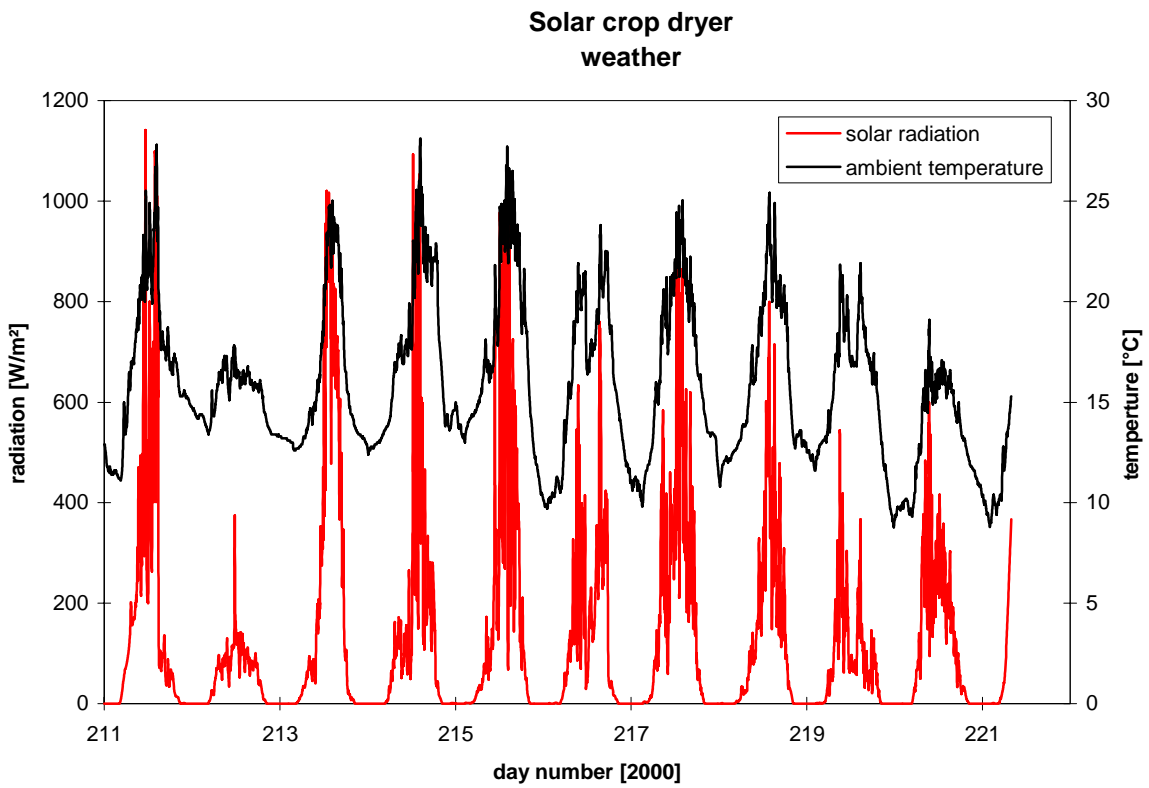


Figure 5.4. Solar radiation and ambient temperature during the period July 29-August 8.

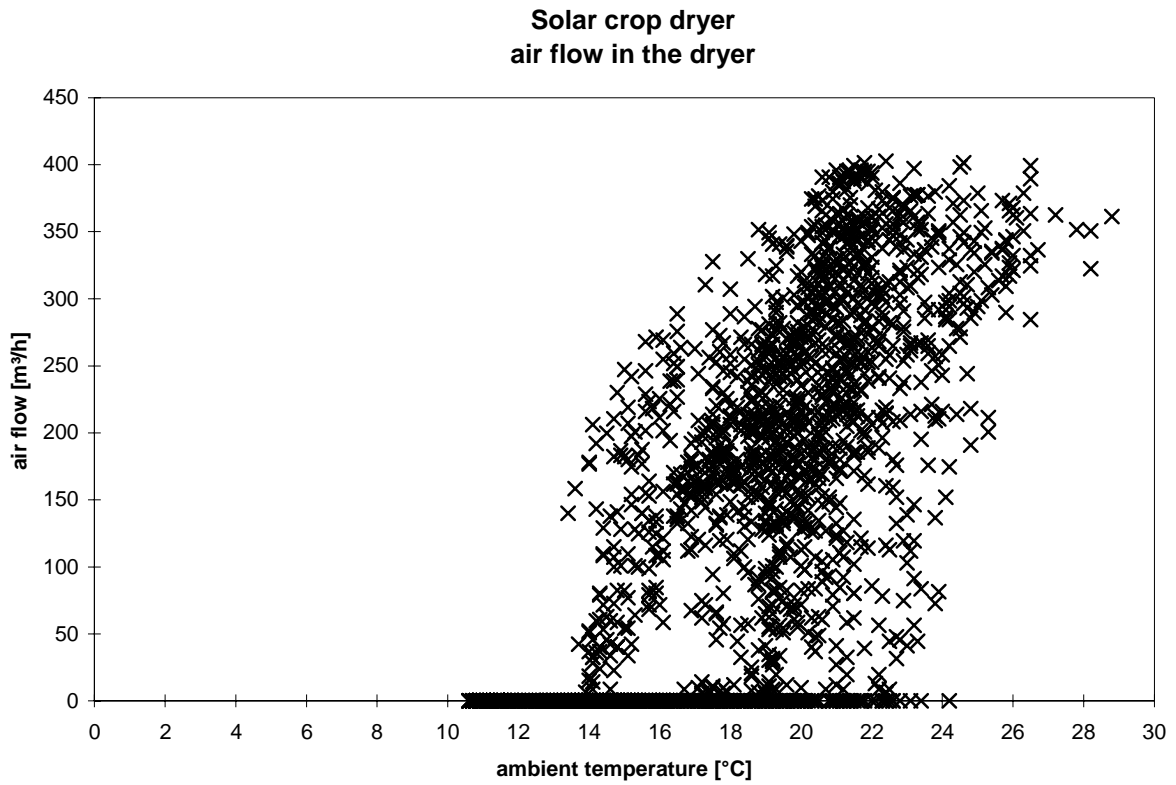


Figure 5.5. The air flow rate dependent on the ambient temperature during the period July 18-28.

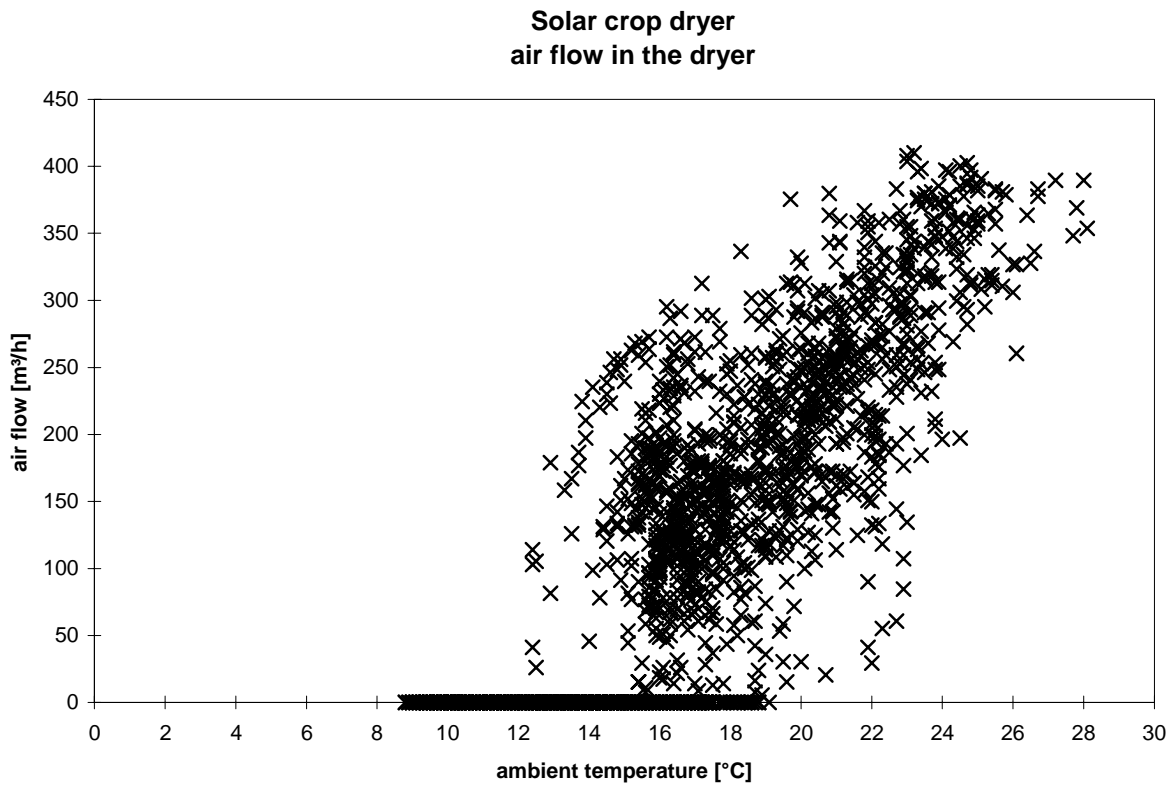


Figure 5.6. The air flow rate dependent on the ambient temperature during the period July 29-August 8.

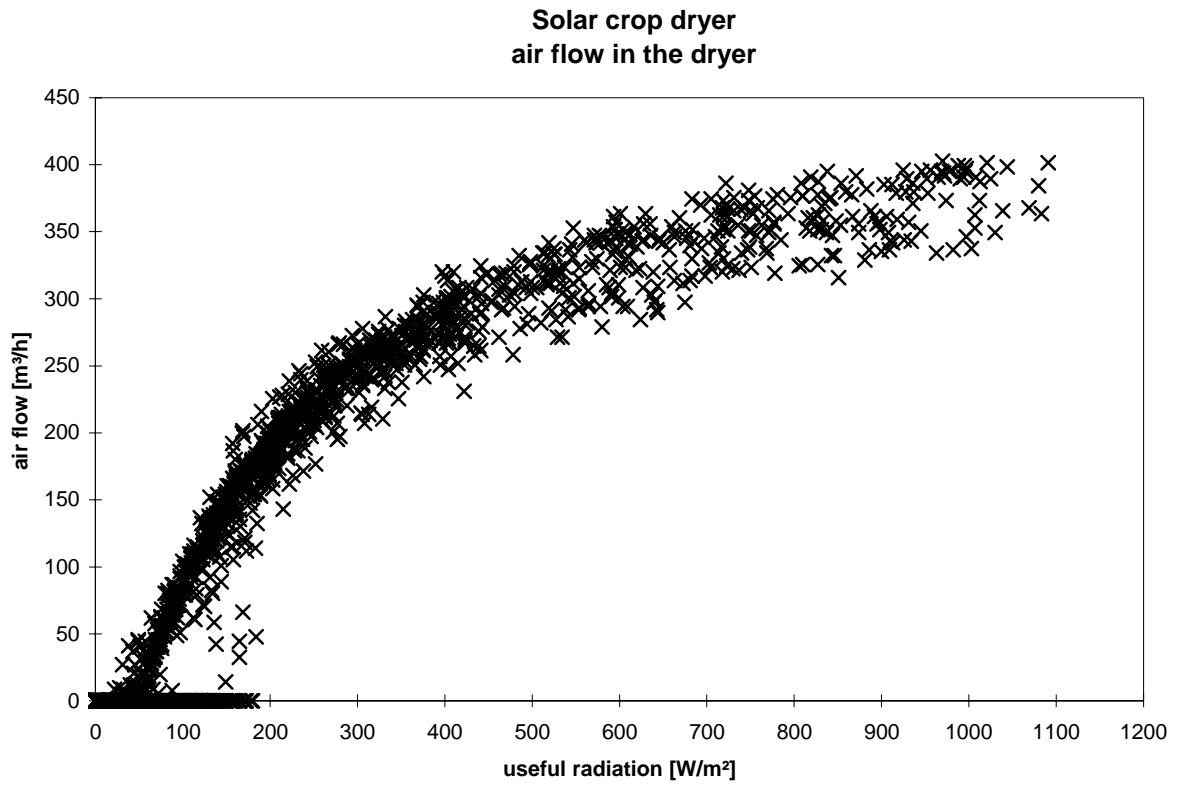


Figure 5.7. The air flow rate dependent on the useful radiation on the PV-panels for the period July 18-28 without the maximum power point tracker.

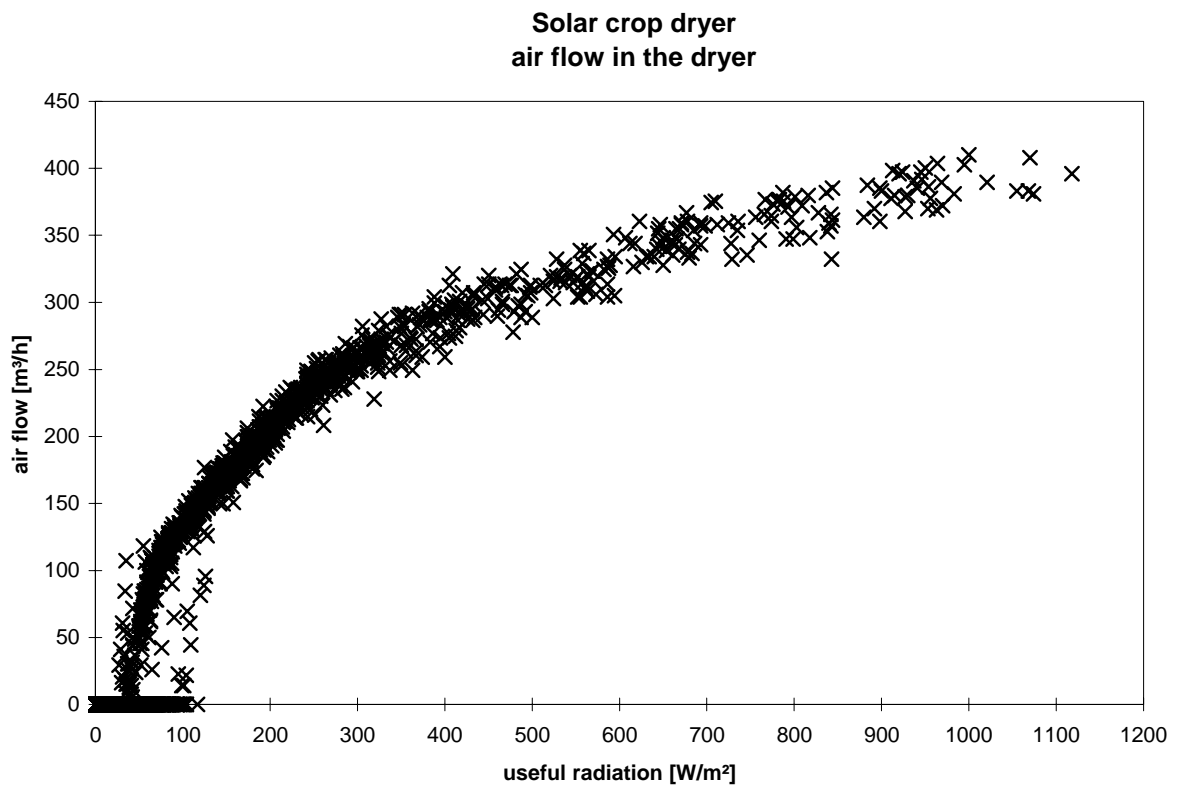


Figure 5.8. The air flow rate dependent on the useful radiation on the PV-panels for the period July 29-August 8 with the maximum power point tracker.

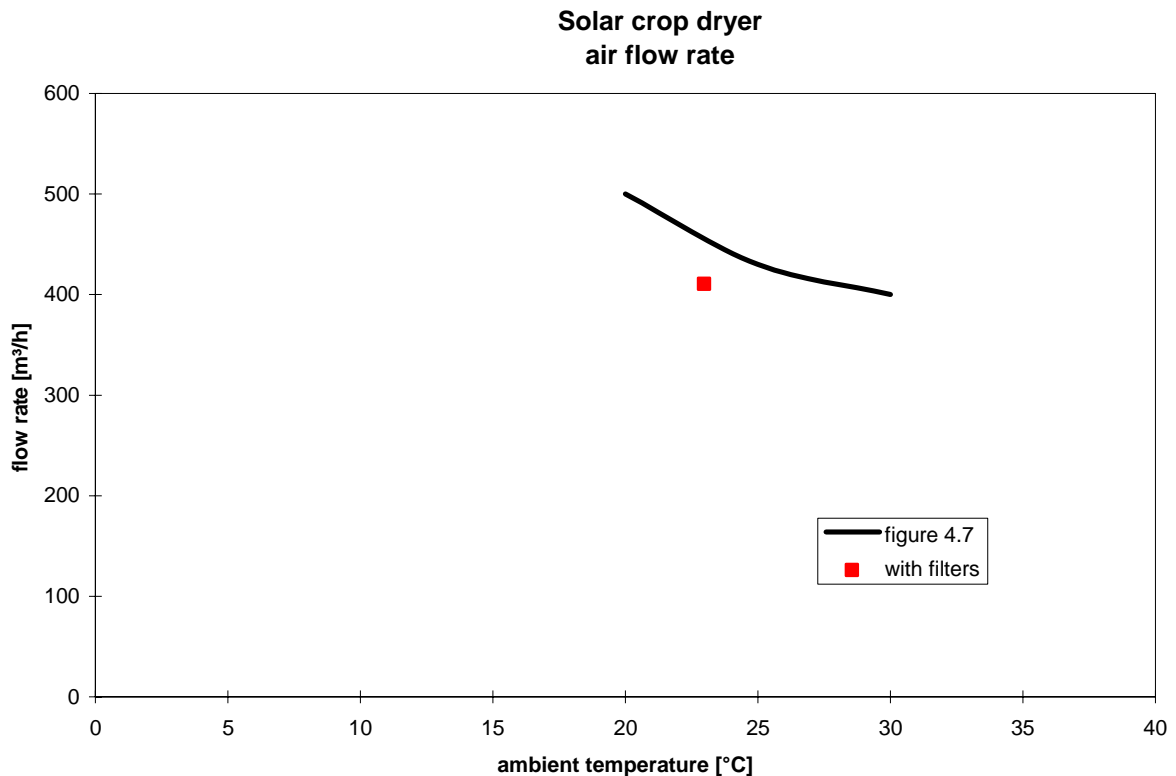


Figure 5.9. The max air flow rate dependent on ambient temperature showing the decrease in air flow due to the filters. However, the uncertainty is large due to a limited number of values.

The air flow rate further increases more rapidly with the maximum power point tracker than without. With the maximum power point tracker an air flow rate of 100 m³/h is reached at about 65 W/m² while it without the maximum power point tracker first is reached at a radiation level of 110 W/m². Figure 5.7 further shows air flow rates being zero up to a radiation levels of just below 200 W/m² this is with the maximum power point tracker (figure 5.8) reduced to just above 100 W/m². The graphs thus show that radiation levels below 200 W/m² is utilized better with a maximum power point tracker.

The conclusion that the maximum power point tracker has a positive influence at low radiation levels and none at high radiation levels is supported by the measured voltage, current and power to the fan as shown in figures 5.10-12. Figures 5.10-11 show the voltage and current to the fan with and without the maximum power point tracker (mppt) as a function on the total radiation on the PV-panels. There is only data available with the maximum power point tracker until before noon August 1. Figures 5.10-11 show a little higher voltage with maximum power point tracker at low radiation levels but especially that the fan starts earlier. The flat finger at the curve in figure 5.10 (at the green arrow) showing that the radiation level has to reach a certain level before the fan starts is nearly not present in figure 5.11.

Figure 5.12 shows a more or less identical amount of power to the fan dependent on the total radiation on the PV-panels, however, with a tendency to a bit higher power at low radiation levels with a maximum power point tracker.

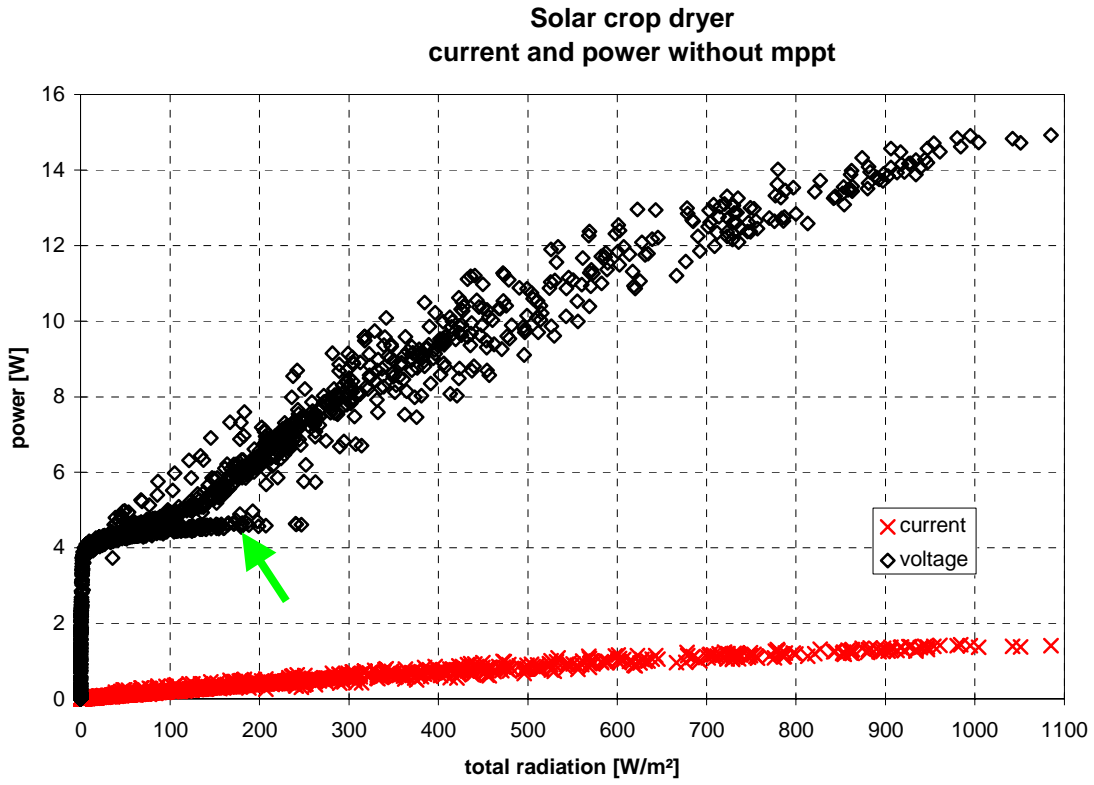


Figure 5.10. Voltage and current to the fan for the preiod without maximum power point tracker.

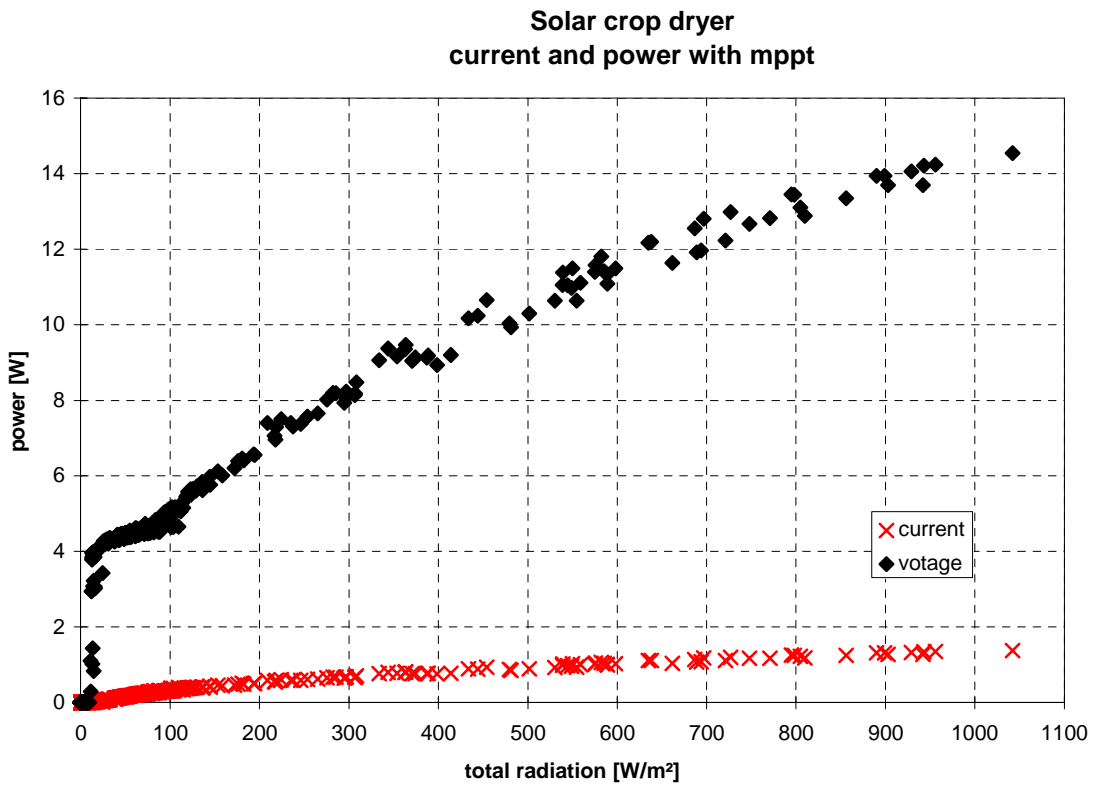


Figure 5.11. Voltage and current to the fan for the preiod with maximum power point tracker.

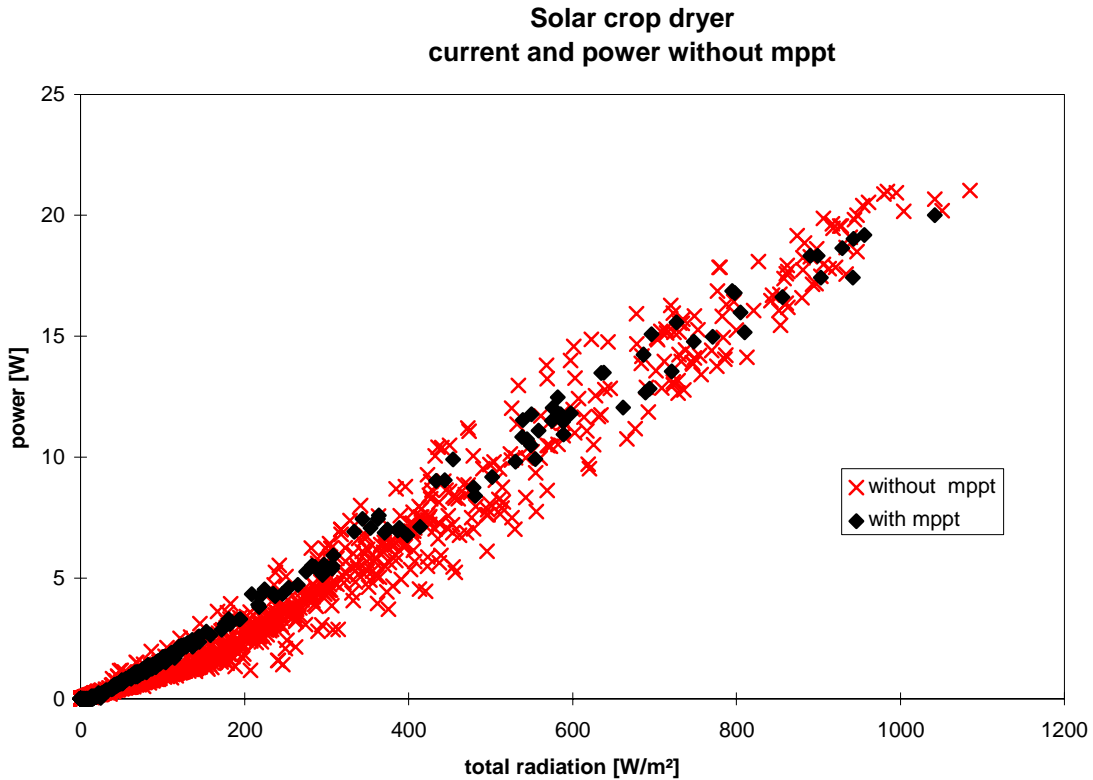


Figure 5.12. Power to the fan with and without maximum power point tracker.

The chosen maximum power point tracker has as seen a limited effect on the air flow rate in the system. In order to gain a higher effect it is necessary to introduce a more advanced maximum power point tracker as earlier mentioned which is able to boost the voltage level if excess energy is available from the PV-panels. This will increase the air flow rate at higher radiation levels especially at high ambient temperature levels.

5.3.1. Temperature of the air to the drying bed

Due to the reduction of the air flow rate the maximum temperature of the air to the drying bed did of course increase - to more or less the same level as before the pressure drop of the system was decreased in chapter 3. The maximum increase from ambient of the air to the drying bed is now again around 20 K at a solar radiation of 900 W.

6. Test with thermal mass in the pressure chamber under the drying bed

One modification was made to the dryer prior to the test. Thermal mass was added in the pressure chamber under the drying bed in the form of stones on a steel grill.

The reason for this test was that the temperature of the air to the drying bed may get too high due to the reduction of the air flow rate caused by the filters at the inlets to the solar air collector as mentioned in the former chapter. This may damage the seed. Thermal mass will to a certain extent even out the temperature swing of the air to the drying bed and in this way reduce the maximum temperature of the air to the drying bed.

The maximum power point tracker from the former chapter was also applied in the present test. There was dry maize in the drying bed.

6.1. Thermal mass

A steel grill was installed in the middle of the pressure chamber as illustrated in figure 6.1. Because of this the shape of the pressure chamber was changed – compare figure 6.1 with 2.1.

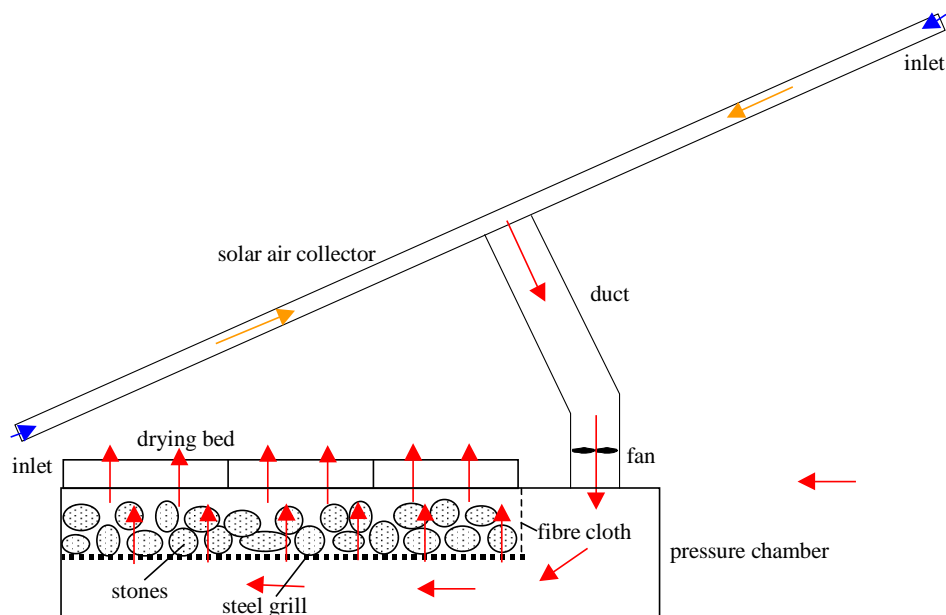


Figure 6.1. Principle drawing of the location of the thermal mass in the pressure chamber.

150 kg of stones was located on the steel grill in the pressure chamber. Figure 6.2 shows a picture of the stones.

The stones were located in such a way that the air flow was mainly below the layer of stones and then up through the stones in order to create a good heat transfer coefficient between the stones and the air. A fibre cloth identical to the filters at the inlets to the collector was located in front of the stones – as shown in figure 6.1 – in order to prevent opposite direction of the air flow in the system during night time due to the warm stones.



Figure 6.2. Picture of the stones in the pressure chamber.

6.2. Measuring results

The following graphs show the results obtained from two warm sunny days in August – August 26-27 (day number 239-240).

Figure 6.3 shows the solar radiation and ambient temperature for the two days. Figure 6.4 shows the maximum flow rate through the system dependent on the ambient temperature. The maximum flow rate from figure 5.9 is also shown. Figure 6.4 shows that the reduction in air flow rate compared to the system without filters are more or less the same as in the previous chapter. This shows that the stones and the fibre cloth don't introduce a pressure drop of importance.

Figure 6.5 shows the temperature increase of the air to the drying bed compared to the ambient temperature. A black x is a value from August 26, while a red square is a value from August 27. Figure 6.6 shows the same for July 4 (day number 186) which was a day with rather stable clear sky conditions as shown in figure 4.1. The arrows in the figures show the heating up and cooling down of the air in the dryer: a red arrow is warming up, while a blue arrow is cooling down.

Figures 6.5 and 6.6 show very different patterns. While the pattern of the curve for heating up and down without stones is very similar the pattern of the curve for heating and cooling down in figure 6.5 is very different. This is because heat is stored in the stones. Smaller peak values are, therefore, experienced in the system with the thermal mass. The maximum increase from ambient of the air to the drying bed is now again down around 16 K at a solar radiation of 900 W. The thermal mass thus has a positive effect on the maximum temperature of the air to the drying bed.

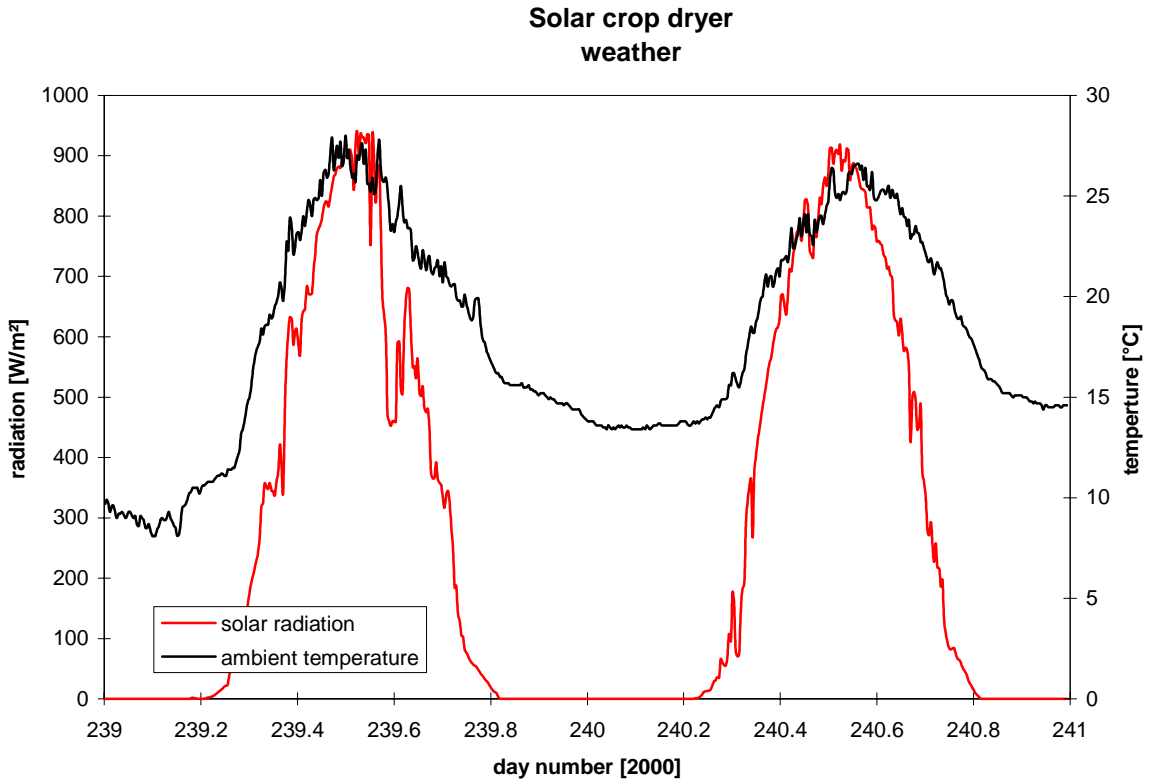


Figure 6.3. Solar radiation and ambient temperature during the period August 26-27.

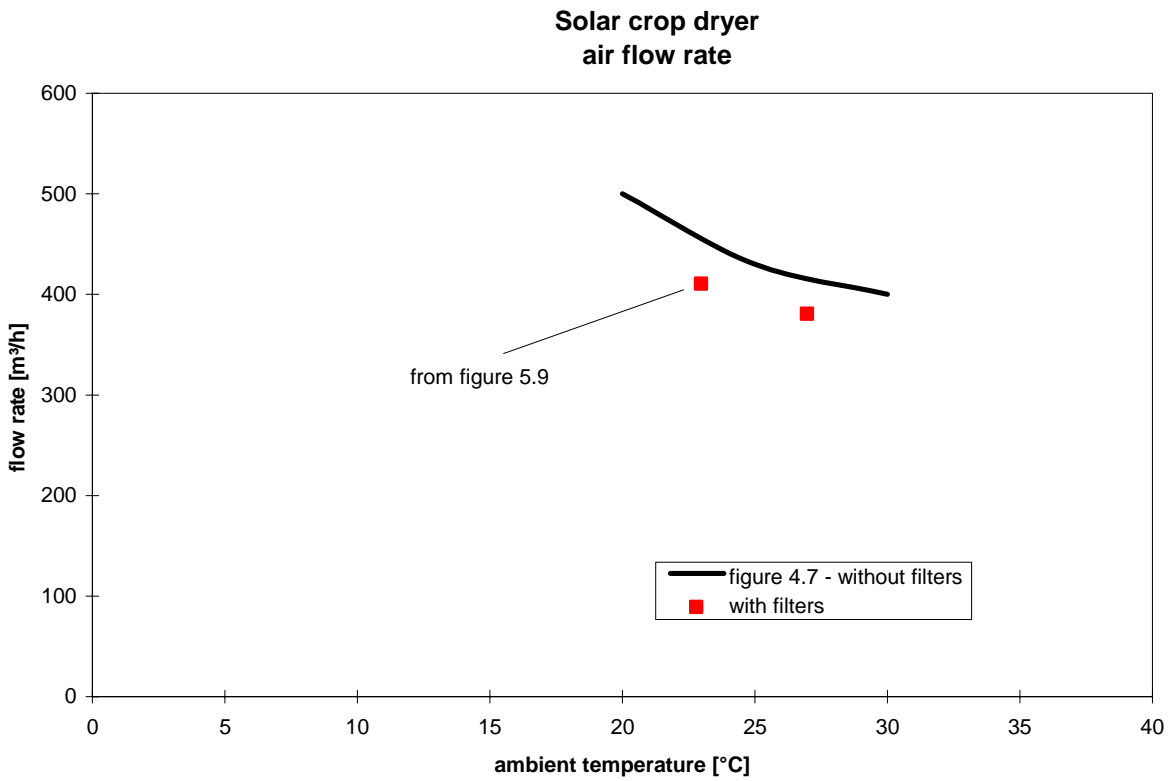


Figure 6.4. The max air flow rate dependent on ambient temperature for the system with filters in the inlets compared to a system without filters.

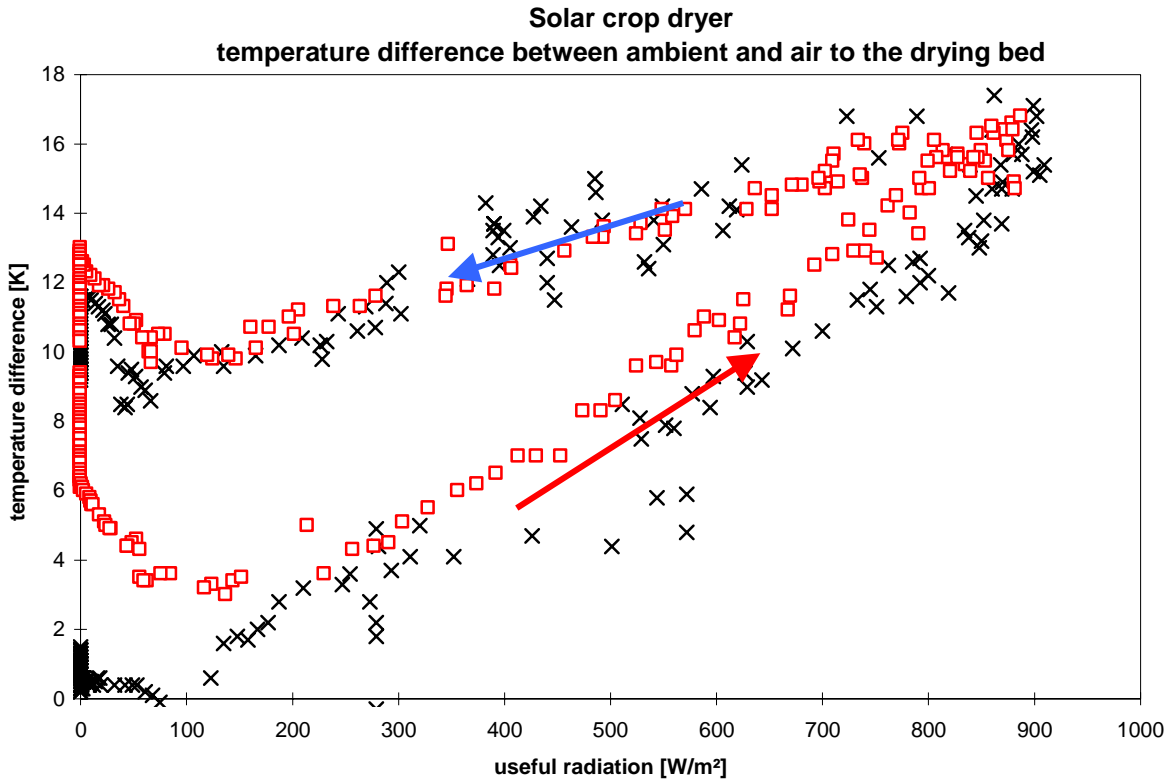


Figure 6.5. The difference between the air temperature to the drying bed and the ambient temperature dependent on the useful radiation for the period August 26-27.

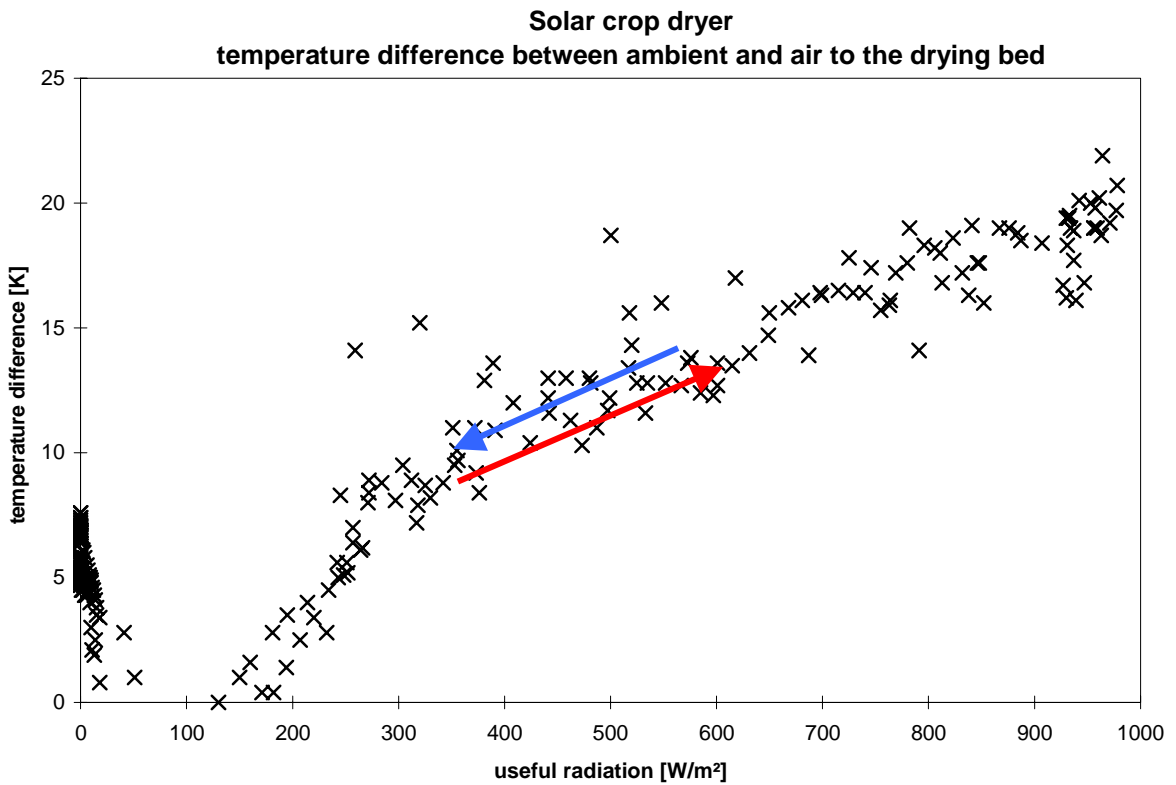


Figure 6.6. The difference between the air temperature to the drying bed and the ambient temperature dependent on the useful radiation for Juli 4.

The curves for the two days in figure 6.5 show a different pattern in the morning. This is because the stones were put in during August 25 and not heated prior to the night between August 25 and August 26.

The difference in patterns between heating up and down in figure 6.5 is a picture of the heat store in the stones. The difference in temperature level of the stones between sunset and dawn (around 100 W/m^2) is around 7 K ($10 - 3 \text{ }^\circ\text{C}$ for August 27). This illustrates the heat lost during the night – heat which really does not participate in the drying of the maize as no air stream through the maize is present during the night. Heat which else could have been used during the day to dry maize. This capacity loss can be estimated.

The heat capacity of stones is about 0.9 kJ/kgK . With 150 kg of stones and a temperature drop of 7 K this leads to a capacity loss of approximately 0.26 kWh .

During daytime the collector delivered 12.2 and 13.7 kWh by the air to the drying bed (after the stones) for the two days August 26 and 27 respectively. This means that the capacity loss is about 2% . This is not a great loss to pay considering the reduced risk of damaging the seed.

6.2.1. Heat losses from the ductworks

The heat loss from the ductworks has as yet not been considered. At first because the ductworks was made of 12 mm plywood which has an insulating effect. However, as part of lowering the pressure losses in the system the wooden ductworks was partly replaced by metal ducting without this insulating effect.

For the two days considered here the energy from the collector to the drying bed (after the stones) was measured to be 12.2 and 13.7 kWh as mentioned above. However, for the same periods 17.7 and 18.6 kWh was delivered from the collector to the ductworks. This means a loss of 31 and 26% . Less than one half of the losses is due to the ductworks while the rest is due to the heat losses in the pressure chamber and heat stored in the stones as seen in figure 6.7. The rather high heat loss in the drying chamber in the morning is of course due to the heating up of the stones. However, without the stones the losses over the pressure chamber is still a bit higher than over the ductworks as seen in figure 3.10. In figure 3.10 there is no peak loss in the morning because of the lower thermal mass here.

If the heat loss was reduced the drying capacity of the dryer would increase but so would the risk of overheating the seed. The dryer should, therefore, either be equipped with movable insulation on the ductworks or better with a control system, which could lead ambient air into the hot air stream when the temperature to the drying bed gets too high. Both solutions are expensive – the first is expensive in manpower, while the other demands a thermostatic regulated damper. The first solution may be chosen later by the owner of the dryer, while the latter is for future further development of the concept.

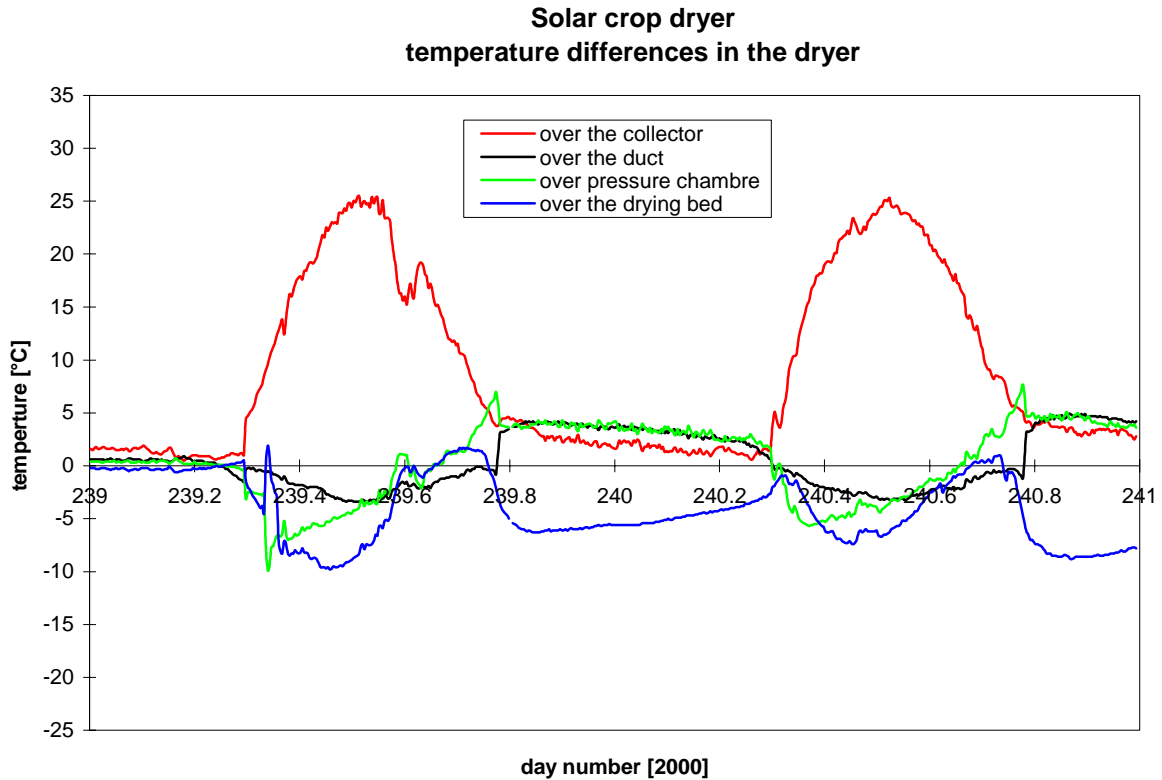


Figure 6.7. Temperature differences in the system.

6.2.2. Efficiency

The weather conditions were as shown in figure 6.3 rather stable. So stable that it was possible to determine a steady state efficiency comparable to the one shown in figure 4.10. Figure 6.8 shows the found efficiency together with the efficiency from 4.10 and the efficiency of the collector of the Summer House Package.

Figure 6.8 shows that the collector is as efficient as the collector of the Summer House Package. The latter collector is one of the most efficient solar air collectors on the market today (Fechner, 1999).

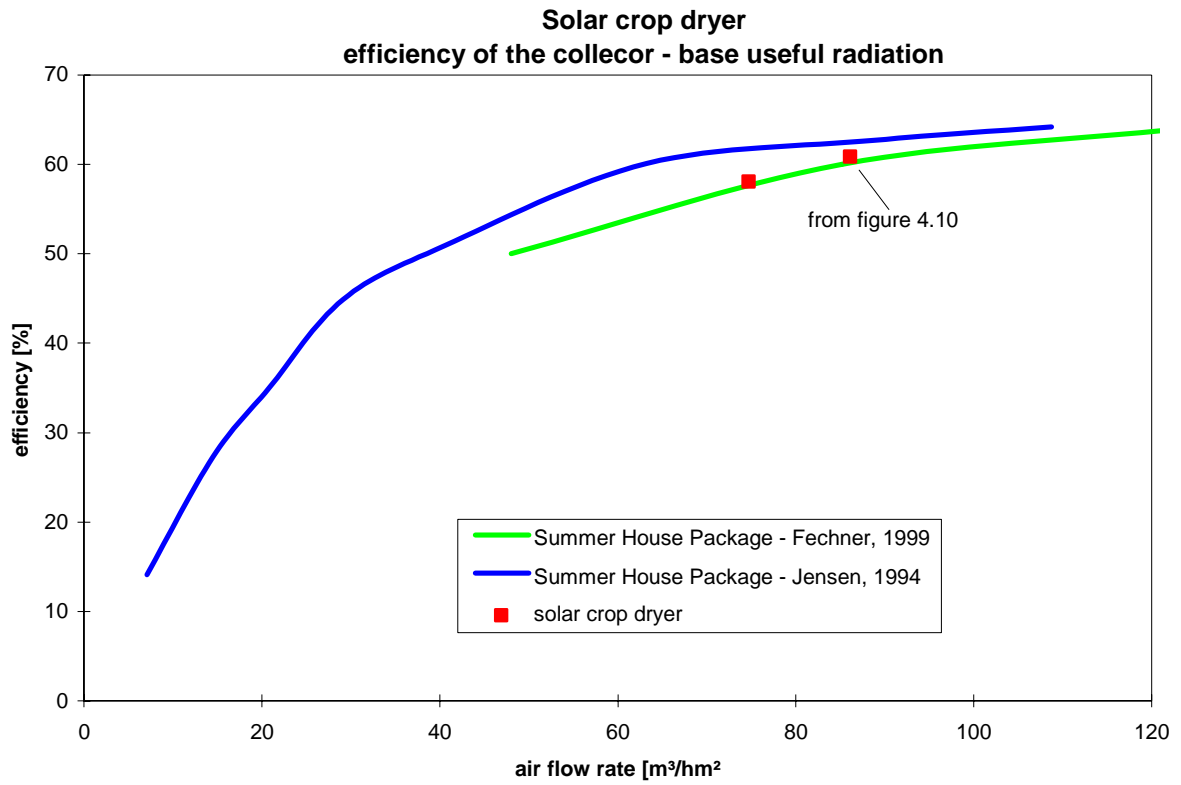


Figure 6.7. The efficiency based on the useful radiation during stable conditions compared with the efficiency of the collector of the Summer House Package.

7. Economical considerations

The chapter contains some preliminary economical considerations regarding the solar crop dryer. The solar crop dryer is compared with conventional maize drying plants in Ghana. The calculations are based on estimates of costs, capacity and thermal performance of the prototype solar crop dryer as shipped to Ghana. The calculations are the first attempt to evaluate the economy of the solar crop dryer. Several of the used parameters are, therefore, very uncertain and should not be regarded as the final truth of the economical benefit of the solar crop dryer.

The solar crop dryer is here compared with the existing batch grain dryer at Silwood Farms. The Silwood Farms dryer is of a type commonly used in Ghana. The used data on capacity, energy consumption, etc., for the dryer is in accordance with information received from the manager at Silwood Farms.

The dryer consists of a container, which may hold about 2 tonnes of maize as a maximum. Normally, about 1.4 tonnes of maize is filled into the plant. Heated air is blown into the container by means of a fan. The air is pressed up through the maize via a distributing chamber at the bottom of the container. The fan is run by a diesel engine, and the drying air is heated by means of a directly fired kerosene burner. The Silwood Farms dryer is shown in figure 7.1.



Figure 7.1. The batch dryer at Silwood Farms used for drying of maize

The solar crop dryer used for the economic comparison is the plant described in the previous paragraphs. In table 7.1 some basic data for the two drying plants are given.

The capacity of the solar crop dryer is indicated for a drying plant with eight sections, each with a capacity of about 120 kg. The maize is expected to be dried within two days. The investment costs for the solar crop dryer are based on the Danish price, which amount to a total

of US\$2,000 per section. To this must be added local costs, such as labour costs, costs for pouring of base and floor, costs for erection of the dryer, etc. The local costs are estimated to be US\$2,000 for a drying plant with eight sections. The initial costs of a solar crop dryer are thus estimated to be US\$2,250 per section, corresponding to a total cost of US\$18,000 for eight sections.

At Silwood Farms the conventional dryer is filled with about 1.4 t of maize. After three hours of drying a moisture content of 18% will be obtained, after which threshing will take place. On subsequent drying for three hours, a moisture content of about 14.5% will be obtained. Hereafter the maize will be cleaned and dried again for six hours to achieve a final moisture content of 10.5%. This procedure is estimated to last two working days of eight hours, corresponding to a capacity of 700 kg/day. Introducing twenty-four-hour production (2.1 t/day) can however, triple the capacity, but this would involve additional costs of US\$8 per night for operation of generator, etc. Also a bit higher energy consumption per tonnes of maize will occur due to low air temperature and high air humidity during the night period.

The approximate purchase price of the conventional dryer at Silwood Farms is quoted to be 15 mill. Cedi, or about US\$2,000.

Plant	Units	Solar crop dryer	Silwood Farms
Capacity	kg/day	500	700
Initial costs	US\$	(uncertain, about 18.000)	2.000
Annual interest rate	%	30 (36) ¹	30 (36) ¹
Annual inflation	%	18 (29.9) ¹	18 (29.9) ¹
Annual real interest rate	%	10.2 (4.7) ¹	10.2 (4.7) ¹
Depreciation/lifetime	years	15	15
Running costs	US\$/t		
Energy		0	14.18 ²
Labour ³		11.0	7.9
Annual maintenance costs	US\$	3 ⁴	80
Increased value on sun drying	US\$/t	0–100 ⁵	0

¹ The figures in brackets indicate values from the end of 2000. The other figures indicate expected values for 2001. Interest is the short-term inter-bank rate. Source: Economist Intelligence Unit, Ghana.

² 3.2 l of diesel (US\$0.21/l) and 48 l of kerosene (US\$0.40/l) is needed to dry 1,400 kg of maize.

³ At Silwood Farms 10 workers are occupied with the operation of the plant. A similar occupancy rate is expected for sun drying (daily wages: US\$0.55).

⁴ 1 worker for 1 week.

⁵ The solar crop dryer is suitable for drying of maize for seed grain. The price of maize for seed is US\$27/hkg and maize for consumption US\$17/hkg.

Table 7.1. Key figures for the plants. All prices are in US\$. For conversion of Cedi into US\$ the following exchange rate has been used: 1 US\$ = 6500 Cedi.

Table 7.2 shows the drying costs involved with the solar crop dryer in proportion to the costs involved with the existing drying plant at Silwood Farms. The costs are allocated as fixed and running costs. The comparisons that are shown in this table are only valid when the solar crop dryer are used for drying of maize within the traditional maize drying season. Therefore, see also table 7.3 where comparisons for other assumptions are made.

Capacity data	Units	Solar crop dryer	Silwood Farms
Working hours	days/year	50	50
	h/day	8	8
	hours/year	400	400
Capacity	kg/day	500	700
	t/year	25.00	35.00
Financial data			
Real interest rate	%	10.2	10.2
Depreciation period	year	15	15
Capital gain factor	%	13.27	13.27
Fixed costs			
Initial cost	US\$	18,000	2,000
Total capital costs	US\$/year	2,389	265
Capital costs/running hour	US\$/h	5.97	0.66
Capital costs/t	US\$/t	95.58	7.59
Running costs			
Wages	US\$/t	11.00	7.86
<i>Energy</i>	US\$/t	0.00	14.18
<i>Maintenance</i>	US\$/t	0.120	2.286
Total running costs	US\$/t	11.12	24.32
Total costs			
	US\$/t	106.70	31.91

Table 7.2. Comparison between sun drying plants and conventional maize drying plants in Ghana

For the calculations in table 7.2 to be valid, both plants must be used for 50 days a year, corresponding to one month in the major harvesting season from August to September and 20 days in the minor harvesting season from January to February. The calculations are based on the expected inflation and interest rates for 2001. However, when using the real interest rate rather than the interest rate it is assumed that the inflation is identical for all parameters of the calculation – materials, components, labour and maize – this introduce an uncertainty.

Under the conditions in table 7.2 the additional price involved with sun drying will be US\$74.79/t. This extra cost must be seen in proportion to the increased prices up to US\$100/t that might be obtained from sun dried maize for seeds compared to the price for maize for consumption. Silwood Farms produces both maize for seed and maize for consumption. To make the solar crop dryer profitable under the assumptions made in table 7.2 the production of maize for seed must, therefore, be increased.

If the values for capital costs, interest and inflation from the end of 2000 are used, the costs of sun dried and conventionally dried maize would amount to US\$79.07/t and US\$29.72/t, respectively, corresponding to an additional price of US\$49.35/t for sun drying. If the solar crop dryer could be financed by means of loans from the International Bank for Reconstruction and Development, the real interest rate might be zero. In that case the drying cost involved with solar crop dryers would be only US\$59.12/t

In the case of 24-hour operation, the capacity of the Silwood Farms plant would be increased by a factor 3. Thereby, the annual capacity would be increased by up to 105 t, and the drying costs would amount to US\$29.14/t, given that the costs of wages per tonne of maize would be the same, and that the lifetime of the dryer and the maintenance costs would remain unchanged. The costs would only drop slightly, because of the additional expenses on generator operation during night periods (US\$8/night).

If only the operating costs are considered, the costs involved with sun drying would in any case be lower than what is seen for the drying plant presently in use at Silwood Farms. Under the given circumstances, the actual running costs will be US\$11.12/t in the case of sun drying, which is US\$13.20/t less than for conventional drying.

The relatively high fixed costs per tonne involved with the solar crop dryer are due to a low annual capacity in relation to the invested capital. If the plant is used for drying other crops, e.g. chile pepper or fruit, the annual capacity may be increased, and the fixed costs per tonne of maize may then be reduced. If the sun drying plant is used e.g. 300 days per year, the total cost will be only US\$26.95 per tonne, and the costs will thus be very competitive. The importance of the number of operational days per year is shown in figure 7.2.

The curve for the Silwood Farms dryer is only indicated for a period of maximum 50 operational days per year. This is due to the fact that the dryer is constructed for drying of grain and unfit for drying of alternative products, such as fruits and vegetables due to the direct burning of kerosene in the drying air. The kerosene leaves taste and unhealthy combustion waste products in the food.

There may be some uncertainty as to the price of sun drying plants. Figure 7.3 shows the possible investment rates for solar crop driers at different drying volumes, if they are to compete with the drying plant at Silwood Farms. The assumptions are the values stated in table 7.1. The values for capital costs, interest and inflation are the values expected for year 2001.

Figure 7.3 shows that if no additional price for sun dried maize can be obtained, and provided that 60 t of maize are produced every year, investment costs of about US\$7,600 will be maximum in order to obtain the same income as would be obtained from the conventional plant. Providing an additional price of US\$100/t could be obtained, an annual investment of about US\$19,300 would be sufficient for drying as little as 20 t/year in a sun drying plant with a daily capacity of 500 kg. At the given investment of US\$18,000, the costs involved with sun drying at annual capacities of 10, 20, 40 and 60 t would be US\$250, 131, 71 and 51/t, respectively. Compared with conventional drying, the additional costs would likewise be US\$194, 91, 40 and 23/t, respectively, as shown in figure 7.3.

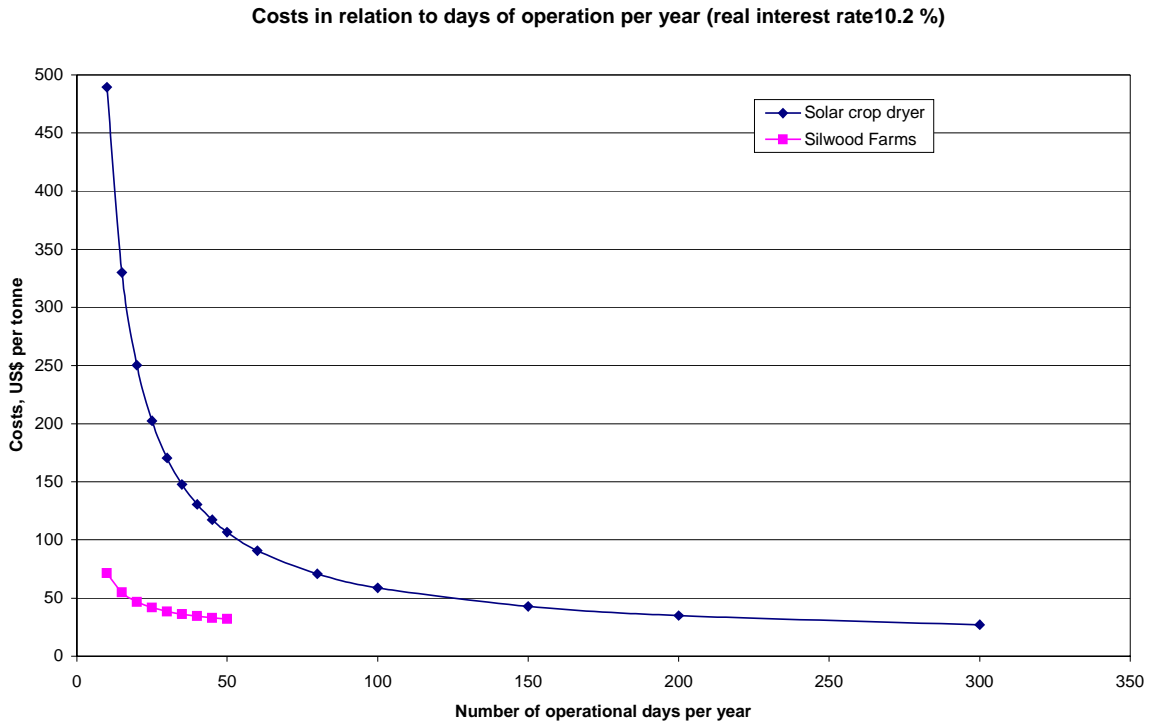


Figure 7.2. Expenses per tonne in relation to the number of operational days per year.

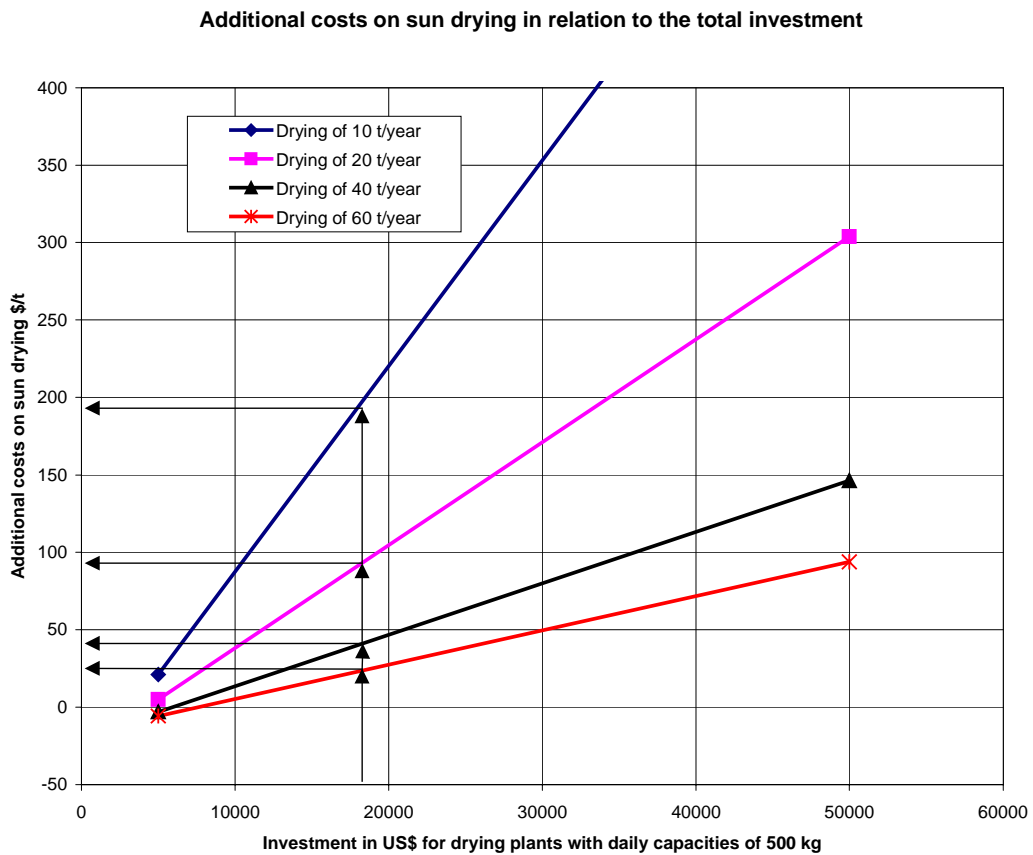


Figure 7.3. Additional costs on sun drying in relation to the total investment in a solar crop dryer of different annual capacities.

As it appears from the above-mentioned calculations, even minor changes in assumptions with regard to operational days, investment, inflation, interest rate, etc., will have a strong influence on the cost comparison. Table 7.3 shows the calculations results obtained from a comparison between the solar crop dryer and the conventional Silwood Farms maize drying plant in the case of changed, but still realistic assumptions.

It is here assumed that the solar crop dryer is used for drying of other products as well as maize. The total number of operational days per year are set to 150. If more solar crop dryers are to be produced, the Danish manufacture assume that the production costs of the plant can be reduced with 25 %. This is taken into account in table 7.3. It is hope that the price of the solar crop dryer may further be reduced when produced in Ghana. The Ghanaian partner DENG Ltd has been able to reduce the price of a solar water heater with one third compared to the price when produced in Denmark. The values for capital costs, interest and inflation from the end of 2000 are used. Increased energy prices are expected in Ghana. The stated calculations are based on a 50% increase in diesel and kerosene prices.

Capacity data	Units	Solar crop dryer	Silwood Farms
Working hours	days/year	150	50
	h/day	8	8
	hours/year	1200	400
Capacity	kg/day	500	700
	t/year	75.00	35.00
Financial data			
Real interest rate	%	4.7	4.7
Depreciation period	year	15	15
Capital gains factor	%	9.44	9.44
Fixed costs			
Initial cost	US\$	13,500	2,000
Total capital costs	US\$/year	1,274	189
Capital costs/running hour	US\$/h	1.06	0.47
Capital costs/t	US\$/t	16.99	5.39
Running costs			
<i>Wages</i>	US\$/t	7.86	7.86
Energy	US\$/t	0.00	21.27
Maintenance	US\$/t	0.040	2.286
Total running costs	US\$/t	7.90	31.41
Total costs			
	US\$/t	24.88	36.81

Table 7.3 Comparison of drying costs at a high utilisation rates for the solar crop dryer and increased energy costs

Under the above-conditions and assumptions the costs of sun dried and conventionally dried maize would amount to US\$24.88/t and US\$36.81/t, respectively, corresponding to a cost sav-

ing of US\$11.92/t when using sun drying. It is thus seen that the solar crop dryer might be very competitive to conventional drying.

The method of using solar energy further has the advantage of being independent to supply of electricity and fuel. This enhanced operational reliability compared to conventional crop drying technology is difficult to convert into money, but it certainly offers great advantages.

7.1. Conclusion

The above-calculations show that the solar crop dryer will be economical feasible under different sets of realistic assumptions. The main parameters determining the economy for the solar crop dryer is the price of the dryer, how much it is used and if the drying in the solar crop dryer will add value to the crops compared to the drying methods used today. The uncertainty of these parameters are, however, rather high as indicated above. The economy of the solar crop dryer can, therefore, first be determined when the dryer has been tested in Ghana and when the marked price for the dryer in Ghana has been found.

To the above considerations should be added the following considerations of major importance: that the oil prices most probably will increase more rapidly in the future due to a beginning shortage of oil, that an energy system based on solar energy thus is more stable than when based on fossil fuel and that an energy system based on solar energy is without pollution in the running phase.

8. Conclusion

Based on a survey in Ghana it was decided to develop a dryer for drying of maize for seed as the increase in value of the crop due to the drying here would be high – the dryer may, however, also be used to dry other crops or other items – one unit will e.g. be erected in Ghana to test drying of fish. The capacity of the dryer was defined to be 600 kg having a collector area of approx. 24 m². It was decided to let the dryer consist of 5 separate units each with a transparent collector area of 4.77 m² and a capacity of approx. 120 kg. The modulized concept has several benefits: If one drying bed is operated improperly this will not affect the total quantity of crops being dried at that time. It is possible to dry different crops (creating different pressure drop) side by side without risking that the crop with the highest pressure drop will be dried improperly. Small dc fans are often cheaper than larger dc fans. The system will be less complex, and an even air distribution over the drying bed is easier obtainable. Finally it is possible to start with only one unit and then gradually increase the capacity of the solar dryer - this will make it easier to invest in a solar dryer.

It was further decided that the fans of the dryer should be powered directly by PV-panels in order to make the dryer independent of an often unreliable, missing or expensive grid. Direct PV-control of the fan is beneficial when a solar collector delivers the heat to the dryer, as the fan will run at high speed at high irradiation levels where the collector is able to deliver much heat, while the fan will run at low speed at low irradiation levels where the collector only is able to heat the air stream a little. This means that the amplitude of the temperature of the air to the drying bed is lower than with a fixed air flow rate.

The main problem with a PV powered solar crop dryer is the fan: the fan should be inexpensive, durable and produce high flow rates at a high pressure while having a low power consumption in order to keep the price of the solar crop dryer down and at the same time ensure an efficient drying process.

In order to limit the necessary size of the PV-panel the flow rate through the crop was decreased considerably compared to conventional dryers. With an air flow in the design case of 300 m³/h per unit the air speed through the drying bed was 0.06 m/s. This is very low compared to the 0.3-0.7 m/s in conventional cross flow dryers and also low compared to the 0.1 m/s in conventional platform dryers. However, a rapid drying process can be obtained despite the low air speed because of a rather thin layer in the dryer.

The dryer is going to be erected and tested at Silwood Farms situated close to Accra. Silwood Farms has total land acreage of 210 acres where 176 acres are used for cultivating maize - the rest is used for growing pineapples. A majority of the maize is processed into seed. The main harvest season for maize at Silwood Farms is August/September with a smaller harvest period in January. During the rest of the year other crops may be dried in the solar crop dryer.

However, before shipping the solar crop dryer to Ghana one unit was tested in Denmark in order to test any malfunction of the concept or the components. Test and measurements went on from mid May until mid September, 2000.

The initial design of the dryer had a too high pressure drop in order to meet the design air flow rate of 300 m³/h per unit. The first test further showed that it was necessary to increase the flow rate above 300 m³/h in order to prevent a too high temperature of the air to the drying

bed. A temperature of above 45°C for a longer period will decrease the germination capacity of the maize.

A new test unit of the dryer was constructed based on the findings from the first unit. The pressure loss of the dryer was reduced by more than 50% at the design air flow rate. This led to an increase of the air flow rate through the system of between 30 and 60% - highest at high air flow rates with a max air flow rate of about 500 m³/h.

However, during the period December – February very fine dust is blown to Ghana from Sahara by the wind called the Hamatan. This very fine dust may by time totally block the absorber if not prevented from entering the collector. For that reason filters were designed and located at the inlet of the solar air collector - filters that may easily be taken down and washed. The filters, however, increase the pressure drop of the system leading to a decrease in the air flow rate of about 10%.

In one test 120 kg of maize with a moisture content of 20% was dried down to 10% within 1½ day. This was, however, under very favourable conditions with a rather low ambient humidity level. From the tests it is hoped that it is possible to dry the maize within 2-3 days under Ghanaian weather conditions.

The efficiency of the solar air collector was found to be as high as the best solar air collectors on the market today.

The tests showed a problem with the concept of PV driven fans. The air flow rate is very dependent on the ambient temperature. The performance of PV-panels is reduced by increasing ambient temperature (or more precisely increasing cell temperature). However, the tests revealed that the air flow rate decreased much more than the power from the PV-panels decreased due to the increase in the temperature of the PV-panels. The tests showed that this was because the speed of the fan was controlled by the voltage and not by the available power. This means that an increase of the area of the PV-panels (with same V_p) or a maximum power point tracker (which ensures max power from the PV-panels by adjusting the voltage and current from the PV-panels) will not increase the air flow rate. In order to be of benefit a maximum power point tracker should be able to boost the voltage from the PV-panels if excess power at a lower voltage is available from the PV-panels.

High ambient temperatures will thus reduce the air flow rate in the system leading to a risk of damaging the seed. It was, therefore, tested if an increase of thermal mass in the system would dampen the peak temperatures in the system so much that the risk of overheating of the maize would be minimized. 150 kg of stones were for that reason placed on a steel grid in the pressure chamber below the drying bed. The test showed that the additional thermal mass reduced the peak values of the air temperature to the drying bed with several degrees and will thereby reduce the risk of overheating of the seed. However, for other crops (and not used for seed) a higher temperature level will often not create problems.

The solar crop dryer for test and use in Ghana was shipped by the beginning of August, 2000 and will be erected at Silkwood Farms during the beginning of October, 2000. It is planned to monitor drying of maize in January, 2001. The monitored tests will show if the conclusions reached by the tests in Denmark will stand also under Ghanaian conditions. Especially if there is a risk of damaging the maize for seed due to too high temperatures to the drying bed. The five units shipped to Ghana are all equipped with a thermometer in the pressure chamber under

the drying bed so that the people at Silkwood Farms may intervene if the air temperature to the drying bed gets to high.

One unit of the solar crop dryer will further be erected at Elitet Enterprise Limited for the purpose of testing if the concept also is valuable for drying of fish.

The economical considerations show that the solar crop dryer will be economical feasible under different sets of realistic assumptions. The main parameters determining the economy for the solar crop dryer is the price of the dryer, how much it is used and if the drying in the solar crop dryer will add value to the crops compared to the drying methods used today. The uncertainty of these parameters are, however, rather high as indicated above. The economy of the solar crop dryer can, therefore, first be determined when the dryer has been tested in Ghana and when the marked price for the dryer in Ghana has been found.

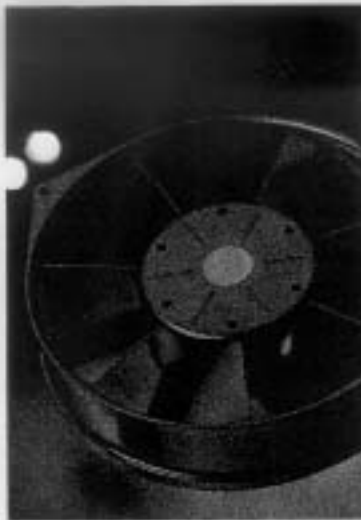
To the above economical considerations should be added the following considerations of major importance: that the oil prices most probably will increase more rapidly in the future due to a beginning shortage of oil, that an energy system based on solar energy thus is more stable than when based on fossil fuel and that an energy system based on solar energy is without pollution in the running phase.

9. References

- Akufo, F.O., 1991. Climate Data for Solar and Wind Energy Applications in Ghana. University of Science & Technology, Kumasi, Ghana.
- Duffie, J.A. and Beckman, W.A., 1991. Solar Engineering of Thermal Processes. John Wiley & Sons, New York. ISBN 0-47-51056-4.
- Fechner, H., 1999. IEA Task 19 Solar Air Systems. Investigation on Series Produced Solar Air Collectors. Arsenal Research. Department of Renewable Energy. Austria.
- Jensen, S.Ø., 1994. Test of the Summer House Package from Aidt Miljø. Thermal Insulation Laboratory. Technical University of Denmark. Report no. 94-1.
- Jensen, S.Ø., Frank, F.C. and Kristensen, E.F., 1999. Survey on solar dryers for drying of food and wood in Ghana. Solar Energy Centre Denmark and Wood Technology, Danish Technological Institute and Department of Agricultural Engineering, Danish Institute of Agricultural Sciences. ISBN
- Jensen, S.Ø., 2000. Ghanaian weather data for simulation purposes. Solar Energy Centre Denmark, Danish Technological Institute. ISBN
- Nielsen, J.E., 1995. Documentation of KVIKSOL – a program for simulation of solar heating systems – version 5.0 (in Danish). The Solar Energy Laboratory, Danish Technological Institute.

Appendix A

Data sheet for the fan



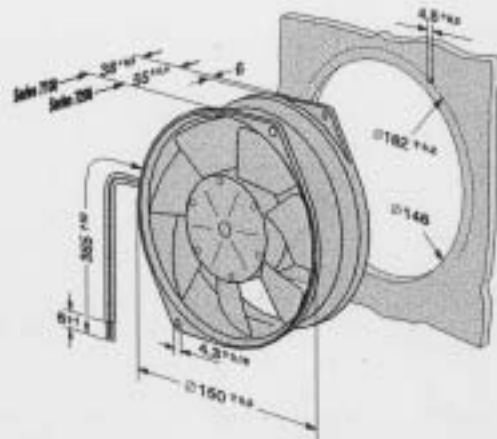
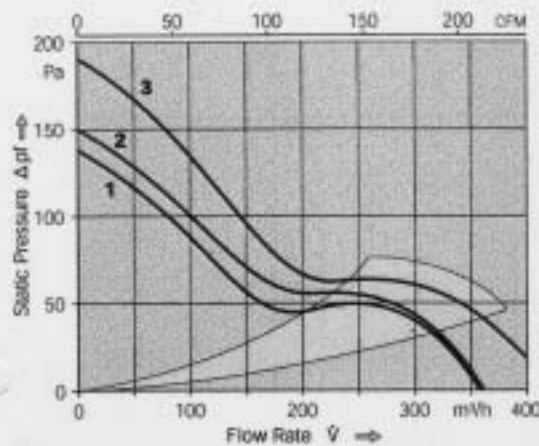
- DC fans with electronically commutated external rotor motor. Fully integrated commutation electronics. With electronic protection against reverse polarity and blocking.
- Metal fan housing, Series 7100 impellers of metal, Series 7200 of fibreglass reinforced plastic PA.
- Air exhaust over struts. Rotational direction CCW looking at rotor.
- Electrical connection via 2 leads AWG 22, TR 84. Stripped and tinned ends. Housing with ground lug for screw M4.
- Mass 620/725 g.

SERIES 7100/7200

150Øx38mm / 150Øx55mm

Air flow	Air flow	Nominal Voltage	Voltage Range	Noise	Static-Current Bearing Ball Bearings	Power Input	Nominal Speed	Temperature Range	Service Life L ₁₀ at 40 °C	# Leads	Curve	Type
m³/h	CFM	VDC	VDC	dBS(A)	mm	Watt	rpm	°C	Hours	Hours		
Series 7100												
360	211.9	12	6...15	55	6.5	●	12	2850	-25...+72	80000 / 37500	1	7112N
360	211.9	24	12...30	55	6.5	●	12	2850	-25...+72	80000 / 37500	1	7114N
420	247.2	24	12...26.5	59	7.0	●	19	3350	-25...+72	75000 / 35000	3	7114NH
360	211.9	48	24...60	55	6.5	●	12	2850	-25...+72	80000 / 37500	1	7118N
Series 7200												
360	211.9	12	6...15	50	6.2	●	12	3050	-25...+72	80000 / 37500	2	7212N
360	211.9	24	12...30	50	6.2	●	12	3050	-25...+72	80000 / 37500	2	7214N
360	211.9	48	24...60	50	6.2	●	12	3050	-25...+72	80000 / 37500	2	7218N

⊕ 48V Type with grounding screw M4x8 (TORX).



Appendix B

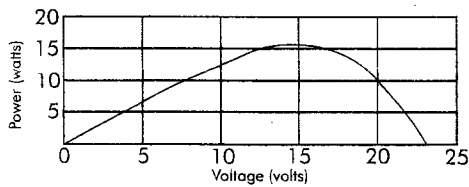
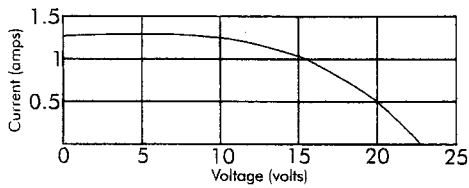
Data sheet for the PV-panels

ELECTRICAL CHARACTERISTICS

Rated power (+/- 15%) 14 Wp
Typical values (+/- 15%)
 Current @ 15.8V 0.94 Amps
 Open circuit voltage 24 Volts
 Short circuit current 1.2 Amps

Temperature co-efficients

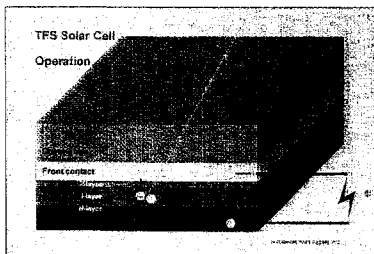
Voltage - 0.29% degrees C.
 Current + 0.08% degrees C



End-of-line testing: a sample of Intersolar's test results.
 Data collected at noon (1200 hrs) on 09 July 1997
 in Bridgend, South Wales, United Kingdom
 (Latitude 51.5N Longitude 3.6W).

Performance Guarantee

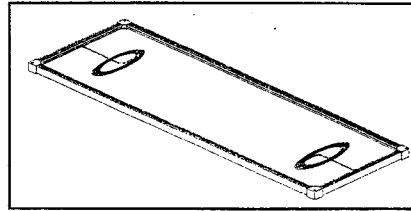
All Phoenix™ panels manufactured by Intersolar carry a limited 6 year manufacturers' warranty guaranteeing performance at the rated power. Due to the Stabler-Wronski effect, TFS modules can deliver typically 15% more than their rated power when first installed and for the first few weeks of operation.



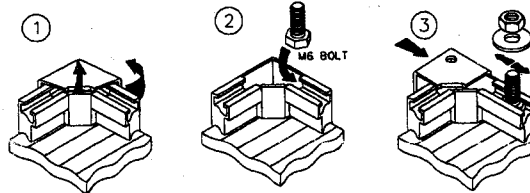
TFS solar cell operation

PHYSICAL CHARACTERISTICS

Electricity generation: Thin film silicon (a-Si)
 29 cells per panel
 Frame: high grade anodised aluminium
 Corners: UV stable ABS / co-polymer polypropylene
 Cables: 3 metres (red = positive, black = negative)



Rear view of module



Fixing and Mounting

Remove black corner cover. Slide M6 bolts (not supplied) and fix to a suitable mounting structure with nuts and washers. Replace corner cover. Front of module should face midday sun.

Nett Weights and Dimensions

Model	B108D
Length	940 mm / 37 inches
Width	340 mm / 13.4 inches
Depth	30 mm / 1.2 inches
Weight	4.6 kg / 10 lbs

Shipping Weights and Dimensions

	Carton (10 units)	Pallet (90 units)
Length	99 cm / 39 in	99 cm / 39 in
Width	43 cm / 17 in	130 cm / 51.5 in
Depth	41 cm / 16 in	140 cm / 55 in
Weight	50 Kg / 110lbs	465 Kg / 1023 lbs

Intersolar Limited

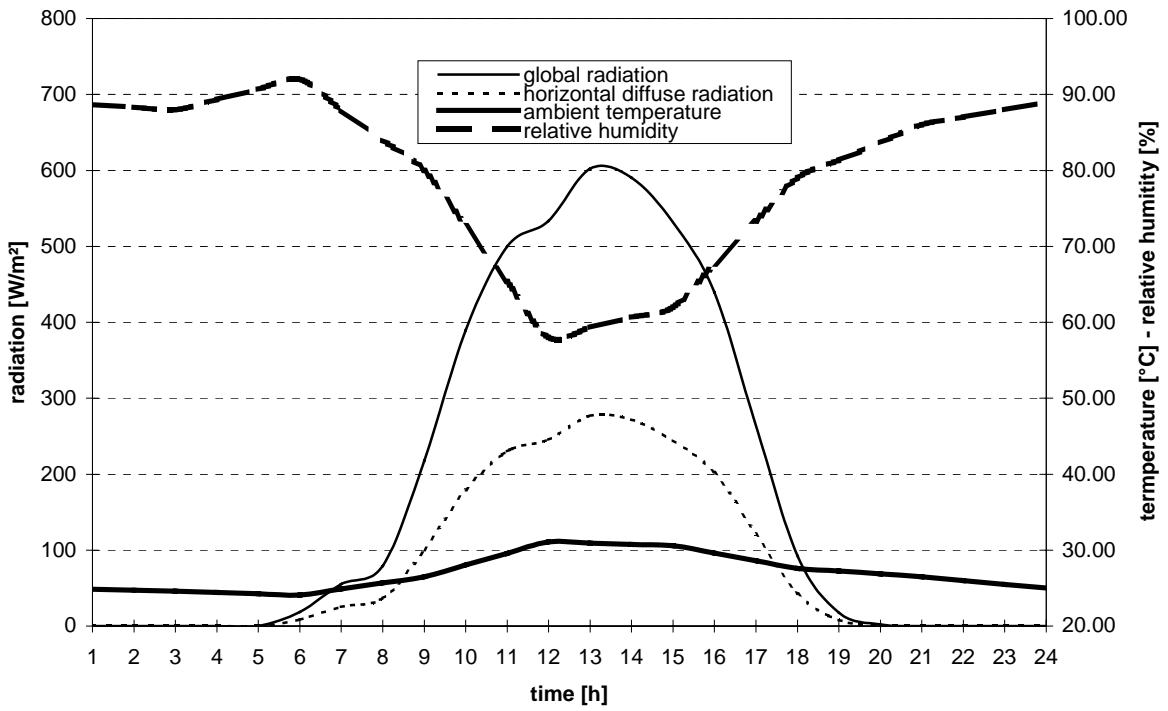
Cock Lane, High Wycombe,
 Bucks HP13 7DE U.K.
 Tel: [44] (0) 1494 452945
 Fax: [44] (0) 1494 437045
 Internet: www.intersolar.com
 E-Mail: intersolar@intersolar.com



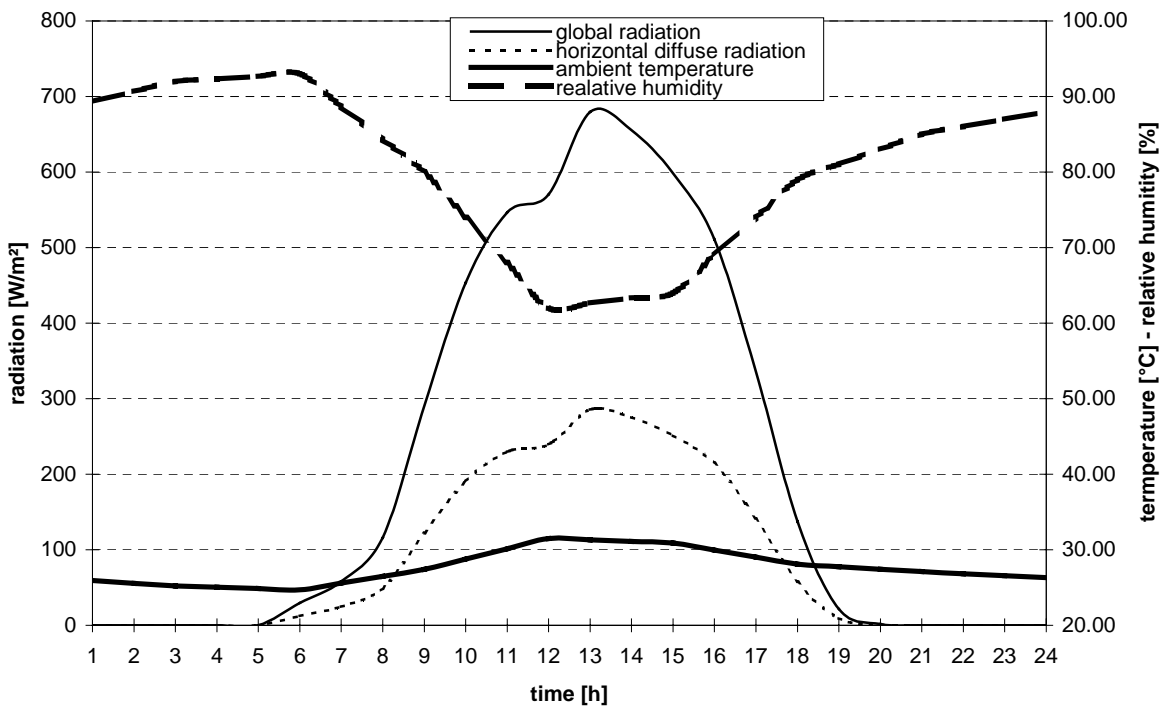
Appendix C

Weather conditions in Accra

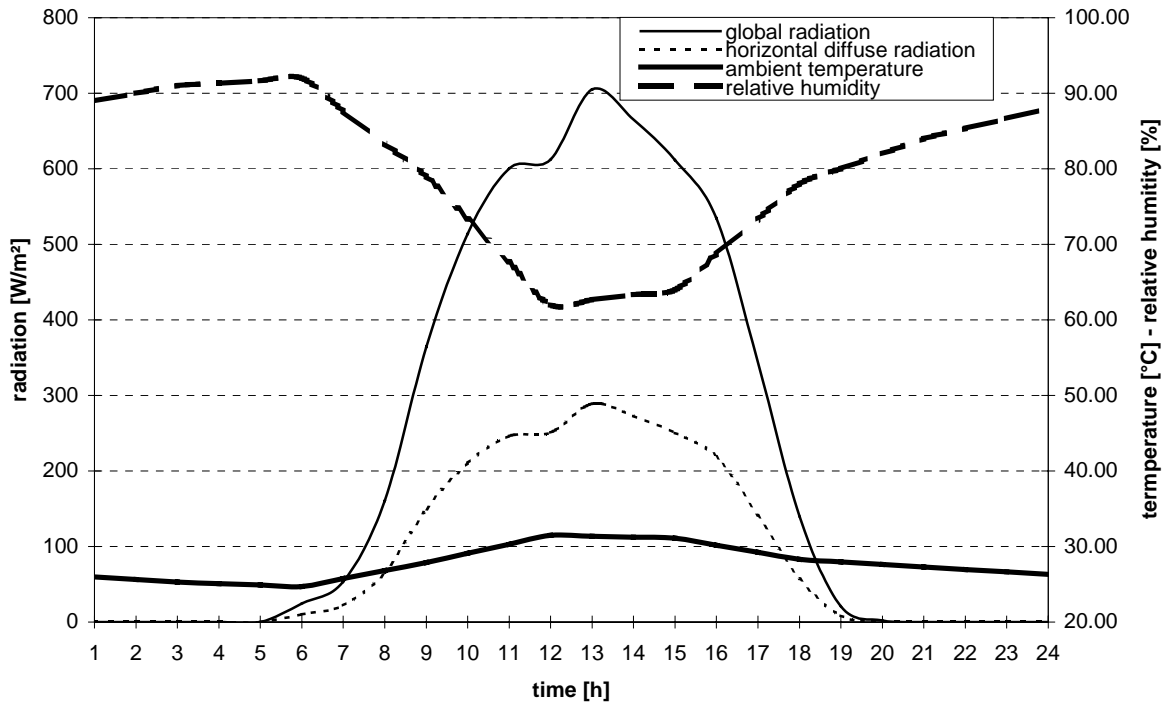
Accra - January



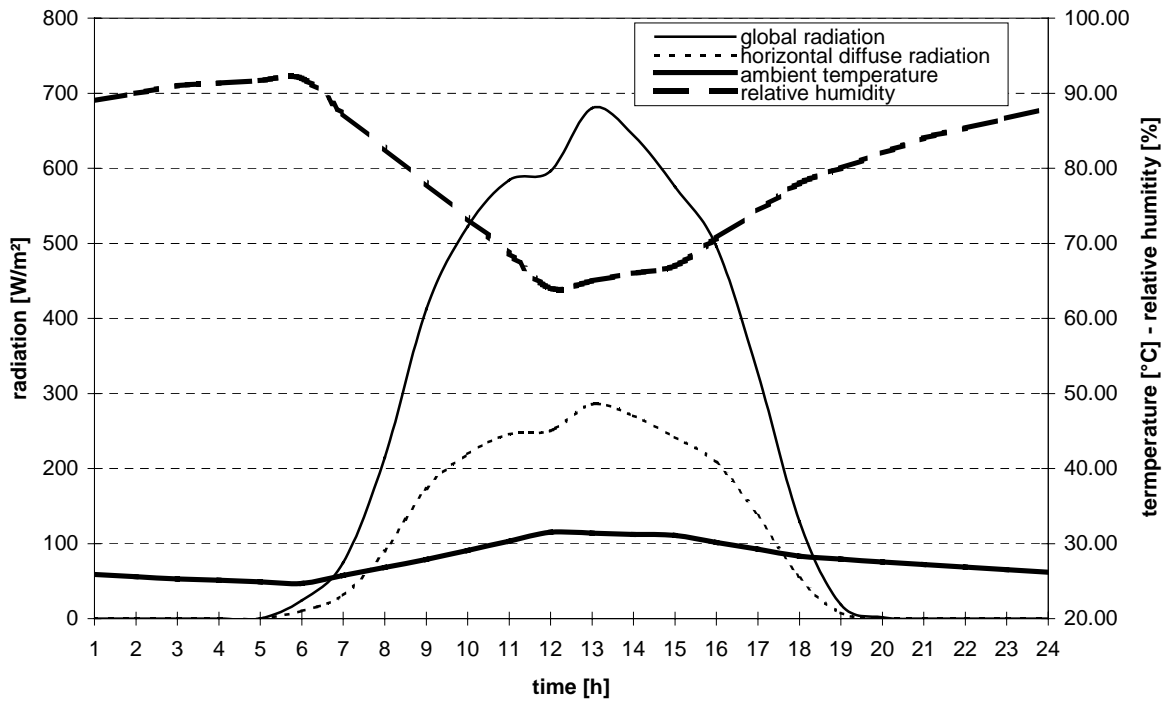
Accra - February



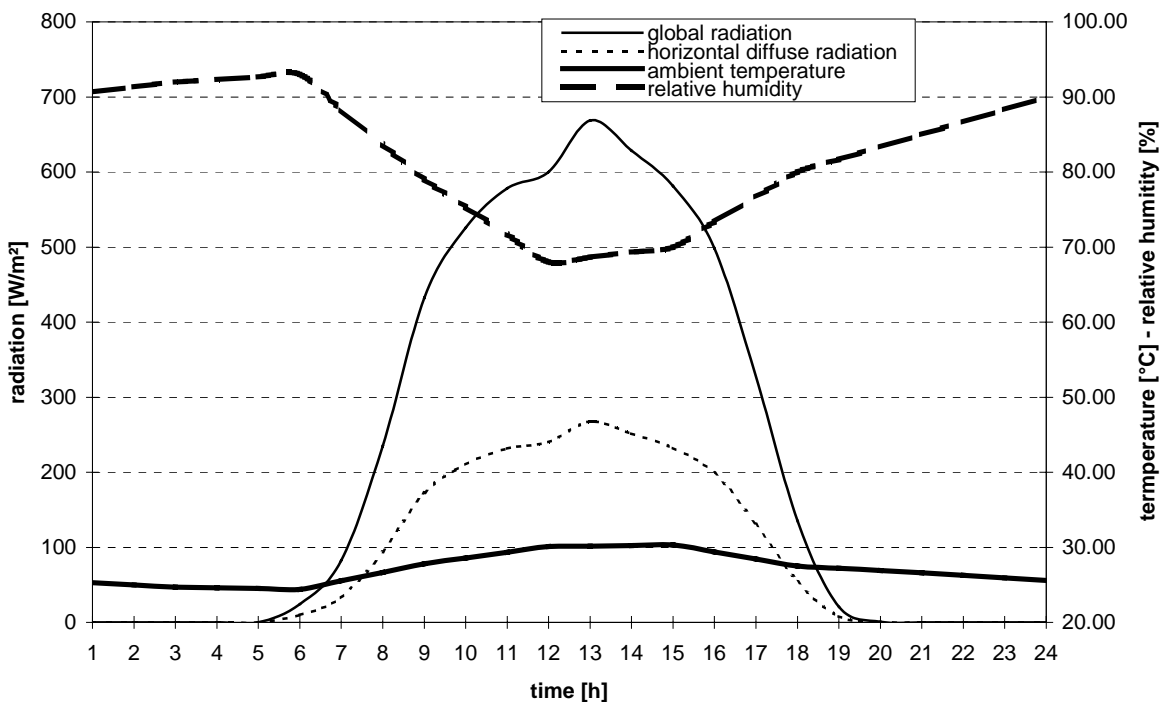
Accra - Marts



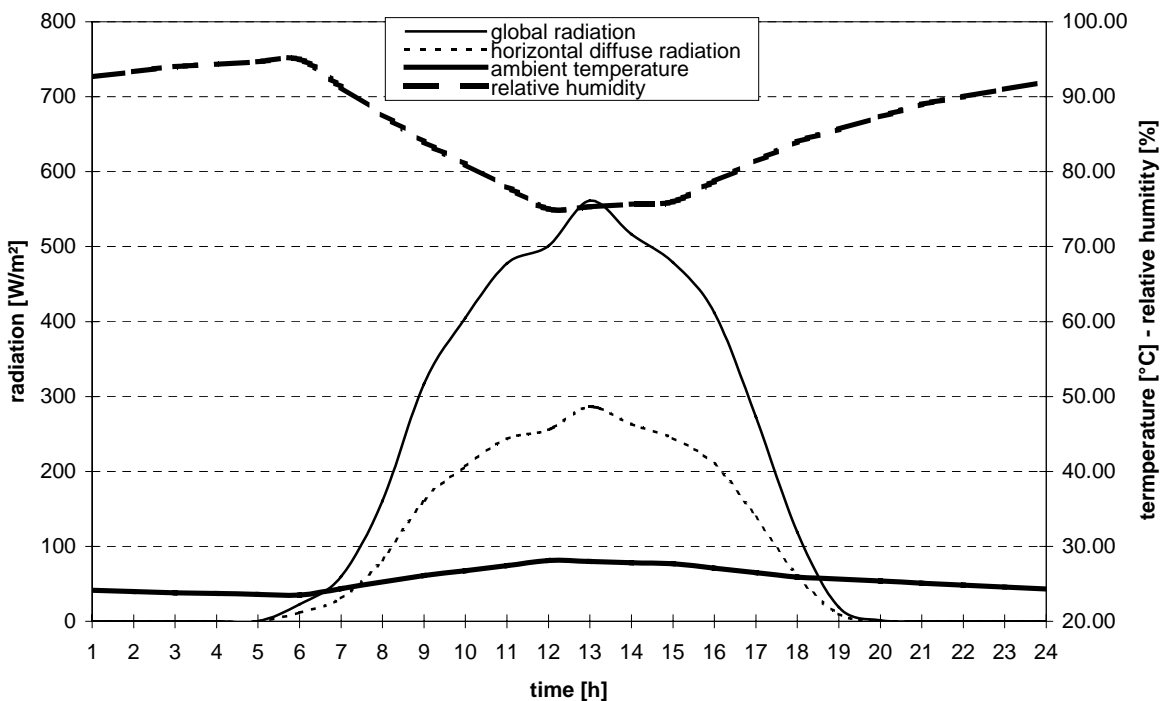
Accra - April



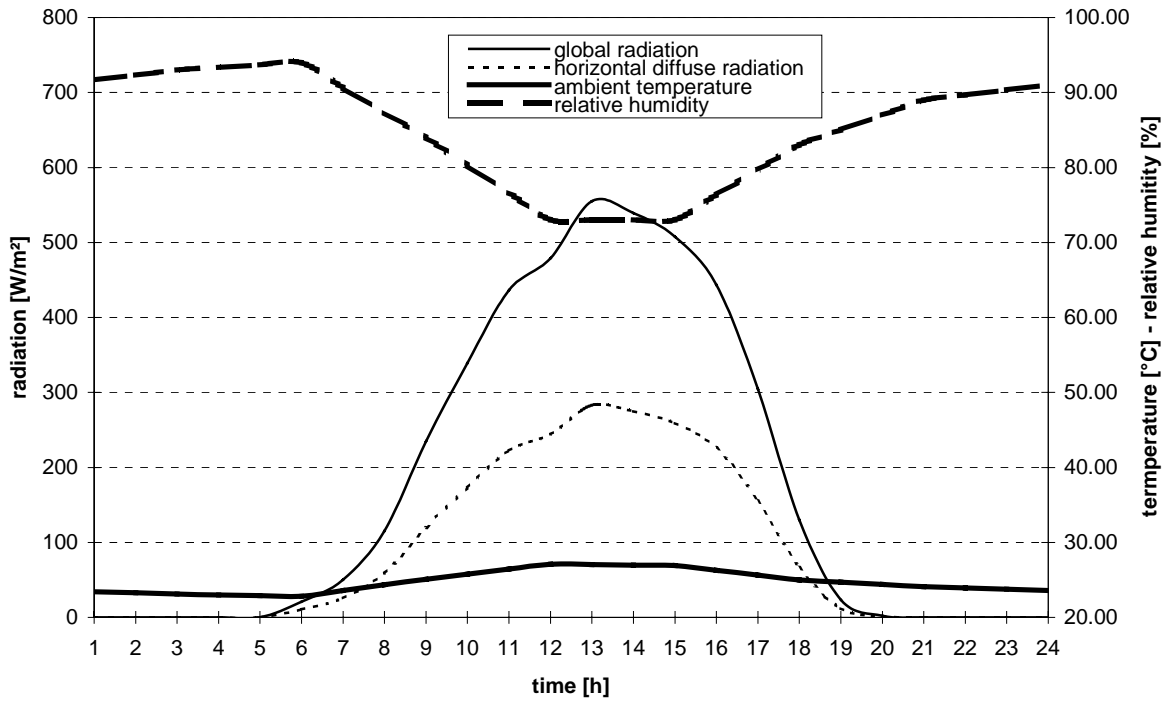
Accra - May



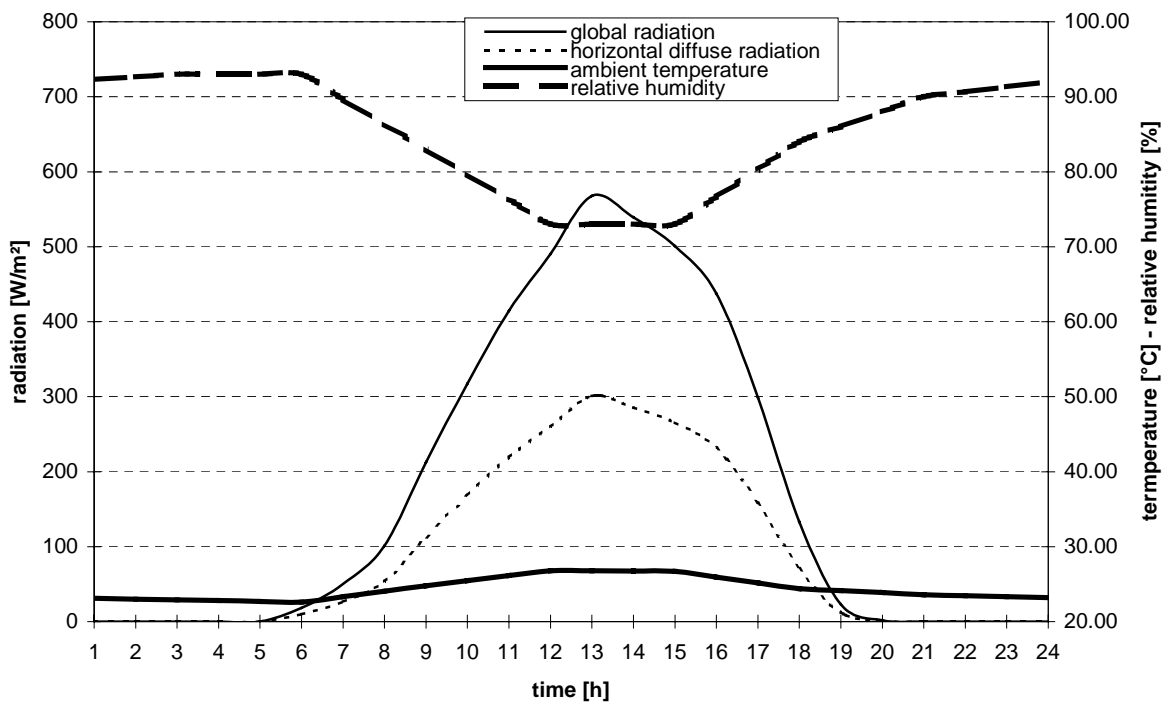
Accra - June



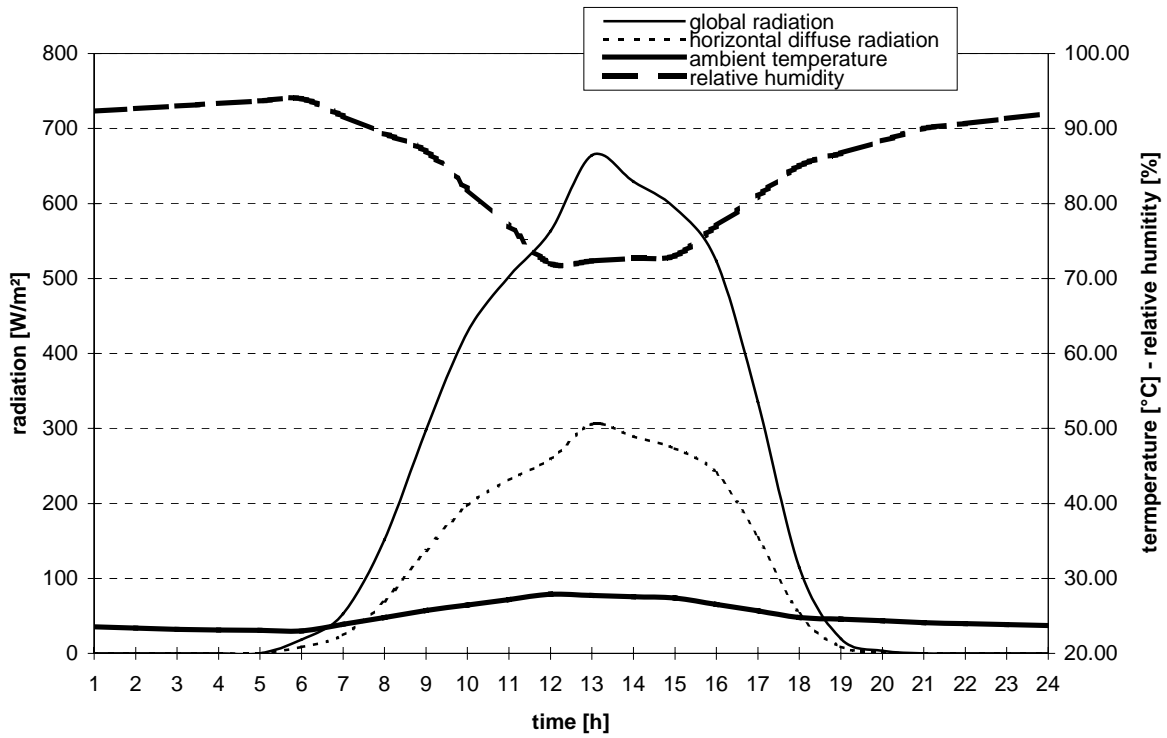
Accra - July



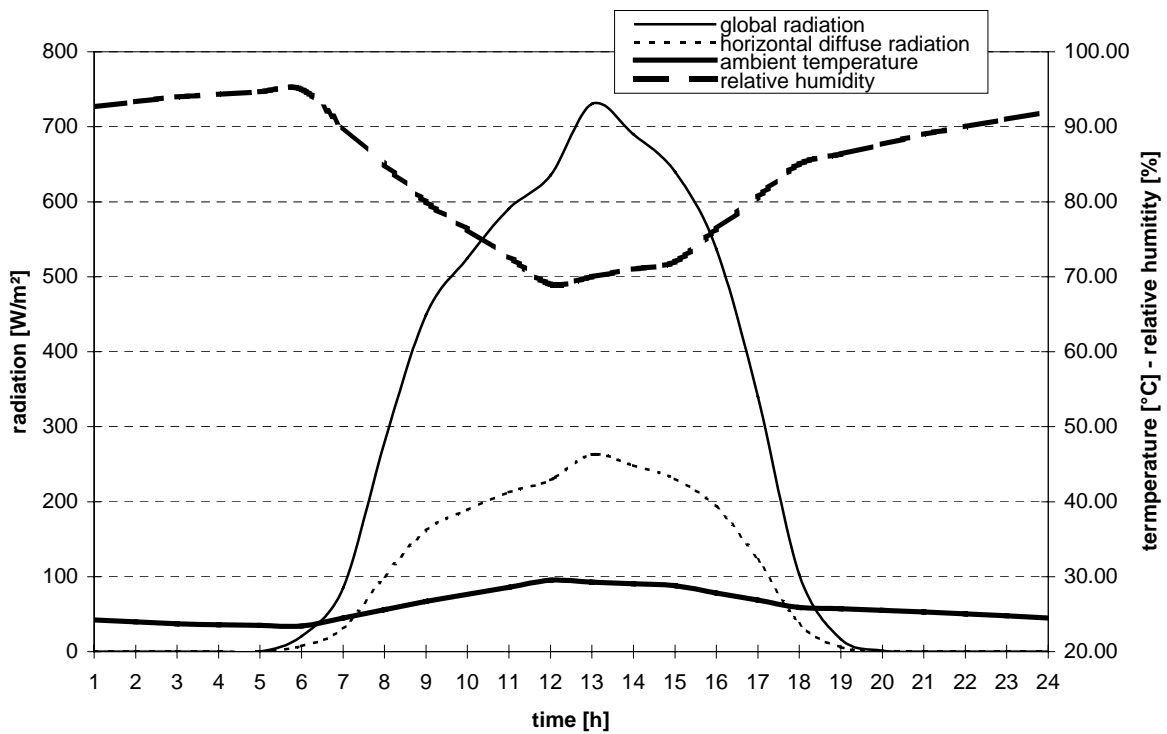
Accra - August



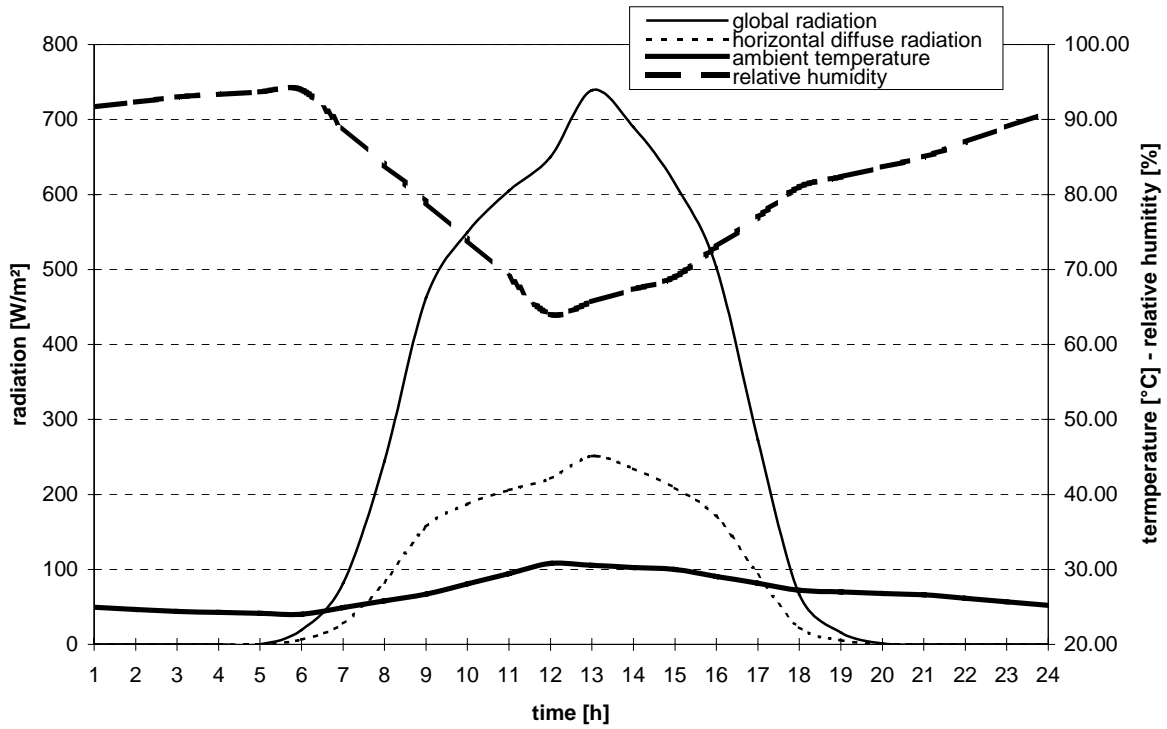
Accra - September



Accra - October



Accra - November



Accra - December

